

**THE EFFICIENCY OF THE BURN-LEACH METHOD IN ASSESSING THE
INTEGRITY OF TRISO COATED PARTICLE LAYERS**

by

ANDILE KENNETH NTLOKWANA

Submitted in fulfilment of the requirements for the degree

Master of Applied Sciences (Metallurgy)

in the

Faculty of Engineering, Built Environment and Information Technology

UNIVERSITY OF PRETORIA

Pretoria, South Africa

July 2013

©University of Pretoria

TITLE: The efficiency of the Burn-Leach method in assessing the integrity of TRISO coated particle layers

STUDENT: Andile Kenneth Ntlokwana

NUMBER: 28613202

DEGREE: Master of Applied Sciences (Metallurgy)

DEPARTMENT: Department of Materials Science and Metallurgical Engineering

FACULTY: Faculty of Engineering, Built Environment and
Information Technology

UNIVERSITY: University of Pretoria, South Africa

SUPERVISOR: Dr. D.R. Groot

CO-SUPERVISOR: Prof. J.P.R. de Villiers

STUDY YEARS: 2009-2012

DECLARATION OF ORIGINALITY

This is to certify that the work is my own and not that of any other person, unless explicitly acknowledged (including citation of published and unpublished sources). The work has not previously been submitted in any form to the University of Pretoria or to any other institution for assessment for any other purpose.

Signed _____

Date _____

ABSTRACT

The basic fuel unit of the High Temperature Reactor (HTR) of the Pebble Bed Modular Reactor (PBMR) is a uranium dioxide kernel coated with a buffer layer, an inner pyrolytic carbon (IPyC) layer, a silicon carbide (SiC) layer and an outer pyrolytic carbon (OPyC) layer and is commonly referred to as a TRISO particle. Thousands of these micro-spheres are embedded in a graphite matrix and pressed to form a fuel sphere. During the manufacture of the TRISO particles and the fuel spheres there is a production of TRISO particles with cracked/broken layers, especially the SiC layer. Before the irradiation of the fresh fuel in the nuclear reactor it is of the utmost importance to quantify the failed fractions in fresh fuel as this information is very useful in the general understanding of fuel behaviour, calculation of risk and safety margins, and prediction of long term fuel behaviour. For this reason the burn-leach method has been applied for the quality control of the fresh fuel. In this work, several aspects of the burn-leach method that affect the efficiency of the method were studied. Aspects that were investigated are: qualitative aspects, layer properties, quantitative aspects, variants of the burn-leach method and lastly statistical information from the burn-leach data.

The results obtained were as follows:

- Studies in this dissertation suggest that partial leaching of uranium in TRISO particles with a defective SiC layer was a phenomenon that exists. Although UO_2 kernel equivalents were successfully determined by burn-leach method for particles with fully broken SiC layers, certain particles leached uranium amounts that did not correspond to single UO_2 kernel equivalents;
- Evidence of occurrences of 'slow leaching' in an acidic medium were evident for certain particles. There were remnants of uranium dioxide kernels that had been partially leached after the full 16 hours. This behaviour led to inconclusive results on the absolute number of defective particles in a given population;
- Investigations suggest that there is at least circumstantial evidence that the BL method combined with X-ray tomography provides information about the integrity of the SiC layer, and why one particle leaches and the other does not.
- Neither the burn-leach nor the leach-burn-leach analysis is sufficient to be used as a stand-alone method to quantify the number of particles with defective SiC layers in a given TRISO particle population. The two tests need to be coupled to

other techniques such as high resolution tomography for an extensive quantification of the layer defects;

- Burn-leach has to be designed to test for the layer integrity on a microscopic level as opposed to testing for the broken shells only, as was done by the normal burn-leach based on the German program. The leach time was not sufficient in its present form;
- Burn-leach results indicated that oxidation times of 96 hours at 750 °C under atmospheric pressure did not negatively affect the mechanical strength of the silicon carbide layer of freshly-manufactured TRISO particles, as these particles did not have a high failure fraction.

Keywords: Burn-Leach, TRISO particles, Layers, Uranium.

ACKNOWLEDGEMENTS

I praise God for the gift of knowledge and wisdom He gave me during the completion of this work.

I hereby would like to thank my supervisors Professor Johan de Villiers and Dr. Dick Groot for their guidance, great ideas, suggestions, patience and encouragement during this study. This work would not have been of this standard without them.

I thank my wife Zanele for her patience during my long hours in the laboratory and in front of the computer screen.

I am grateful to my employment supervisors Dr. Fanie Venter and Mr. Dieter Zimolong for allowing me to conduct this research on their departmental budget.

I hereby thank the laboratory head, Mrs. Leoni Strauss for giving me access to the experimental equipment. I thank Mrs. Corrie Strauss for the X-ray images and the OIAS system, and PAL for the ICP-MS.

I am grateful to Mr. Kwena Morifi and Mr. Pieter Steyn for keeping the burn-leach apparatus neat and tidy. For their insights, I thank Mr. Peter Jackson and Dr. Pradish Rampersadh.

I thank both Mr. Cliff Thompson and associated helper for grammatically editing this dissertation. Without their help it would not read so smoothly.

TABLE OF CONTENTS

ABSTRACT	4
ACKNOWLEDGEMENTS	6
LIST OF FIGURES	10
LIST OF TABLES	12
ABBREVIATIONS	14
CHAPTER 1	16
1. INTRODUCTION	16
1.1. Pebble Bed Modular Reactor (PBMR) description	16
1.2. Aim of this investigation	19
1.3. Manufacture of UO ₂ kernels.....	19
1.4. Manufacture of TRISO particles	24
1.5. Description of the Pebble Bed CVD Coater	24
1.6. Manufacture of fuel spheres	27
1.7. Roles played by each layer in the performance of TRISO fuel.....	30
CHAPTER 2	33
2. LITERATURE SURVEY	33
2.1. Burn-leach method.....	34
2.2. Mercury intrusion method	35
2.3. Chlorine gas method.....	35
2.4. Leach-burn-leach method	36
2.5. Gaseous acid leach method	37
2.6. Organic chemistry of uranium	37
2.7. Thermal degradation of fuel spheres and TRISO particles	37
2.8. High temperature chemistry of SiC.....	38
2.9. Reactivity of SiC.....	39
2.10. Summary.....	40

CHAPTER 3	41
3. STATISTICAL TOOLS	41
3.1. Determination of layer thickness values	41
3.2. Analysis of variance (ANOVA) in layer thickness values.....	42
3.3. Determination of the failure fraction of TRISO-coated particles	43
3.4. Calculation of the 95% Poisson confidence level	45
3.5. Sampling statistics of TRISO particles.....	45
CHAPTER 4	48
4. EXPERIMENTAL	48
4.1. Qualitative aspects of the BL test	48
4.1.1. Density difference method for the broken SiC layers	48
4.2. Characterisation of TRISO particles	48
4.2.1. Introduction	48
4.2.2. Determination of the layer thicknesses of TRISO particles	49
4.2.3. Determination of the total uranium content of TRISO particle batches	49
4.2.4. Density determination: Buffer, IPyC, SiC and OPyC	50
4.3. Quantitative aspects of the BL test	52
4.3.1. As-manufactured (fresh) TRISO particles.....	52
4.3.2. Leach-burn-leach test of TRISO particles.....	52
4.3.3. Fuel spheres	53
4.4. Variants of BL test.....	54
4.4.1. Effect of burn time on the amount of leached uranium	54
4.4.2. Effect of sequential leaching on the amount of uranium released.....	55
4.4.3. Defective IPyC	55
CHAPTER 5	56
5. RESULTS AND DISCUSSION	56
5.1. Qualitative analysis of TRISO particles	56
5.1.1. Introduction	56

5.1.2.	Separation of the SiC layer shards by the density difference	56
5.2.	Characterisation of TRISO particles	59
5.2.1	Introduction	59
5.2.2	Determination of layer thickness values of TRISO particles.....	59
5.3	Quantitative analysis of TRISO particles by BL method	65
5.3.1	Introduction	65
5.3.2	Fresh TRISO particles	67
5.3.3	BL results by PBMR	69
5.3.4	LBL results by ORNL	71
5.3.5	Fuel spheres by BL	78
5.3.6	Comparison of results with Nukem fuel testing.....	80
5.4.	Variants of BL method	84
5.4.1	Effect of burn time on the amount of leached uranium.....	84
5.4.2	Effect of leaching time on the amount of uranium released	87
5.4.3	Defective IPyC layer	88
5.5	Statistical treatment of the BL results	93
5.5.1	Fresh fuel	93
5.5.2	Sampling risks of the BL method	94
6.	CONCLUSION AND RECOMMENDATIONS	99
6.1	Conclusion	99
6.2	Recommendations	100
	BIBLIOGRAPHY	101
	APPENDICES	107

LIST OF FIGURES

- Figure 1.1:** PBMR fuel sphere design, courtesy of the PBMR Fuel design group.
- Figure 1.2:** UO₂ kernel production.
- Figure 1.3:** Casting process.
- Figure 1.4:** A picture of the PBMR CVD coater, courtesy of the PBMR Advanced Coater Facility group.
- Figure 1.5:** The flow diagram for the manufacture of TRISO particles.
- Figure 1.6:** Example of the CVD process control screen, courtesy of the ACF group.
- Figure 5.1:** A photomicrograph showing shards from the BL test indicating a single broken particle (64X magnification).
- Figure 5.2:** A shell with a hole collected after a positive BL test for one particle (64X magnification).
- Figure 5.3:** Shards that were collected after BL testing (16X magnification).
- Figure 5.4:** Photomicrograph showing a rough surface SiC layer (32X magnification).
- Figure 5.5:** Statistical distribution of buffer layer thickness values of TRISO particles inspected in this dissertation for $n = 1\ 000$.
- Figure 5.6:** Statistical distribution of IPyC layer thickness values of TRISO particles used in this study for $n = 1\ 000$.
- Figure 5.7:** Statistical distribution of SiC layer thickness values of TRISO particles used in this study for $n = 1\ 000$.
- Figure 5.8:** Statistical distribution of OPyC layer thickness values of TRISO particles used in the study for $n = 1\ 000$.
- Figure 5.9:** Amount of uncontained uranium for each of the 60 BL tested samples, 20 g of each sample were tested.

- Figure 5.10:** The total uncontained uranium as a function of the mean layer thickness of the silicon carbide layer for the batches SiC 101-SiC 110.
- Figure 5.11:** The total uncontained uranium as a function of the mean layer thickness of the inner pyrolytic carbon layer for the batches PyC 101-PyC 110.
- Figure 5.12a:** TRISO particles before LBL testing and (b) Particles after LBL test.
- Figure 5.13a:** High resolution X-ray tomography of a SiC defect particle after the kernel was removed by acid leaching at ORNL. The white ring shows the SiC layer, the damaged porous layer below the white ring pointed by the arrow is the IPyC layer.
- Figure 5.13b:** Same particle as in Figure 5.13a showing a crack in the SiC layer (arrow).
- Figure 5.14:** High resolution tomography of a SiC defect after the kernel was partially removed by acid leaching.
- Figure 5.15:** J10-FSA-G12, particles that floated in methylene iodide after BL test (48X magnification).
- Figure 5.16:** Photomicrographs showing strange-looking particles (from fuel sphere) after BL test. Magnification is 32X and 48X respectively.
- Figure 5.17:** Micro X-rayed images of particles with a peculiar SiC layer.
- Figure 5.18:** Uncontained uranium released (mg/l) as a function of burn time (hours).
- Figure 5.19:** A schematic representation of a log normal leak channel size distribution.
- Figure 5.20:** X-ray microradiographs of particles with two layers: buffer and IPyC. About 1 % of the population had defective IPyC layer that leached uranium within the first two hours in nitric acid.
- Figure 5.21:** A low resolution X-ray image of a TRISO particle with uranium dispersion caused by a crack in the IPyC layer.
- Figure 5.22:** An image of a crack marked by a ring in the IPyC layer of a TRISO particle, showing uranium deposits through the crack, performed at ORNL.

Figure 5.23: Design of acceptance sampling plans. Steep curves indicate high sampling rates or large sample sizes. Dashed line indicates the sampling rate employed in this study.

Figure 5.24: An outline of risks associated with each sampling plan.

LIST OF TABLES

- Table 1.1:** Technical design requirements of PBMR fabricated TRISO particles.
- Table 1.2:** Summary of roles played by each component of a TRISO particle.
- Table 5.1:** A comparison of qualitative versus quantitative BL.
- Table 5.2:** Summary of statistical treatment of buffer layer thickness values.
- Table 5.3:** Summary of statistical treatment of IPyC layer thickness values.
- Table 5.4:** Summary of statistical treatment of SiC layer thickness values.
- Table 5.5:** Summary of statistical treatment of OPyC layer thickness values.
- Table 5.6:** ICP-MS results ($\mu\text{g/L}$) of water, reagents and reference samples.
- Table 5.7:** Results ($\mu\text{g/L}$) of uranium contamination studies on dummy samples.
- Table 5.8:** Results (mg/L) of uranium leached during BL testing of B_5 TRISO particles.
- Table 5.9:** Summary of the SiC defect analysis for CPU-L- H101.
- Table 5.10:** Comparison of the failure fractions between PBMR fuel versus Nukem fuel after 1985.
- Table 5.11:** Summary of BL test results (number of failed particle equivalents) in fuel sphere manufacturing.
- Table 5.12:** Layer properties of coated particle batch CPT-T-C7.
- Table 5.13:** Summary of BL results of TRISO particles burned for various times.

Table 5.14: Mass difference for 16- and 32-hours burn times.

Table 5.15: Decrease in uranium concentration ($\mu\text{g/L}$) with successive leach steps.

Table 5.16: A comparison of BL results of fuel spheres using Poisson distribution.

Table 5.17: Design of acceptance sampling plans for BL testing of particles.

Table 5.18: Producer's risk (α) and consumer's risk (β) computed for each sampling plan.

ABBREVIATIONS

ACF	Advanced Coater Facility
ADU	Ammonium diuranate
ANOVA	Analysis of Variance
AVR	ArbeitsgemeinschaftVersuchsreaktor (Jointly operated prototype reactor)
BAF	Bacon Anisotropy Factor
BL	Burn Leach
CVD	Chemical Vapour Deposition
FDL	Fuel Development Labs
FP	Fission Product
FS	Fuel Sphere
HF	Hydrofluoric acid
HNO ₃	Nitric acid
HTR	High Temperature Reactor
ICP-MS	Inductively Coupled Mass Spectrometry
IPyC	Inner Pyrolytic carbon layer
LBL	Leach Burn Leach
LEU	Low enriched uranium
MBL	Modified Burn Leach
OAF	Optical Anisotropy Factor

OC	Over-coating layer
OIAS	Optical Image Analysis System
OPyC	Outer Pyrolytic carbon layer
PBMR	Pebble Bed Modular Reactor
PyC	Pyrolytic carbon
QC	Quality Control
QCTL	Quality Control Test Lab
RCF	Research Coater Facility
SiC	Silicon carbide layer
STA	Simultaneous Thermal Analyser
TRISO	Tristructural-isotropic
VHTR	Very High Temperature Reactor

CHAPTER 1

1. INTRODUCTION

1.1. Pebble Bed Modular Reactor (PBMR) description

The PBMR is a graphite-moderated, gas-cooled, nuclear reactor. It is a type of very high temperature reactor (VHTR), one of the six classes of nuclear reactors in the Generation IV initiative. The basic design of pebble bed reactors features spherical fuel elements called pebbles. These tennis ball-sized pebbles are made of pyrolytic graphite (which acts as the moderator), and they contain thousands of micro fuel particles called TRISO particles. These TRISO fuel particles consist of a fissile material (such as U^{235}) surrounded by a coated ceramic layer of silicon carbide for structural integrity and fission product containment. In the PBMR, thousands of pebbles are amassed to create a reactor core, and are cooled by a gas, such as helium, which does not react chemically with the fuel elements.

This type of reactor is passively safe (Kasak 2005), that is, it removes the need for redundant, active safety systems. Because the reactor is designed to handle high temperatures, it can cool by natural circulation and still survive in accident scenarios, which may raise the temperature of the reactor to 1 600 °C. Because of its design, its high temperatures allow higher thermal efficiencies than possible in traditional nuclear power plants (up to 50%). It has the additional feature that the gases do not dissolve contaminants or absorb neutrons as water does, so the core has less in the way of radioactive fluids.

The concept was first suggested by Farrington Daniels in the 1940s, but commercial development did not take place until the 1960s in the German AVR reactor by Rudolf Schulten (Association of German Engineers 1990) but this system was plagued with problems and political and economic decisions were made to abandon the technology. The AVR design was licensed to South Africa as the PBMR and China as the HTR-10, the latter currently the only such design operational. In various forms, other designs are under development by MIT, University of California at Berkeley, General Atomics (U.S.), the Dutch company Romawa B.V., Adams Atomic Engines, and Idaho National Laboratory.

A pebble bed power plant combines a gas-cooled core and a novel packaging of the fuel that dramatically reduces complexity while improving safety.

Figure 1.1 is a schematic of PBMR fuel. The uranium nuclear fuel contained within a spherical pebble is a little smaller than the size of a tennis ball and made of pyrolytic graphite, which acts as the primary neutron moderator. The pebble design is relatively simple, with each sphere consisting of the nuclear fuel, fission product barrier, and moderator.

The pebbles are held in a vessel, and an inert gas such as helium circulates through the spaces between the fuel pebbles to carry heat away from the reactor. The preferred gas, helium, does not easily absorb neutrons or impurities. Therefore, compared to water, it is both more efficient and less likely to become radioactive. If helium is used, because it is lighter than air, air can displace the helium if the reactor wall is breached.

Pebble bed reactors need fire-prevention features to keep the graphite of the pebbles from burning in the presence of air. Ideally, the heated gas is run directly through a turbine. However, if the gas from the primary coolant can be made radioactive by the neutrons in the reactor, or a fuel defect could still contaminate the power production equipment, it may be brought instead to a heat exchanger where it heats another gas or produces steam. The exhaust of the turbine is quite warm and may be used to warm buildings or chemical plants, or even run another heat engine.

A large advantage of the pebble bed reactor over a conventional light-water reactor is in operating at higher temperatures. The reactor can directly heat fluids for low pressure gas turbines. The high temperatures allow a turbine to extract more mechanical energy from the same amount of thermal energy; therefore, the power system uses less fuel per kilowatt-hour.

For maintenance, many designs include control rods, called "absorbers" that are inserted through tubes in a neutron reflector around the reactor core. A reactor can change power quickly just by changing the coolant flow rate and can also change power more efficiently by changing the coolant density or heat capacity.

The core generates less power as its temperature rises, and therefore cannot have a criticality excursion when the machinery fails. At such low power densities, the reactor

can be designed to lose more heat through its walls than it would generate. In order to generate much power it has to be cooled, and then the energy is extracted from the coolant.

The PBMR core consists of spherical fuel elements which contain uranium in the form of uranium dioxide kernels of a strictly controlled density. The uranium oxide fuel generates heat by means of the fission reactions which occur in the core. The fuel sphere is manufactured by pressing a core of coated particles surrounded by a matrix graphite composite, which is a mixture of natural graphite and electro graphite bound together by a phenolic resin. There are two zones that define a fuel sphere. The inner core is called the fuel zone and the outer 5 mm the fuel-free zone. The fuel zone contains a large number of uniformly dispersed spherical-coated particles while no coated particles appear in the fuel-free zone.

FUEL ELEMENT DESIGN FOR PBMR

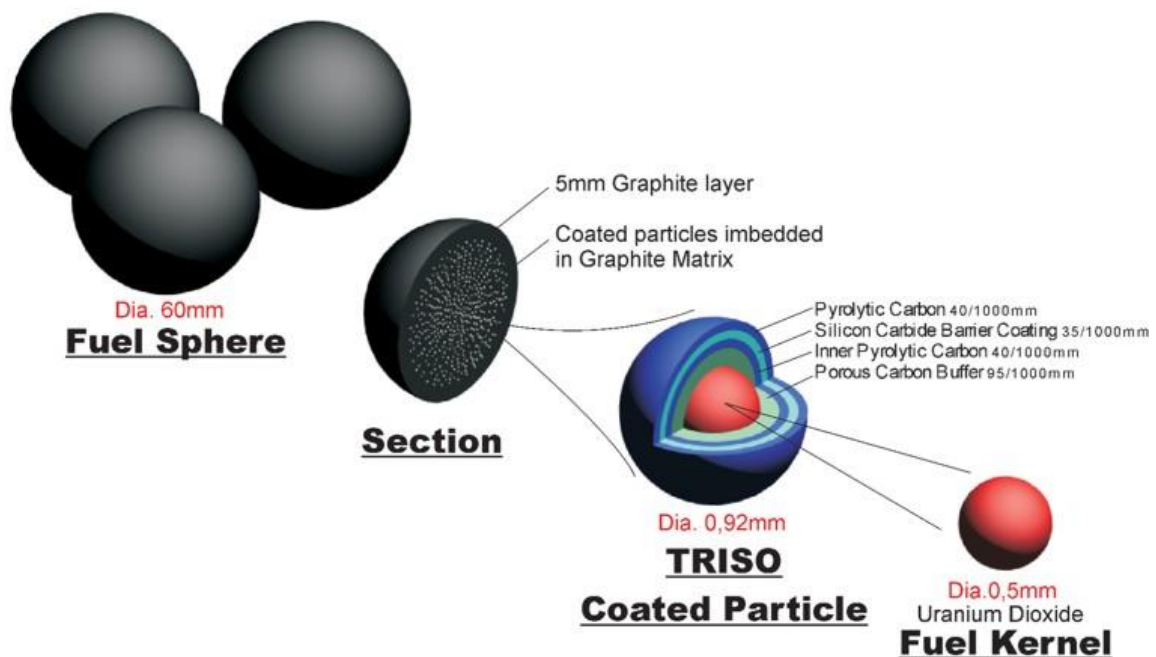


Figure 1.1: PBMR fuel sphere design, courtesy of the PBMR Fuel Design group.

Each coated particle consists of a UO_2 kernel with a nominal diameter of $500 \mu\text{m}$ and a density of 10.4 g/cm^3 . The kernel is surrounded by four different layers, namely the buffer (innermost layer), the inner pyrocarbon (IPyC), the silicon carbide (SiC) and the outer

pyrocarbon (OPyC) layers. This coated particle design is known as the Tri-structural Isotropic (TRISO) design.

1.2. Aim of this investigation

This study sought to investigate the following aspects of the burn-leach method:

1. Qualitative aspects;
2. Layer properties of TRISO particles;
3. Quantitative aspects;
4. Variants of the burn-leach method;
5. Statistical treatment of data from burn-leach.

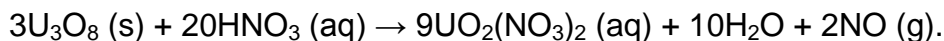
The main emphasis of this study was on the silicon carbide layer and to a lesser extent on the inner pyrolytic carbon layer. The strengths and weaknesses of the burn-leach method compared to other available alternatives were investigated.

1.3. Manufacture of UO₂ kernels

The process schematic for UO₂ kernel production is given in Figure 1.2. This process is based on the external gelation process also known as the gel-precipitation process. The feed material is uranyl nitrate solution and is prepared by dissolving fine U₃O₈ powders in nitric acid.

1.3.1. Preparation of the feed solution

The U₃O₈ feed powder is dissolved in nitric acid to form a uranyl nitrate solution according to the chemical reaction:



The uranyl nitrate solution is pre-neutralized with dilute ammonium hydroxide to just prior to precipitation of the uranium according to the following reaction:



A casting solution is prepared by adding small amounts of polyvinyl alcohol and

Tetrahydrofurfuryl alcohol to the pre-neutralized uranyl nitrate solution. These additives adjust the surface tension and viscosity to ensure proper droplet formation and also assist with later uniform shrinkage of the kernels as well as crystals growth.

1.3.2. Casting of microspheres

Casting is carried out in a glass column filled with the concentrated ammonium hydroxide precipitation solution as shown in Figure 1.3.

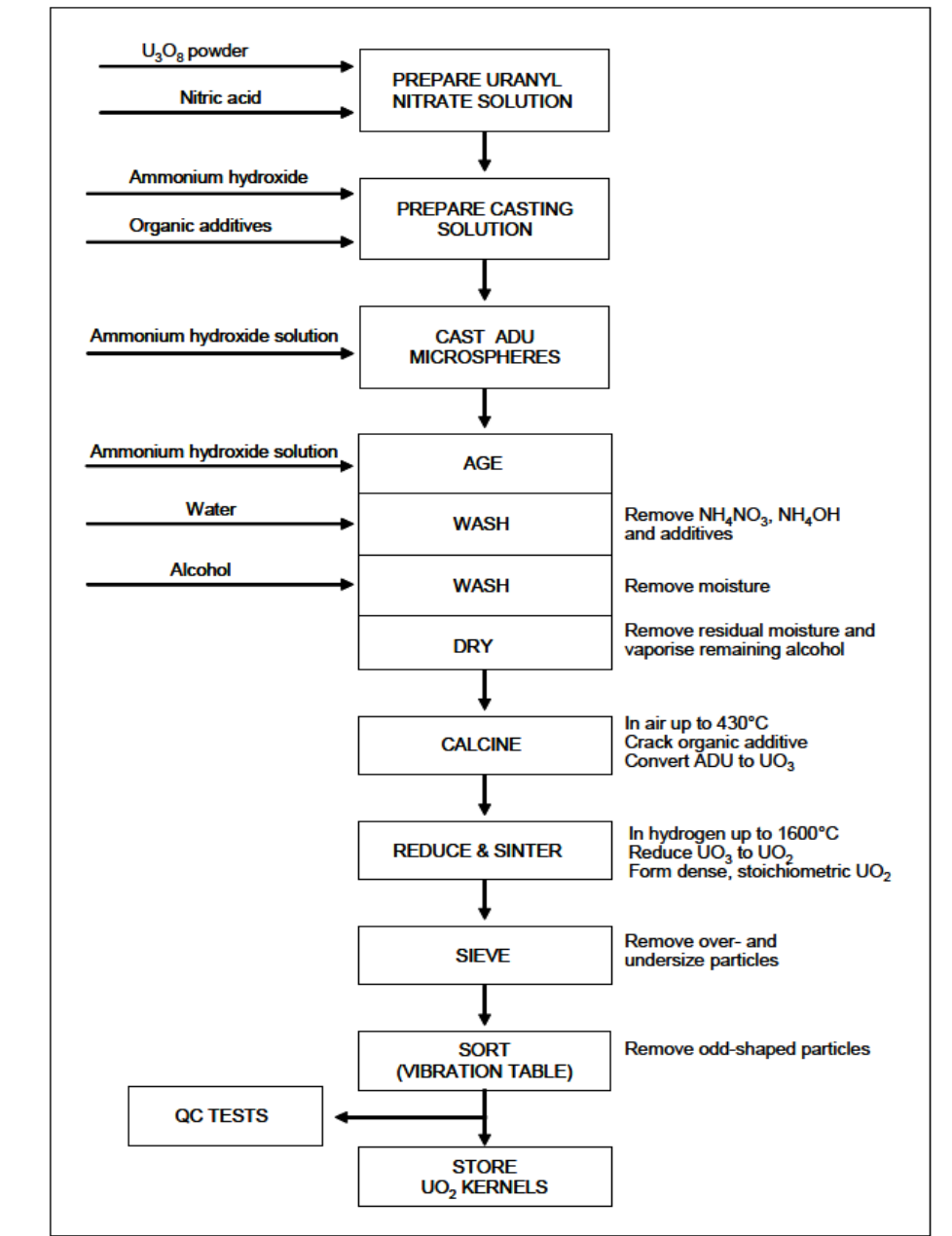
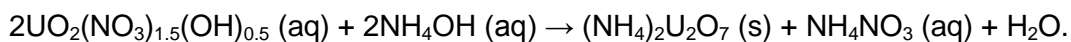


Figure 1.2: UO₂ kernel production.

The casting solution is pneumatically fed to the nozzles (typically between 4 and 6) at the top of the column, where a vibrator shakes off droplets from the feed stream at a rate of ~100 discrete droplets per second from each nozzle.

The droplets first fall a short distance through air where they attain a spherical shape as a result of surface tension. The spherical droplets then fall a further short distance through an ammonia atmosphere (ammonia gas is blown directly onto the droplets), where a chemical reaction occurs with the uranyl nitrate on the surface of the droplets. The uranyl nitrate precipitates as ammonium diuranate (ADU) in the outer layer of the droplet, forming a protective film. This protective skin enables the droplets to retain their spherical shape on impacting the precipitation solution without deforming. As the reaction continues in the casting column, ADU forms throughout the kernels, with ammonium nitrate as a by-product:



The precipitation solution is circulated from the bottom of the casting column to the top of the column via a cooled circulation line. The precipitation solution is saturated in the circulation line to ensure a high ammonia concentration at the top of the column where the chemical reaction in the droplet initiates. The precipitation solution in the casting column is also saturated by bubbling ammonia through the solution. Ammonia vapors from the casting process are scrubbed with water in a glass column filled with stainless steel rings.

The kernels are kept in the casting column until they are strong enough to be processed further. The diameter of a cast gelled sphere is about 1.8 mm (UO_2 kernels that have a final diameter of 500 μm after sintering).

1.3.3. Ageing, washing and drying

After casting, the wet kernels and the accompanying precipitation solution are transferred from the casting column to a jacketed rotary flat vessel for ageing, washing, and drying. During ageing, the vessel rotates and is heated with steam to 80°C. The ageing process fully converts the gelled spheres to solid ADU kernels, and initiates

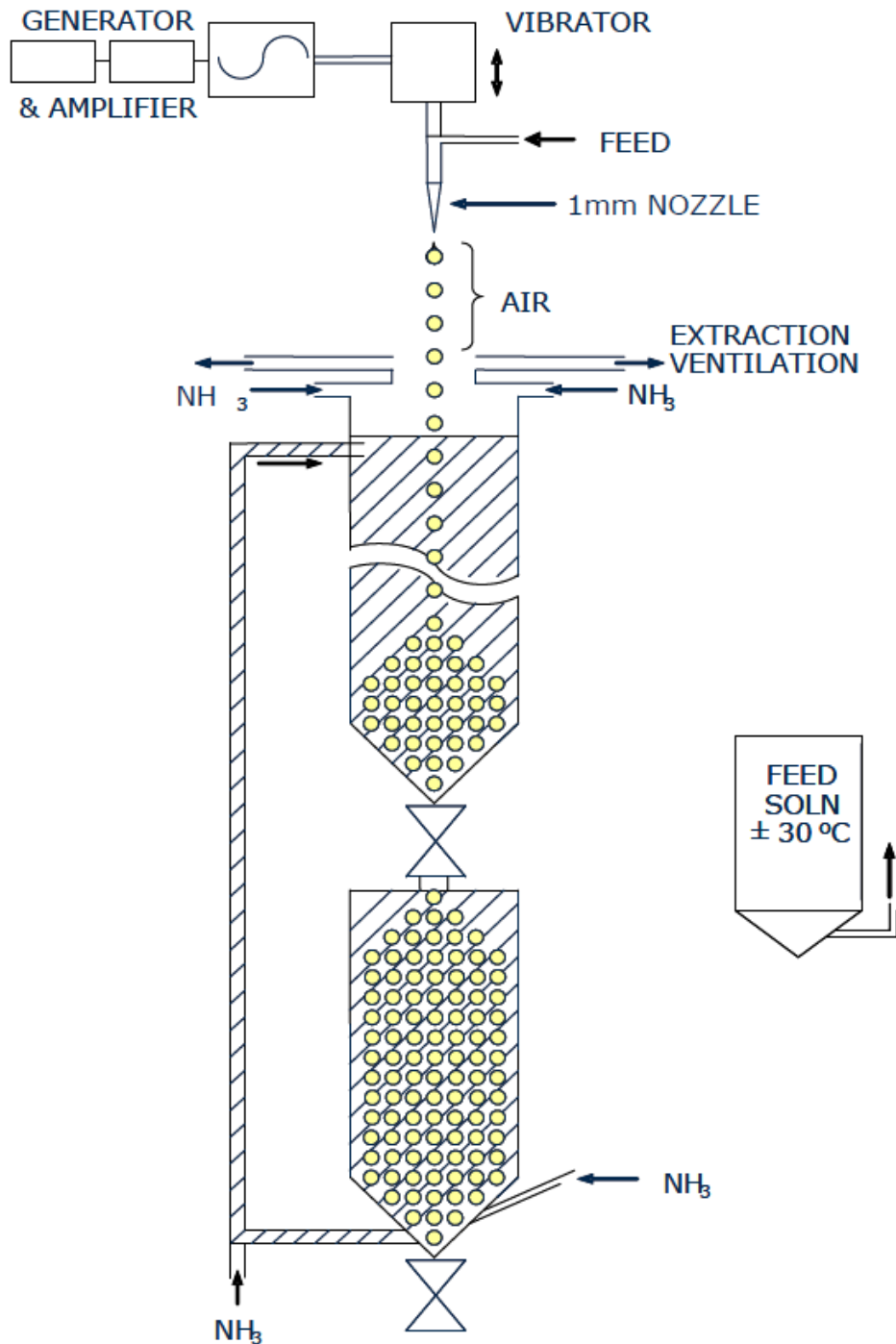


Figure 1.3: Casting process.

crystal growth in the kernels. The precipitation solution may be used as an ageing solution, or fresh diluted precipitation solution may be prepared for use as the ageing solution. Thereafter the kernels are washed with isopropyl alcohol (IPA) to remove moisture and any remaining ammonium nitrate, ammonium hydroxide and

tetrahydrofurfuryl alcohol. The final step is to dry the kernels at 80°C under vacuum at a slow rotation speed. The dried ADU kernels have a diameter of about 1 mm.

1.3.4. Calcining

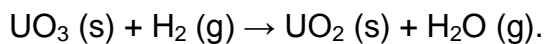
After completion of the ageing, washing, and drying processes, the ADU kernels are calcined in air up to 430°C in a batch furnace. The remaining organic additives are cracked and driven off during a gradual temperature increase. Above 300°C the ADU is converted to UO_3 according to the following reaction:



The mean diameter of a calcined kernel is about 750 μm .

1.3.5. Reduction and sintering

After calcining, reduction and sintering follows at a high temperature to reduce the UO_3 to UO_2 , to remove remaining impurities and densify the kernels. This process is carried out under a hydrogen atmosphere. The reduction step takes place between 450°C and 650°C according to:



Thereafter, the temperature is increased to 1 600 °C in order to form dense, stoichiometric UO_2 kernels that have a diameter of 500 μm and a density just below the theoretical value of 10.96 g/cm^3 .

1.3.6. Sieving and sorting

The final production steps are sieving to remove any under and over sized kernels, followed by sorting to remove any odd-shaped particles. The latter is performed on a sorting table that is slightly inclined to allow spherical kernels to roll downhill while odd-shaped particles are vibration transported along a perpendicular direction and collected for recycling. The vibration sorting is a very slow but effective method to ensure that any odd-shaped kernels are removed from the batch.

1.4. Manufacture of TRISO particles

The fundamental design for the High Temperature Gas-Cooled Reactor relies on the behaviour of the coated fuel particle at elevated temperatures. The success of gas-cooled reactors depends upon the safety and quality of TRISO-coated particles used to manufacture the final fuel, for both the fuel sphere type as pursued by the Pebble Bed Modular Reactor (PBMR) company and for the cylindrical compact type fuel as pursued in other parts of the world (Venter 2006). The TRISO particles are manufactured by a process using Chemical Vapour Deposition (CVD). The PBMR particle manufacturing process uses a spouted bed coating furnace shown in Figure 1.4. There were, however, a proportion of defective IPyC and SiC layers present during the manufacture of TRISO particles by the CVD process.

The Fuel Development Labs (FDL) facility of the PBMR is situated at Pelindaba, 30 km West of Pretoria, RSA. Most of the work in this dissertation was carried out locally at the FDL. The TRISO particles evaluated were manufactured locally within the Advanced Coater Facility (ACF) and the Research Coater Facility (RCF). The testing equipment was also locally based. The site is owned by the Nuclear Energy Corporation of South Africa and is designated for most nuclear research and technology activities. Figure 1.5 is a schematic of the CVD process for the manufacture of TRISO particles. The order starts from the top to the bottom.

1.5. Description of the Pebble Bed CVD Coater

The CVD spouted bed coating furnace consists of the reaction chamber and computer-interfaced associated equipment, ranging from vacuum pumps to instrumental measuring devices for controlling the temperature, pressure and the gas flows.

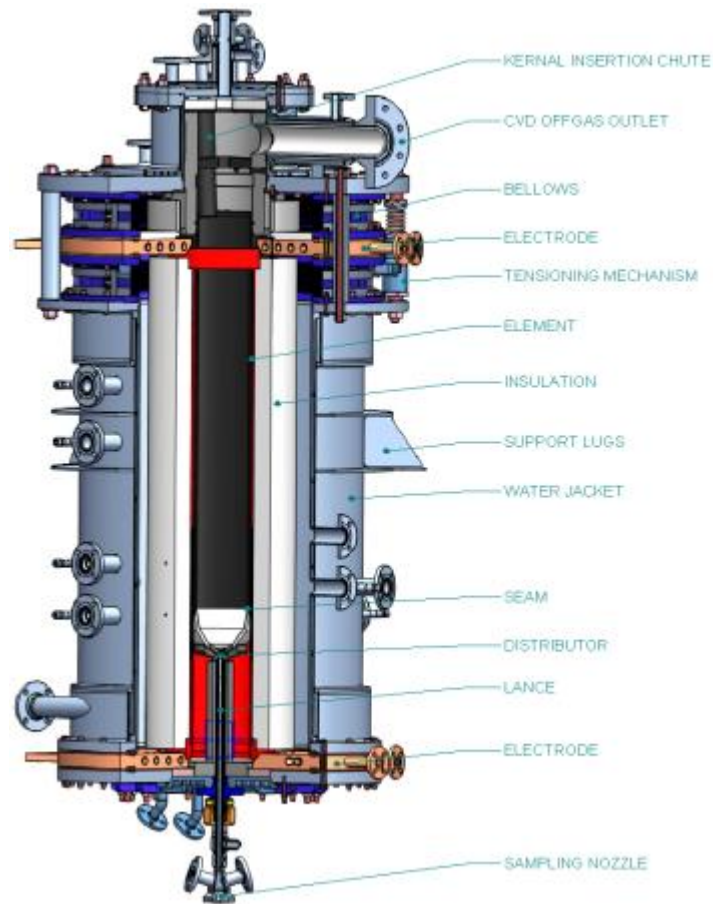


Figure 1.4: A picture of the PBMR CVD Coater, courtesy of the PBMR Advanced Coater Facility group.

The UO_2 kernels are suspended in an argon gas stream (Figure 1.5) at about $1\ 000\ ^\circ\text{C}$ by the force coming from the gas flow. The buffer layer is deposited using acetylene (C_2H_2) as the CVD precursor. The gases that are used as CVD precursors for the deposition of the inner and the outer pyrolytic carbon layers are acetylene (C_2H_2) and propylene (C_3H_6), respectively, while methyl-trichloro-silane (CH_3SiCl_3) and hydrogen (H_2) are used as CVD precursors for the deposition of the SiC layer. At the temperature of the CVD reactor these gases decompose and form agglomerates which build up on the surface of the UO_2 kernels.

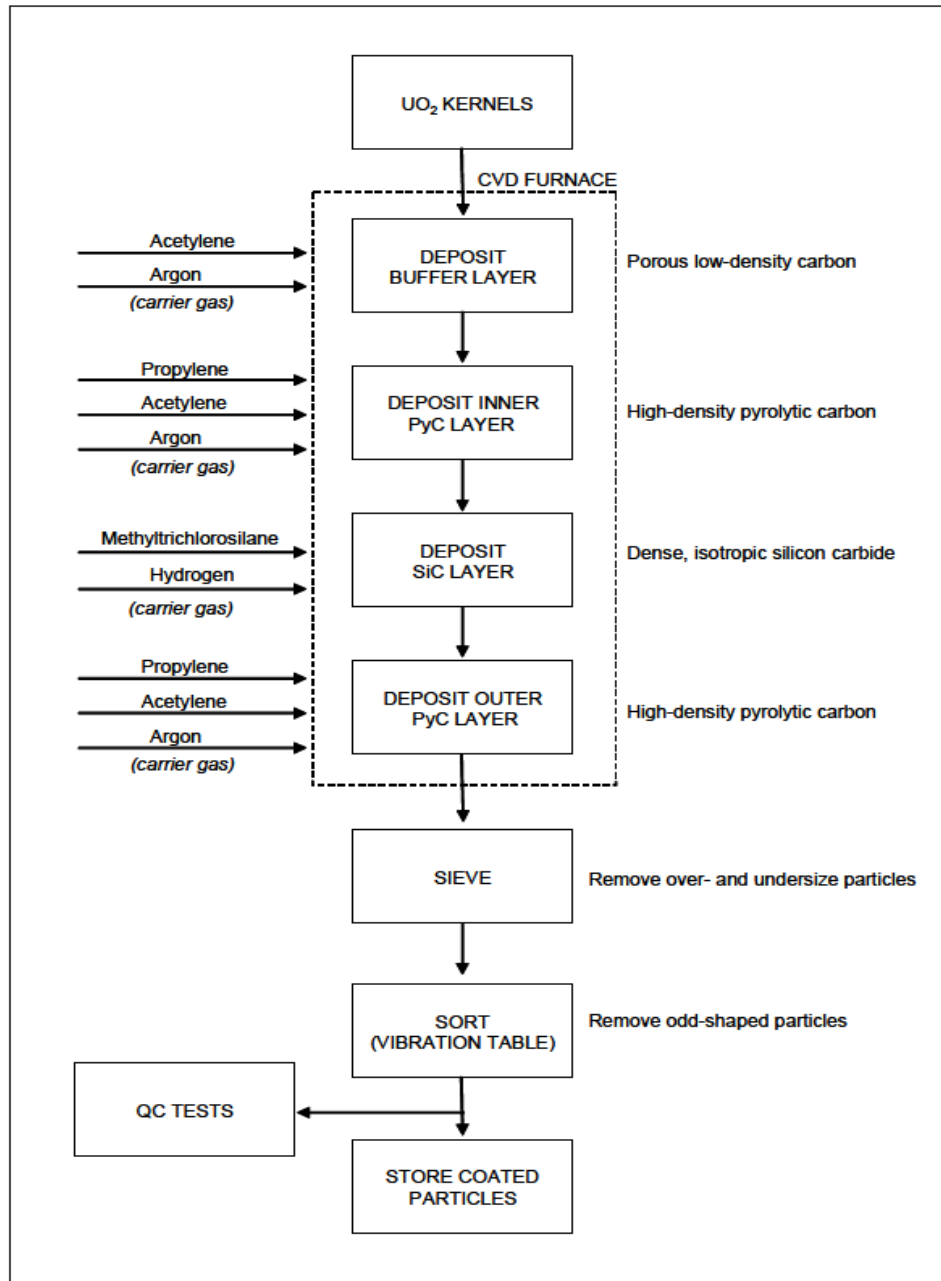
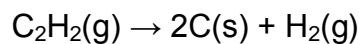


Figure 1.5: The flow diagram for the manufacture of TRISO particles.

A summary of the chemical equations depicting the CVD coating process:

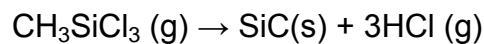
- Deposit a porous pyrocarbon (PyC) layer (the buffer layer) on the kernels by the decomposition of acetylene (C₂H₂) according to:



- Deposit an inner, dense layer of isotropic pyrocarbon (IPyC) on the porous carbon layer by the decomposition of a mixture of acetylene and propylene (C_3H_6):



- Deposit a dense, isotropic layer of SiC on the IPyC layer by the decomposition of Methyl-tri-chlorosilane (CH_3SiCl_3) according to the following reaction:



- Deposit an outer, dense layer of isotropic pyrocarbon (OPyC) on the SiC layer by the decomposition of C_2H_2 and C_3H_6 .

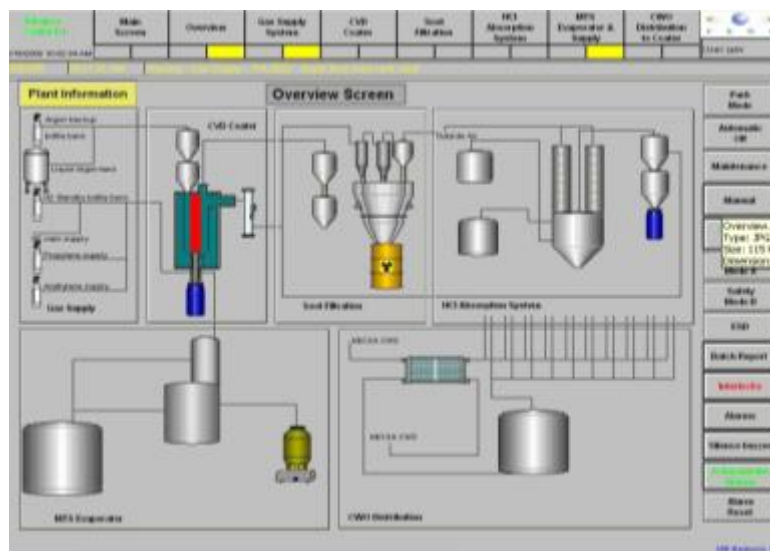


Figure 1.6: Example of the CVD process control screen, courtesy of the ACF group.

Figure 1.6 shows a snapshot of the control room computer screen of the CVD reactor.

1.6. Manufacture of fuel spheres

1.6.1. Introduction

A PBMR fuel sphere consists of two regions: a spherical fuel region of 50 mm diameter containing TRISO-coated particles, and a surrounding shell of nominal 5 mm referred to as a fuel-free zone. Both regions contain matrix graphite, which is a mixture of electro-

graphite and natural graphite glued by a phenolic resin. Good quality TRISO particles which are sieved to remove the oversize and the undersize particles are then used for the manufacture of the fuel spheres.

The fabrication process for fuel spheres was developed and improved by NUKEM, Germany and consists of the following steps (Basak 2010):

- resinated graphitic matrix powder preparation;
- overcoating of particles;
- pre-molding of fuel zone and high-pressure isostatic pressing of the complete fuel element;
- machining; and
- carbonisation at 800°C and heat treatment at 1 900-1 950°C.

1.6.2. Preparation of resinated graphite matrix powder

The matrix graphite powder (MGP) for the spherical fuel consists of approximately 64% natural graphite (NG), 16% electro-graphite (EG), and 20% phenolic resin binder. The fabrication process includes the mixing of NG and EG powders, and kneading of the graphite powders and binder, drying and milling. The manufacturing process of the graphitic matrix powder is as follows:

- NG and EG powders are mixed in a four-to-one ratio in a conical mixer.
- The mixture is fed into a kneading machine where phenolic resin binder, dissolved in alcohol, is added and the mixture is homogenised.
- The paste-like mixture is extruded through a punched screen creating strings that are cut into small pieces.
- These small pieces are placed in drying trays which are heated to approximately 100°C.
- The dried graphitic mass is transferred into a hopper that feeds a hammer mill used to grind the material into powder of the desired grain size.
- The milled powder is homogenized and ready for pressing.

1.6.3. Overcoating of TRISO coated particles

Overcoating the TRISO particles prevents direct particle-to-particle contact which may induce cracking of the particle coating layers during sphere formation. The overcoating graphitic matrix material is about 200 μm thick and is applied to TRISO coated particles already placed in a rotating drum. The overcoating dry resinated graphitic matrix material and solvent are added simultaneously into the rotating drum in order to maximize adherence and obtain a uniform thickness. Then, the moist overcoated particles are dried at about 80°C to remove any remaining solvent. The dried overcoated particles are sieved to select proper sized particles within the range of 1.1 mm and 1.5 mm. An inclined vibrating table is used to remove oddly shaped, twin, or nonspherical overcoated particles.

1.6.4. Molding and pressing of fuel spheres

The fuel spheres are manufactured by quasi-isostatic pressing at room temperature using silicon rubber molds. The pressing operation consists of taking overcoated TRISO particles together with graphite matrix powder and molding them in a pre-pressing operation to form the internal fueled zone. Additional matrix material is added to form the fuel-free shell around the fueled core using a final high pressure molding process. The sphere molding and pressing process consists of the following steps:

- Combine overcoated particles with matrix graphite powder to form the fueled zone.
- The MGP volume is carefully controlled along with the overcoated particle volume and the mixture is homogenised.
- The homogenised mixture is injected into the pre-pressing mold and pressed at approximately 5 MPa pressure.
- The pressed fuel zone spheres are then transferred into the final mold. The lower half of the final mold contains MGP. The fuel zone sphere is placed into the center and the second half of the mold is placed on top. More matrix material is added through a feeder and final pressing process is performed at about 300 Mpa pressure.

1.6.5. Lathing the elements

After pressing, the fuel spheres are transported to the lathing process where they are machined in a two step process to obtain uniform spheres with specified dimensions.

1.6.6. Carbonisation and removal of impurities

After machining, the spheres are heat-treated in two distinct processes; carbonisation and annealing. In the carbonising process, the fuel spheres are heated to 800°C in an inert argon atmosphere furnace in order to carbonise the phenolic resin binder to provide strength. The annealing process is carried out under vacuum at a temperature range between 1 900-1 950°C for one hour to eliminate residual impurities in the matrix graphite. After a cool down phase, the fuel spheres are removed for inspection.

1.7. Roles played by each layer in the performance of TRISO fuel

The innermost element of this particle is a UO_2 kernel which is coated with a low-density pyrolytic carbon (PyC) buffer layer which contains about 50% voids. The next layer is a high-density inner pyrolytic carbon (IPyC). This layer is followed by a high-density silicon carbide (SiC) layer. The outer pyrolytic carbon layer is the outermost layer of the TRISO particle.

The buffer layer has a nominal density of 1.0 g/cm^3 and performs several functions including the absorption of fission product recoils from the kernel, provides a reservoir for fission product gases, and accommodates kernel swelling without transmitting forces to the outer coatings.

The inner pyrolytic carbon layer has a nominal density equal to 1.9 g/cm^3 and is isotropic. This layer protects the UO_2 kernel from reactions with chlorine vapours during the deposition of the SiC layer. In addition, this layer provides structural stability for the SiC layer, and protects the SiC from fission products and carbon monoxide that is generated in the UO_2 kernel-buffer region during reactor operation. Carbon monoxide is generated by the reaction that occurs between the UO_2 kernel and the pyrocarbon buffer at high temperatures around $2\,000 \text{ }^\circ\text{C}$ (Ikawa *et al.*1978).

The SiC layer is a high-density layer with its nominal density equal to 3.2 g/cm^3 . It is a high strength layer which provides the TRISO particle the ability to contain the high pressure that is generated in the kernel-buffer region. It also provides the structural support to withstand the stresses that develop in the pyrolytic carbon layers due to irradiation.

The outer pyrolytic carbon layer has a nominal density of 1.9 g/cm^3 and is isotropic. This layer protects the SiC layer during the remainder of the fabrication process and provides the structural stability to the particles during irradiation.

Table 1.1 is a summary of the design characteristics of the PBMR fabricated TRISO-coated particles, and Table 1.2 gives a summary of roles played by each component of TRISO particles.

Table 1.1: Technical design requirements of PBMR fabricated TRISO particles.

Property	Units	Nominal	Actual Value	Specification Value
Buffer thickness	(μm)	95	90 ± 11	50 to 140
IPyC thickness	(μm)	40	37 ± 3	25 to 55
SiC thickness	(μm)	35	36 ± 2	25 to 45
OPyC thickness	(μm)	40	33 ± 2	25 to 55
Buffer bulk	(g/cm^3)	1	0.94 ± 0.02	≤ 1.05
IPyC density	(g/cm^3)	1.9	1.916 ± 0.012	1.8 to 2.0
SiC density	(g/cm^3)	≥ 3.18	3.204 ± 0.001	≥ 3.18
OPyC density	(g/cm^3)	1.9	1.930 ± 0.005	1.8 to 2.0
IPyC anisotropy	(BAF)	≤ 1.08	1.03 ± 0.01	≤ 1.08
OPyC anisotropy	(BAF)	≤ 1.08	1.01 ± 0.02	≤ 1.08

Because of the elevated temperatures of the advanced high temperature reactors (HTR's), the SiC layer is critical for the sufficient retention of the metallic fission products, especially the more volatile cesium (Cs) radionuclides namely Cs-134 and Cs-137.

Table 1.2: Summary of roles played by each component of TRISO particles.

Component	Function
UO ₂ kernel	<ul style="list-style-type: none"> • Contains Fuel Material; • Diffusion Barrier; • Structural Base of Particle.
Buffer	<ul style="list-style-type: none"> • Void Volume for Gaseous FP absorption; • Accommodates Kernel Swelling; • Sacrificial Layer for Fission Fragments.
IPyC	<ul style="list-style-type: none"> • Gastight Coating/Protects Kernel from Cl₂; • Diffusion Barrier for Metallic FP; • Reduces Tensile Stress on SiC.
SiC	<ul style="list-style-type: none"> • Primary metallic fission product diffusion barrier; • Primary Pressure Retaining Layer.
OPyC	<ul style="list-style-type: none"> • Gaseous fission product barrier; • Diffusion Barrier Metallic FP; • Reduces Tensile Stress on SiC; • Provides Bonding Surface for Overcoating, or Matrix Material, respectively;

CHAPTER 2

2. LITERATURE SURVEY

2.0 Preamble

Burn-leach method has until now been used as an indicator of the defective fractions in the fuel elements (Myers 1989). Some limited references about the use of this method are reported in the literature, and the alternatives to the burn-leach method are also reported. The fundamental design for a High Temperature Gas-Cooled Reactor (HTR) relies on the structural integrity of the coated particles. The most critical component of this fuel is the SiC layer, which is a ceramic material. As described earlier, the chemical vapour deposition (CVD) process was used to manufacture the TRISO-coated particles. This process produces a proportion of defective layers due to a number of limiting factors present in controlling the dynamics of the CVD process. The success of gas-cooled reactors depends upon the safety and quality of the TRISO coated particles used to manufacture the final fuel, and therefore determining the quantity of broken or cracked particles is central to predicting the expected behaviour of fuel when irradiated in the reactor (Venter 2006).

From the observations of several hundreds of TRISO coated particles by Petti and co-workers (Petti *et al.* 1986), it was determined that failures of coatings occur during:

- particle fluidization in a spouted bed by mechanical shock and chemical reactions;
- the unloading of the particles from the coater by mechanical shock;
- during the compacting processes to fabricate the final product; and
- U-235 fission reaction that induces thermal shock.

The release of the fission products into the reactor core of the PBMR under normal operating conditions depends to a large extent on the quality of fuel spheres in the core, and specifically on the amount of free uranium in the fuel spheres (Venter 2006). The free uranium is defined as all the uranium in the fuel sphere that is not covered by an intact SiC layer. This situation can arise due to the following:

- Uranium contained in the TRISO particles with damaged SiC layers;

- Uranium deposited as contamination on the outer surface of the (OPyC); and
- Natural uranium contained as an impurity in the MGP.

The free uranium fraction is the measured amount of free uranium in the fuel sphere expressed as the fraction of total uranium of the fuel sphere. In this study, the ICP-MS was used for the quantitative determination of the uncontained uranium in the solutions that came from the burn-leached samples. The following section outlines a summary of the available literature in this field.

2.1. Burn-leach method

A burn-leach procedure that was employed at the HOBEG fuel manufacturing company in Germany entailed the following (Myers 1989): the spherical fuel spheres were oxidized at 750 °C for 100 hours to remove the carbonaceous material exterior to the SiC layer. The oxidized particles were placed in 6 M HNO₃ and refluxed at a temperature of 95 °C for 16 hours. The special precautions that were taken to ensure a complete leach of the uranium from the particles were: (1) the leach step was repeated if the results of the burn leach method did not yield a positive integer number of kernels i.e. 1, 2 or 3 defective particles; and (2) particles with defective SiC coatings were separated from those having intact SiC coatings on the basis of the density difference by using methylene iodide. The particles that did not have kernels or buffer or IPyC layers would float in methylene iodide due to their lower density, and these particles would be cleaned and radiographed for any uranium remnants. Although this method was reported to be well controlled, some workers elsewhere believed that more work needed to be performed to establish the true efficiency of the burn-leach method (Myers 1986).

Adam and co-workers believed that the burn leach method was not able to extract all the uranium within a reasonable time when the small nanometre size cracks were present in the SiC layers (Adams and Partain 1987). They drilled holes ranging between 10 µm and 52 µm with a laser on loose TRISO-coated particles and observed that the uranium did not readily leach when in contact with the acid medium. At the worst, a leached particle with a 22 µm hole resulted in a recovery of only 82% of the uranium. Another worker, Layton, believed that leaching of uranium was ineffective when cracks in the SiC layer were smaller than 90 nm (Layton 1978).

These authors concluded that the burn-leach method only extracted the heavy metal from a subset of defective TRISO particles. This implied that an under-estimation of the number of failed TRISO particles was certain to occur under these conditions.

2.2. Mercury intrusion method

The detection of micro-cracks in the SiC layer was investigated by high pressure mercury intrusion up to 69 MPa (Goodin 1985). This in turn could help in relating the metallic and gaseous fission product released to the level of the defective SiC layers and could be used as a comparative method to the burn-leach method. Other investigators performed some work on the intrusion method using halogenated hydrocarbons such as methylene iodide or tribromo-methane instead of mercury and had mixed successes (Adams 1983, Cohen 1982, Goodin and Nabelek 1985). The gaseous fission product released during the irradiation was shown to be more accurately predicted when the fraction of the defective SiC layers as determined by the mercury intrusion was taken into account.

The suggested improvement in the detection of the cracked SiC shells by the mercury impregnation method was reported (Kovacs 1981). After acid washing, particles were X-rayed. Cracked shells were identified by viewing the radiographs through a microscope. Mercury impregnation method, while a considerable advancement over the burn-leach method, has some shortcomings. In use, mercury becomes dirty and smears over the particles causing them to adhere to one another. The test is relatively slow because of the need to apply the mercury under pressure and there is an additional requirement of acid washing of the particles. This test has some practical limitations with regard to the sample sizes since the largest sample holder in a mercury porosimeter has a capacity of about 10 000 particles, and yet several tens of thousands are analysed by burn-leach method.

2.3. Chlorine gas method

Other tests, involving the use of chlorine gas, have been suggested for determining the existence of cracks in a carbon coating (Kovacs 1981). A recently proposed test for determining the existence of cracks in the outer carbon coating covering the silicon carbide shell involves subjecting the outer carbon coating to a substantially pure chlorine gas atmosphere at an elevated temperature for an extended period. Radiographing the

treated particles to determine the density changes in the silicon carbide shell indicates the chemical adsorption between the chlorine gas and the silicon carbide due to the cracked outer carbon coatings. However, it is not clear whether this method will see small changes to the SiC given that the product of the chlorination reaction is either Si-Cl_x or Si-OH and the fact that attenuation of X-rays with the different products would be quite small versus SiC.

2.4. Leach-burn-leach method

This method consists of leaching the fuel compact with an acidic solution, oxidizing the compact and leaching again (Myers 1989, Goodin 1985). The first leach extracts the exposed UO₂ kernels and the uranium contamination on the compact. During the burn step, if there is a cracked SiC layer, the buffer, IPyC and OPyC layers are oxidized and removed. The second leaching step facilitates the extraction of the uranium from the failed particles. This method is currently used by the quality control laboratories such as the Oak Ridge National Lab in the United States of America. The two leach steps are identical except that, after the first leach and before oxidation by burning, the TRISO particles are dried overnight at 100 °C. The procedure followed:

- About 15 to 20 fuel cylindrical compacts with dimensions 25 mm height and 10 mm width are placed in a 600 ml quartz beaker and placed in a standing position on the bottom of the beaker. This assembly is then placed inside a 0.28 m³ muffle furnace.
- Air at 0.17 MPa and 27 °C flowing at 2 700 cm³/min is fed onto the furnace held at 750 °C.
- After 50 to 60 hours the compacts are radiographically evaluated to check for remnants of pyrolytic carbon and should such are found, oxidation is continued.
- The particles that are devoid of the OPyC layer are then placed on an Erlenmeyer flask together with 100 mL of acid leach solution made of 1 720 mL concentrated nitric acid, 240 mL H₂O and 2 mL HF.
- The content of the flask is heated at 109 °C and the liquid is refluxed for 24 hours.
- The liquid is then decanted, another 100 mL of leach solution added and again the liquid refluxed for 24 hours.
- The liquids are evaporated to dryness and taken up in 1 M HNO₃ and then measured using ICP-MS.

2.5. Gaseous acid leach method

The gaseous leach technique has been shown to be an effective method for removing the exposed heavy metal from the manufactured fuel compacts (Adams and Partain 1987). The heavy metal includes matrix contamination plus exposed fuel kernels that result from particles broken during the mould injection step of the fuel sphere fabrication process. The determination of the defective TRISO-coated particles with currently available methods depends on the accessibility of uranium oxide by the liquid or gas media being used for the extraction. The extent to which the particles have failed is determined by the amount of the uranium leached by the reactive liquids. It is worth noting that particles with missing buffer layers are not distinguished by the existing methods and these particles have a high probability of failure in the reactor. Below follows a brief review of the chemistry of uranium.

2.6. Organic chemistry of uranium

Spencer and co-workers have investigated the production of organic acids (e.g., carboxylic acids) from the reaction of nitric acid with the metal carbide and buffer carbon. These studies were conducted in order to establish the effect of the organic acids on the solvent extraction process of uranium in defective TRISO-coated particles (Spencer 1982). Their study indicated the formation of organic acids, and also the calculated distribution coefficients confirmed that uranium distributed itself between the aqueous and the organic phases during the dissolution process. It was not clear whether this distribution was significant enough to affect the uranium recovery during the burn-leach analysis.

2.7. Thermal degradation of fuel spheres and TRISO particles

Fresh TRISO particles and fuel spheres undergo oxidation at 750 °C during burn-leach testing. The burn step is necessary to remove the outer pyrolytic carbon of fresh TRISO particles (Neter *et al.* 1982), and the graphite matrix is removed from the fuel spheres at this temperature before leaching of uranium from the defective OPyC denuded particles is performed. The understanding of the three-component system U-C-O involved in the kernel/pyrolytic carbon oxidation during the burn-leach analysis is necessary. Knowledge of the thermodynamics and more-over of pressure laws in the U-C-O system is a

necessary reference to understand the thermo-mechanical strength of the TRISO particles.

2.8. High temperature chemistry of SiC

The oxidation behaviour of *bi*-directional silicon carbide-based composites was studied in the temperature range from 900-1200 °C under an oxygen pressure equal to 1kPa Ehrburger and Vix-Guterl (1996). The composite consisted of silicon-based fibers, separated from the SiC matrix by a pyrolytic carbon layer SiC/C/SiC. Oxidation was carried out by a volumetric technique with a mass spectrometer for the analysis of the gaseous phase. The change in morphology of the composite after exposure to oxygen was followed by scanning electron microscopy on polished sections of the external and the internal parts of the samples. Vix-Guterl and co-workers found that two main phenomena occur during oxidation: the carbon interlayer is gasified resulting in the formation of annular cavities around the fibers whereas the SiC-based fibers and SiC matrix are oxidised leading to the formation of silica layers. Although burn-leach tests are carried out at a lower temperature of 750 °C, these findings are still relevant since the components used in this study were chemically close to the components used in the manufacture of the layers of TRISO particles. In addition, fuel spheres are carbonised at 800 °C and later heat treated at a temperature range of 1 900-1 950 °C.

Other workers (Kleykamp *et. al* 1995) investigated the oxidation behaviour of one-dimensional and two-dimensional SiC fibre-reinforced SiC up to 1 520 °C in air, as well as in water vapour saturated air and argon by calorimetry, DTA and TGA. They found that the the oxidation process takes place in three steps: (1) oxidation of free carbon in the carbon coated composites between 530 and 690°C with mass losses up to 7.5%; (2) a fast exothermal process associated with mass gain starting at 800°C and terminated below 1500°C within 1 h; (3) the diffusion controlled oxidation of bulk SiC. The processes were found to follow a logarithmic rate law between 875 and 985 °C with an effective activation energy $Q = 84$ kJ/mol. The amorphous reaction product SiO₂ transforms to cristobalite at (930 ± 50) °C. The oxidation kinetics were found to follow a quadratic rate law above 1 000°C with rate constants $k = 3.5 \times 10^{-7} \text{g}^2/\text{cm}^4\text{h}$ for 1D SiC/SiC and $k = 5 \times 10^{-8} \text{g}^2/\text{cm}^4\text{h}$ for 2D SiC/SiC at 1 520 °C in air. The rate constants are up to three orders of magnitude higher than that for high density monolithic SiC.

2.9. Reactivity of SiC

Effect of thermal treatment on the reactivity of SiC-based fibres was investigated (Ehrburger 1996). The evolution of the chemical composition of the outer layer of SiC-based fibres was studied under different conditions of temperature and gas environment. After heating the fibres under vacuum or in argon at 1270, 1470, and 1570 K, their reactivity was determined with molecular oxygen at 1170 K and their surface composition was analysed by X-ray photoelectron spectroscopy. Treatment under a vacuum led to severe degradation of the fibres due to chemical reactions between SiC, SiO₂ and carbon. As a result, the silica layer initially present at the surface of the fibre disappeared and an oxygen-deficient silica compound was formed. On the contrary, the formation of silica at the fibre surface was observed during the treatment in argon and the chemical changes were more limited. This work is relevant to our study because the SiC of TRISO particles is ultimately exposed to molecular oxygen under convection during the burn step of burn-leach test. The burn-leach test must ensure that the deficiency of oxygen is prevented at all times during the test. It must be ensured in this study that burn-leach method does create defects that were not there prior to testing.

Other workers (Asha *et. al* 2007) studied ceramic matrix composites (CMCs) as potential structural materials for application of high temperature technologies. Excellent high temperature performance of CMCs requires that fibers must have high enough thermal stability and sufficient mechanical properties throughout the service life. In order to clarify the correlation between the mechanical properties and the microstructure of SiC-based fibers, SiC-based fibers were annealed at elevated temperatures in Ar for 1 h. After annealing, the fracture strengths on these fibers were evaluated at room temperature by tensile test; the microstructural features were characterized by X-ray diffraction (XRD) and field emission scanning electron microscopy (FE-SEM). Furthermore, the fracture mechanics was applied to estimate the fracture toughness and the critical fracture energy of these fibers. They found that excellent microstructure and mechanical stabilities were observed for SiC fibers with near-stoichiometric composition and high-crystallite structure. Combining the microstructure examination with tensile test indicated that the thermal and mechanical stabilities of SiC fibers at high temperatures were mainly controlled by their crystallization and composition.

High-temperature properties of silicon carbide prepared by chemical vapor deposition (CVD) are superior to those of normally sintered and hot-pressed SiC when the structure, characteristics and uses of CVD SiC were reviewed (Hirai *et al.* 1991).

The nature of grain boundaries in pressureless sintered SiC with and without sintering aids was studied in connection with the absence and presence of strength loss at high temperatures (Kurishita *et al.* 1991). They attributed the absence of strength loss to the occurrence of an 'extended grain boundary', whereas the remarkable loss in strength was due to the existence of an amorphous-like second phase at the grain boundaries. This extended grain boundary was not of a special phase but simply of a relaxed structure with some extension, and is most likely composed mainly of SiC itself. It was shown that the concept of extended grain boundaries could explain the observed behaviour in SiC.

2.10. Summary

The available references on the integrity of the TRISO particle layers were outlined. The leaching of the uranium from the defective coatings was reported in the various studies using different methodologies. This research project selected the burn-leach method for the investigation of the integrity of the TRISO particle layers because this method had the added advantage of evaluating thousands of particles in one analysis, and the presence of the defective layers was indicated by the dissolution of uranium in an acidic medium. Also, this method was well-suited to test the pebble bed type fuel because the oxidation step of the burn-leach method reduced the large 60 mm diameter fuel sphere into a manageable remnant in a form suitable to be leached in acid. Not only does this method detect broken/cracked coatings, but it also determines the uncontained uranium coming from the outside of the silicon carbide layer. This contamination usually emanates from the feed material that is used to manufacture the MGP.

CHAPTER 3

3. STATISTICAL TOOLS

3.1. Determination of layer thickness values

The equations that were used in the results section to compute the descriptive statistics of the TRISO particle layer properties are listed below (Neter *et al.* 1982).

$$\bar{X} = \frac{1}{N} \sum_{i=1}^N X_i \quad (1), \text{ Mean value.}$$

$$\sigma^2 = \frac{1}{(N-1)} \sum_{i=1}^N (X_i - \bar{X})^2 \quad (2), \text{ Variance.}$$

$$\sigma = \sqrt{\sigma^2} \quad (3), \text{ Standard deviation.}$$

$$S = \frac{\sum_{i=1}^N (X_i - \bar{X})^3}{(N-1)\sigma^3} \quad (4), \text{ Skewness.}$$

$$C.L. = \bar{X} \pm \frac{ts}{\sqrt{N}} \quad (5), \text{ Confidence Level.}$$

Definitions:

Equation (1): The mean is that value that is most commonly referred to as the average. The mean is the sum of the data points divided by the number of data points.

Equation (2): The variance is the arithmetic average of the squared distance from the mean. Although the variance is intended to be an overall measure of spread, it can be greatly affected by the outlying data points.

Equation (3): The standard deviation is the square root of the variance.

Equation (4): Skewness is a measure of symmetry, or more precisely, the lack of symmetry. A distribution, or data set, is symmetric if it looks the same to the left and right of the centre point.

Equation (5): Confidence limits are limits within which we expect a given population parameter, such as the mean, to lie. Confidence intervals shrink towards zero as the sample size N increases.

3.2. Analysis of variance (ANOVA) in layer thickness values

In statistics, analysis of variance (ANOVA) is a collection of statistical models, and their associated procedures, in which the observed variance in a particular variable is partitioned into components attributable to different sources of variation. In its simplest form ANOVA provides a statistical test of whether or not the means of several groups are all equal, and therefore generalises the t -test to more than two groups.

In this study this test was applied to determine whether the measured layer thickness values of the SiC and the inner pyrolytic carbon were significantly different from each other based on different CVD runs. This information was then correlated with the burn-leach test results to see if there were any trends that could be established.

3.3. Determination of the failure fraction of TRISO-coated particles

It is possible to determine the number of failed TRISO-coated particles in a fresh fuel by means of the destructive burn-leach test. The two important characteristics of fresh fuel can be obtained from the results of burn-leach tests:

- The coated particle failure fraction
- The average number of failed coated particles per fuel sphere

There are two probability distributions that are employed in the determination of the failure fraction in the fresh fuel which are the Binomial and the Poisson distributions.

The Binomial distribution describes processes with a given number of identical trials with only two possible outcomes. In a burn-leach test a large number of coated particles are tested and there are only two possible outcomes: a coated particle can be cracked/broken or it can be intact. Thus binomial statistics can be used to describe the results of a burn-leach test on a sample of coated particles.

During one of the stages in the PBMR fuel manufacturing process a large number of coated particles are mixed with matrix graphite and pressed to form a fuel sphere. It is inevitable that a small number of coated particles will be damaged in the pressing process. The final Quality Control (QC) test on finished fuel spheres is the burn-leach test that measures all uranium in a fuel sphere that is not covered by an intact SiC layer. This includes coated particles with failed SiC layers, enriched uranium contamination on the outside of the outer PyC layer, and natural uranium contamination of the matrix graphite. Provided that the contamination level is kept low it is also possible to determine the actual number of failed coated particles present in a fuel sphere from a burn-leach test. Unfortunately the burn-leach test is a destructive test with the result that only a few fuel spheres from each lot can be tested using this method. One is thus faced with the problem of finding the expected number of failed coated particles per fuel sphere of a large population from the results of a limited sample taken from the population.

Suppose the number of failed coated particles per fuel sphere is determined for a large number of fuel spheres and a normalised frequency distribution is generated from the results showing the frequency distribution for the occurrence of 0, 1, 2, failed coated particles per fuel sphere. From such a distribution one could find the average number of

failed coated particles per fuel element without actually knowing the number of tests that were performed in order to generate the frequency distribution diagram. Such a distribution is described by the Poisson probability equation, provided that the average value is small. The Binomial and Poisson distributions are generally available in most software packages. Microsoft Xcel was used in this study for the computations.

Binomial distribution:

$$P(X = k) = \binom{n}{k} p^k (1 - p)^{n-k}$$

$P(X=k)$ = probability of obtaining k successes out of n trials, each of which has a probability p of success,

X = random variable taking on discrete values $k = 0, 1, 2,$

n = total number particles in the tested sample,

k = number of successes,

p = probability of success in a single trial,

$(1-p)$ = probability of failure in a single trial.

Poisson distribution:

$$P(X = k) = e^{-\lambda} \frac{\lambda^k}{k!}$$

$$P(X = k) = e^{-np} \frac{(np)^k}{k!}$$

$P(X=k)$ = probability of obtaining k events if the mean expected number is λ ,

X = random variable taking on discrete values $k = 0, 1, 2, \dots,$

λ = mean number of events,

n = total number particles in the tested sample,

p = probability of success in a single trial,

k = number of successes.

3.4. Calculation of the 95% Poisson confidence level

When an experiment has two possible outcomes, the results are expressed as a proportion. Out of N burn-leach experiments, an outcome is observed (termed "failure") in F experiments and the alternative outcome in $N-F$ experiments. Failure occurs in F/N of the experiments when a failed TRISO particle is observed, and that proportion is called p (Venter 2006). Since the data are subject to random sampling, the true proportion of failure in the overall population is almost certainly not p . According to Agresti and Coull (1996) a 95% confidence interval quantifies the uncertainty. One can be 95% sure the overall proportion of success is within the confidence interval.

To compute the 95% confidence level for the Poisson distribution of failed coated particles in fuel spheres, the following equations are employed in chapter five:

$$p = (\text{number of failures} + 2) / (\text{number of experiments} + 4) = \frac{F + 2}{N + 4}$$

$$p - 1.96 \cdot \sqrt{\frac{p(1-p)}{N+4}} \text{ to } p + 1.96 \cdot \sqrt{\frac{p(1-p)}{N+4}}$$

3.5. Sampling statistics of TRISO particles

The acceptance sampling is an inspection procedure to decide whether to accept or reject a specific quantity of material based on test results (Krajewski and Ritzman 1985). Burn-leach testing attempts to achieve such by rejecting a population of TRISO particles or accepting a population of TRISO particles based on the quality and the integrity of layers of fresh discrete TRISO particles. The two levels were considered in the design of sampling plans for this study:

The first level was the acceptable quality level (AQL), the quality level desired by the fuel sphere pressing laboratory (consumer). For the TRISO particles, the AQL was 1

defective particle in 100 000 particles or an AQL of 0.00001. The producer's risk (α), which was the risk inherent to the Advance Coater facility, was the risk that the sampling plan would fail to verify the lot's quality, and thus would reject it.

The second level was the lot tolerance proportion defective (*LTPD*), the worst level of quality that the consumer could tolerate. The probability of accepting a population with *LTPD* quality was the consumer's risk (β). There are three most common types of sampling plans: single, double and multiple.

- Single sampling plan: A single sampling plan is the decision rule to accept or reject a population based on results of one random sample from the population. The procedure is to take a random sample of size (n) and to inspect each item.
- Double sampling plan: After the first sample is tested, there are three possibilities
 - Accept the lot
 - Reject the lot
 - No decision

If the outcome is "No decision", and the second sample is taken, the procedure is to combine the results of both samples and make a final decision based on that information.

- Multiple sampling plans: This is an extension of the double sampling plans where more than two samples are needed to reach a conclusion. The advantage of multiple sampling is smaller sample sizes.

This investigation employed multiple sampling to reduce the risk of failing to determine broken/cracked particles in a given population. For this dissertation, the acceptance sampling design was computed and the operating characteristic (*OC*) curves were computed to justify the choice of sample sizes employed for the burn-leach testing of the TRISO particles. This design also revealed that very large sample sizes needed to be taken to reduce the risk of accepting a population which did not meet the specification using the burn-leach method. It was clear that quantifying the defective fraction of the SiC layers accurately was the biggest risk in the characterisation of the HTR fuel as shown by the characterisation curves that were computed.

The sampling distribution to detect a failed particle in a sample is the Binomial distribution because each sample of the TRISO particles inspected either contained a defective (failure) particle or not (success). The probability of accepting a population of TRISO particles equals the probability of taking a sample of size n from a population with a proportion defective of p and finding c or fewer defective TRISO particles. However, should n be greater than 20 and the proportion defective p was less than 0.05, the Poisson distribution approximated the Binomial distribution to take advantage of the tables prepared for the purpose of drawing the OC curves. To draw up the OC curves, this investigation looked up the probability of accepting the population for a range of values of p . The following procedure was followed, for each value of p (the defective proportion):

- multiply p by the sample size n
- find the value of np in the left column of the table (see Appendix B)
- move to the right until a value corresponding to c is found
- record the value for the probability of acceptance P_a

$$P(x \leq c) = \sum_{x=0}^{x=c} e^{-\lambda} \frac{\lambda^x}{x!}$$

When $P = AQL$, the producer's risk, α , equals 1 minus the probability of acceptance.

When $P = LTPD$, the consumer's risk, β , equals the probability of acceptance.

CHAPTER 4

4. EXPERIMENTAL

4.1. Qualitative aspects of the BL test

4.1.1. Density difference method for the broken SiC layers

In this experiment, the TRISO particles which were exposed to the burn-leach test were later submerged in the *di*-iodomethane organic solvent. The purpose of this was to suspend the broken SiC shards on the surface of the solvent. In this way an estimate of the number of TRISO particles with broken SiC shells was determined since the density of the solvent of 3.5 g/cm³ was greater than the nominal density of 3.2 g/cm³ of the SiC shards.

The resulting SiC shards were evaluated under the optical microscope to count the broken shells of the SiC layer equivalent to the discrete number of failed TRISO particles. This methodology was used to study the relationship between the quantitative analytical results from the ICP-MS and the qualitative counting of the SiC shards.

4.2. Characterisation of TRISO particles

4.2.1. Introduction

Single runs of the PBMR Advanced Coater Facility produced a total of 10 kg of TRISO particles in each campaign. These populations were then sieved to be within 800 - 1 000 µm thereby eliminating both the undersized and the oversized TRISO particles. A nominal diameter of around 920 µm was targetted. Once this was performed the remainder of the product was tabled on a vibration sorting table to eliminate Odd shaped particles. The Odd shaped particles refer to non-spherical TRISO particles, twins, triplets and other particles that were attached together in the fluidised bed and came out as agglomerates. The remaining population of near spherical particles amounted to just over 8 kg TRISO particles for each campaign. These TRISO particle batches were then homogenised and riffled for the characterisation experiments. This was achieved by using two different rifflers in a sequential fashion, starting with the rotary 8-way riffler followed by a 30-way riffler. During this study, 250 g batches of TRISO particles were sampled for each of the populations that were investigated.

4.2.2. Determination of the layer thicknesses of TRISO particles

After the homogenisation and the riffing, the particles were ground and polished for the measurement of layer thickness values for the buffer, the inner pyrolytic carbon, the silicon carbide and the outer pyrolytic carbon layers. Metallographic sections were prepared using the equipment listed in Appendix A. Using a clear acrylic, particles were mounted on a grid. The grid was ground fine with 1 200 μm SiC until kernels were exposed. They were then backpotted with fluorescent epoxy to immobilise them. They were then ground to near midplane with 1 200 μm SiC and polished prior to measurement.

From ten ACF runs, a total of 4 000 particles were measured to determine layer thickness values. From these batches 1 000 particles for each layer were evaluated. From these measurements, the statistical distributions of the layer thickness values were established and the resulting descriptive statistics computed. This effort aimed at ensuring that particles which were exposed to the burn-leach test were of acceptable integrity with layer thickness values that met the design specifications.

4.2.3. Determination of the total uranium content of TRISO particle batches

The uranium content or uranium loading of the TRISO particles is the most critical attribute that requires careful control for the successful irradiation performance of fuel. This attribute was determined gravimetrically by crushing the TRISO-coated particles using a ring mill and dissolving the uranium in them in nitric acid. The steps involved in the uranium content determination were as follows:

- 8 g TRISO particles were crushed into fragments.
- The carbonaceous components were oxidized at 750 °C in a furnace for 16 hours. Air flow was through a little hole in the front door of the furnace (convection).
- The remnants were dissolved in 6 M HNO_3 and refluxed at boiling point in acid for 16 hours.
- The shards from the SiC layer were filtered and the remaining uranium solution evaporated until dryness in a hot water bath.
- Total uranium content of TRISO particles was determined gravimetrically.

4.2.4. Density determination: Buffer, IPyC, SiC and OPyC

These attributes were tested by the gradient density column (or sink-float). This test aimed at ensuring that particles which were exposed to the burn-leach test were of acceptable integrity as summarised in Table 1.1 of chapter 1. Two different columns were prepared in-house: one column had a density range of 1.5 – 2.0 g/cm³ for the pyrolytic carbon layers, while the other column had a density range of 2.95 – 3.25 g/cm³ for the SiC layer.

A 100 mL burette with a round bottom was used for the establishment of the gradient density column. The grading increment on the burette was 0.2 mL. The vertical standing burette was filled with liquid mixtures, starting with the highest and ending with the lowest density. This resulted in a column consisting of sections of liquid of different densities. An acceptable fill rate to produce a column with satisfactory properties was found to be < 2 mL/s. The burette was sealed with a stopper and tilted at an angle of < 25° from the horizontal. The burette was then rotated in a mechanical mixing facility around its own axis for approximately 10 seconds, which affected some mixing at the boundaries between the liquid layers. This is a critical step for achieving the sensitivity and the linearity of the column. In the upright burette a relatively smooth density gradient was developed, increasing from the top to the bottom.

Standards of known density were then inserted in the column and allowed to distribute themselves according to their respective densities (approximately 20 minutes) before being read off the scale of the burette. The test pieces and the standards were wetted before they were inserted into the column to prevent adhesion of the air bubbles which could influence the reading. Due to the nature of the column, with mixtures of fluids at different densities, effects such as turbulence, vibration, diffusion and stirring as a result of the sample motion can in principle destroy the density gradient with time. It was however found that if the column was properly prepared, it was robust and stable for at least a week under normal conditions of use. The temperature effects were not studied in detail, as the measurement was performed in an environmentally controlled area. However, the temperature deviations of ± 2°C from the norm had no statistically significant influence on the results obtained.

Standards in the ranges of interest which were small enough to fit into the column without interfering with other standards and test pieces could not be sourced commercially. Standards for a high density column were prepared by mixing teflon powder with copper powder in different ratios and pressing them into cylinders. The low density standards were prepared by the glass blower by preparing hollow spheres. The densities of both sets of standards were carefully and accurately determined by means of the Archimedes method. It is important to consider a possible change in density with time as a result of corrosion or deposition processes. The OPyC layer test pieces were obtained by lightly cracking a number of TRISO-coated particles in a controlled manner. This resulted in the OPyC layer being separated from the SiC layer and test pieces were selected under a microscope. The IPyC layer test pieces were obtained in the same manner using particles coated with only the buffer and the IPyC layers. In some cases, it has proven impossible to separate the buffer and the IPyC layers and in others, a large number of particles needed to be cracked to obtain enough IPyC test pieces. Once the SiC layer had been deposited, it was not possible to separate the IPyC layer. To obtain the SiC layer test pieces, particles coated up to the SiC layer were cracked, placed in a furnace for at least 3 hours at ~ 750 °C, and the test pieces were selected under the microscope.

The chemicals that were used to make up the columns were bromoform and di-iodomethane. For each layer a minimum of 15 fragments were measured at their scale position in the gradient density column and their density values determined using the equation:

$$\frac{\rho_s - \rho_2}{x_s - x_2} = \frac{\rho_3 - \rho_2}{x_3 - x_2}$$

where ρ_s = sample density, ρ_2, ρ_3 are standard densities below and above the sample within the column, with their corresponding scale positions x_i .

4.3. Quantitative aspects of the BL test

4.3.1. As-manufactured (fresh) TRISO particles

For each of the ten ACF runs, at least six samples of 20 g each were subjected to the burn-leach test. Of the six samples, half of them were hydrostatically pressed in a water medium at a pressure of 420 tons before the burn-leach test. It was supposed that the hydrostatic pressing would increase the sizes of the SiC-OPyC cracks if they existed, and would facilitate the extraction of the uncontained uranium during the leaching step. The main two ways that the TRISO particles can become defective are classified as:

- Ones where the uncontained uranium is leached through the cracked SiC shells in the coating layers during the burn-leach test;
- Ones where the free uncoated kernels are present, oxidized, and then dissolved during leaching step.

4.3.2. Leach-burn-leach test of TRISO particles

Some other groups of the world perform the leach-burn-leach (LBL) testing versus the burn-leach test. The LBL test method gives all the information acquired from the burn-leach (BL) test but helps to distinguish the form of the defect, where the first leach would give defects from the uncoated or the exposed kernels. In addition, the LBL is more suited for the small compact fuel design (25 mm x 12 mm) as employed by the Oak Ridge National Lab in the USA.

A total of 110 g particles were selected from the ACF run 5 and divided into five different samples to submit them to the LBL investigation. The LBL entailed leaching the TRISO particles in an acidic medium, evaluating the presence of the exposed or free kernels that dissolved in the leaching acid, drying the intact TRISO particles, oxidizing and leaching once more.

In this study a combination of nitric acid (HNO_3) and hydrofluoric acid (HF) was used as the leaching medium. The final concentration of HF was 0.5% (v/v). These strong acidic conditions would expose any presence of the channels in the SiC layer if they existed.

For comparison purposes, a 10 kg population (CPU-L-H101) from the PBMR ACF was characterised following the same techniques outlined in section 4.2. A 1 kg random sample from this population was sent to the Oak Ridge National Lab for QC testing.

4.3.3. Fuel spheres

Fuel spheres were deconsolidated by means of isothermal oxidation at a temperature of 750 °C for 96 hours. The total carbonaceous material which largely consisted of MGP that was used to hold the fuel core together was removed by this process and the SiC layer of the TRISO particles was also exposed. OPyC denuded particles were placed in 6 M HNO₃ and refluxed at boiling point for 16 hours to leach uranium from the defective SiC shells.

There are several stages which are involved during the production process of the fuel spheres. It is of interest to investigate which of these stages are likely to break or weaken the SiC layer during the manufacturing process. This study attempted to study these stages using the burn-leach method.

Samples at each stage of the manufacturing process (after release of the TRISO-coated particles) were taken and half of these subjected to the burn-leach analysis with the test extended to 96 hours at 750 °C. The reason to extend all the tests to 96 hours was to investigate the thermal strength of the SiC layer as this was the temperature at which the burn-leach testing of the fuel spheres was performed under normal conditions. In this way it was expected that if any single one of the stages damaged the particles, such stage could be identified using the burn-leach method. The burn-leach results were obtained for the following stages:

1. The good particle fraction sorted by the production department using their sorting table (CPU-B-H103);
2. The bad particle fraction sorted by the production department using their sorting table;
3. QCTL bad particle fraction sorted by the quality control department using their sorting table;
4. Particles over-coated and then washed free of the OC layer (OPU-B-H103);
5. Pre-mix and in-mould mix for fuel sphere (FSA-T-J18G(13-18));
6. Core press before final press of fuel sphere (FSA-T-J18G(25-30));

7. Final pressed spheres not carbonised and annealed (FSA-T-J18G(37-42));
8. Final pressed spheres carbonised and annealed (FSA-T-J18G(1-6)).

Particles from (1) were tested to ensure that such particles were mechanically strong enough to be used to manufacture fuel spheres;

Particles from (2) were tested to confirm if these were truly weak to be used to manufacture fuel spheres;

Particles from (3) were tested to confirm if the QCTL sorting table which had more stringent separation parameters than the production department table could successfully remove bad particles that may have been classified as being good by the production sorting table;

Particles from (4) were tested to establish whether it was a good practice to re-use particles that had already been over-coated before for the manufacture of fuel spheres.

4.4. Variants of BL test

4.4.1. Effect of burn time on the amount of leached uranium

Freshly manufactured TRISO particles were exposed to burn times of 16, 22, 46, 70 and 90 hours and uranium leached was recorded.

German BL method prescribed a burn time of 16 hours to be followed by 16 hours of leaching to ensure that all the uranium due to the broken particles was in solution. Under such circumstances the uranium concentration in the leach solution was expected to reflect the presence of a number of failed TRISO-coated particles. For the current test, a TRISO-coated particle batch CPT-T-C7, manufactured on the 1 kg experimental coater at Pelindaba, was sorted using the QCTL vibration table with a working amplitude of 0.4 mm, frequency 54Hz, inclination angle 1.4° and low 85 g.h⁻¹ feed rate until a sample of 100 g was obtained. The sorted coated particles that were deemed to be a good product did not contain completely broken particles such as half particles. The BL test could therefore only give a positive result should the shells contain holes of some kind or another. It was therefore not expected to find a positive BL result on the sorted samples.

For this experiment, the sorted sample was portioned into 20 g sub-samples. The burn duration was varied from 16 hours to 90 hours and BL test was applied

4.4.2. Effect of sequential leaching on the amount of uranium released

Freshly manufactured TRISO particles are generally leached for 16 hours in a normal BL test, and the uranium in solution determined. A test was performed where this action was repeated three more times on the same particles and each time the uranium leached was recorded. To test the effect of multiple leaching, samples 4A and 5A were burned for 21.5 and 16.25 hours respectively, and were leached three more times than the usual, meaning that they were leached for three additional steps of 16 hours. Uranium leach solutions were analysed by the ICP-OES for the concentration values above 1 mg/L and with ICP-MS for the lower range.

4.4.3. Defective IPyC

The IPyC layer forms the first defence in retaining fission radionuclides from leaving TRISO particles. The integrity of this layer was tested by sampling particles from the ACF before the deposition of SiC. These particles were leached using 6 M HNO₃ for 2 hours. Following this step, they were dried and imaged on the Micro XT X-ray microtomography system (Xradia).

A comparison of this method with the ORNL method which was based on the uranium dispersion phenomena was performed (Weber et al. 1976). A considerable quantity of uranium can be transferred from the kernel into the buffer layer during fabrication. An outline of the CVD process in section 1.4 gives evidence of the formation of HCl during the decomposition of methyl-tri-chlorosilane (CH₃SiCl₃). Uranium re-distribution in TRISO particles can result from permeation of the inner pyrolytic carbon by HCl during SiC deposition. Since the SiC deposition employs decomposition of CH₃SiCl₃, HCl is readily available during this process to react with IPyC. The permeability of the IPyC to HCl gas has a marked effect on the extent of this uranium dispersion.

CHAPTER 5

5. RESULTS AND DISCUSSION

5.1. Qualitative analysis of TRISO particles

5.1.1. Introduction

One way to assess whether a sample or a batch of TRISO-coated particles has a single particle or more with a broken SiC layer when inspecting the integrity of the TRISO layers using the burn-leach test is to count the broken SiC shell pieces or shards.

5.1.2. Separation of the SiC layer shards by the density difference

This was achieved by floating the shells that remained after the burn-leach test on *di*-iodomethane high density liquid. The shards were collected for inspection under a light optical microscope. When only a few particles were broken it was often possible to make a final decision on the number of broken particles by simply inspecting the shells. Table 5.1 is the comparison of the qualitative results (UO₂ kernel equivalents) from optical microscopy versus quantitative results (UO₂ kernel equivalents) from the ICP-MS.

Broken SiC shells of aTRISO particle batch CPT-T-C17 were floated on *di*-iodomethane. BL test results indicated the presence of one broken particle. A photomicrograph of the SiC shards is shown in Figure 5.1. SiC fragments were compatible with one broken particle.

Table 5.1: A comparison of qualitative versus quantitative BL.

Batch	Type	Optical Microscopy	ICP- MS
CPT-T-C17	TRISO particles	1	1
FAS-T-E30-G04	Fuel Sphere	1	1
CPT-T-D1	Fuel Sphere	36	30

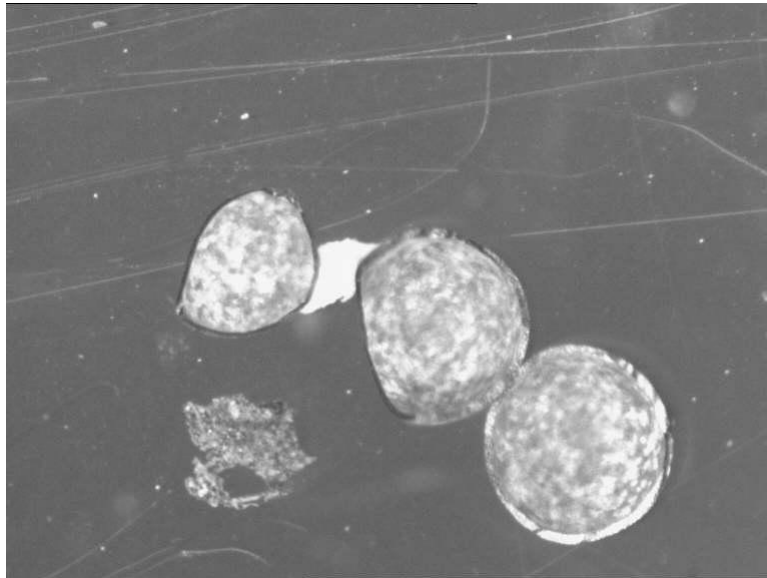


Figure 5.1: A photomicrograph showing shards from the burn-leach test indicating a single broken particle (64X magnification).

Burn-leach analysis was performed on a fuel sphere batch FSA-T-E30-G04. Figure 5.2 shows a particle that floated on *di*-iodomethane. This type of failure was different in that there was no SiC breakage but a little hole in the SiC shell. ICP-MS results indicated one UO₂ kernel equivalent.

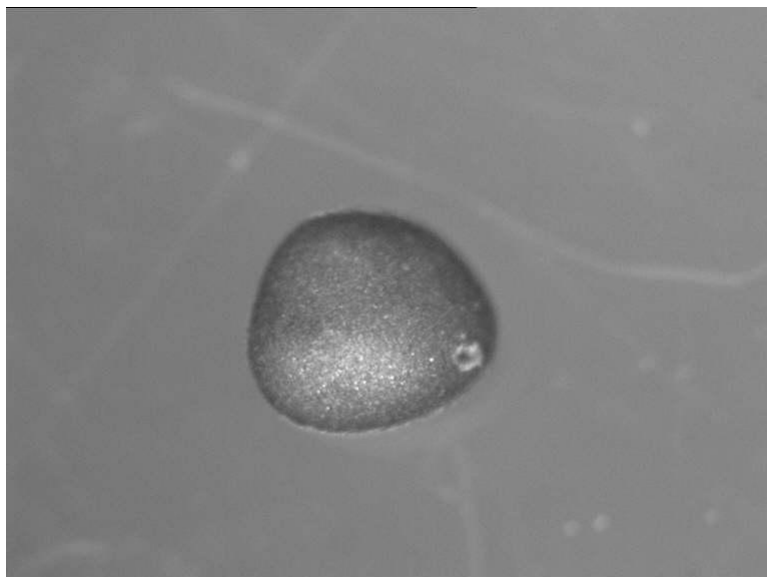


Figure 5.2: A shell with a hole collected after a positive BL test for one particle (64X magnification).

BL test was performed on a fuel sphere sample CPT-T-D1. Figure 5.3 shows broken SiC shells that floated on *di*-iodomethane. The estimated number of failed TRISO particels was 36. Figure 5.3 shows the broken SiC shells collected from this sample. The ICP-MS results indicated 30 UO₂ kernel equivalents. It was supposed the broken particle fraction increased markedly due to pressing during fuel sphere manufacture. This suggested a mechanical failure of coated particles of this particular batch under pressure.

In general it was concluded that the qualitative burn-leach test could be used as a rigorous testing technique provided that there were not large numbers of failed TRISO particles. The effort of counting the broken fragments became tedious, and it became difficult to identify each fragment belonging to a certain particle. The reason was that a single SiC shell did not always break into two equal pieces. There were many possible ways of breaking.

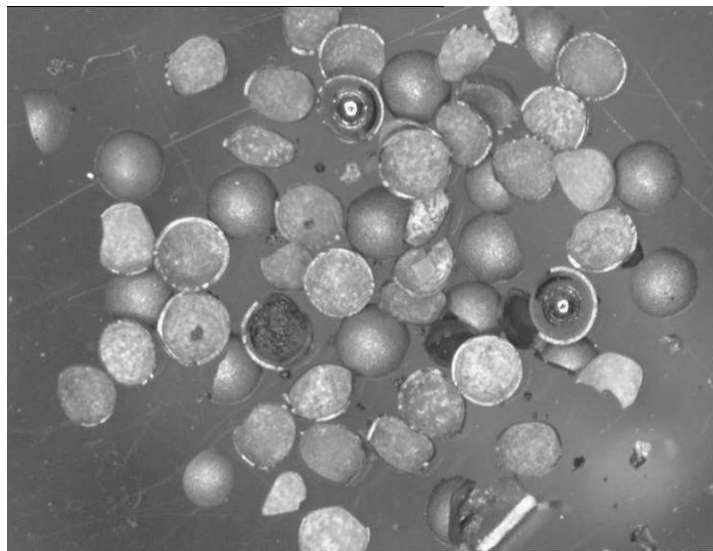


Figure 5.3: Shards that were collected after burn-leach testing (16X magnification).

The frequency of the appearance of the rough-surfaced SiC particles shown in Figure 5.4 could not be ignored. The SiC layer of these particles was intact and survived the BL test. Their existence could not be explained. There is currently no evidence of scientific work that has established whether or not such particles will fail during the irradiation in the nuclear reactor.

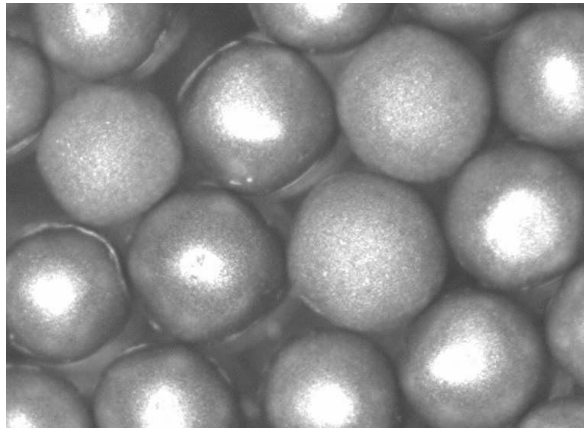


Figure 5.4: Photomicrograph showing a rough surface SiC layer (32X magnification).

5.2. Characterisation of TRISO particles

5.2.1 Introduction

BL analysis of TRISO particles would not have been meaningful if the layer thickness values of TRISO particle batches which were tested were outside the required specification detailed in Table 1.1 of chapter one. Layer thickness distributions were confirmed in this study to be *nearly* normally distributed (see section 5.2.2) and hence this study was confident that the BL results came from TRISO particle populations with attributes that met the specification requirements.

5.2.2 Determination of layer thickness values of TRISO particles

After the homogenisation and riffing of the sub-sample, the particles were mounted in epoxy resin and polished to the midplane as per preparation for the measurement of the layer thickness values for the buffer, the inner pyrolytic carbon, the silicon carbide and the outer pyrolytic carbon layers. The numbering B101-B110 refers to batch number 101 to batch number 110. From ten different CVD runs a total of 4 000 particles were measured to determine layer thickness values; 1 000 particles for each layer of the four. The raw data are available in the Appendix section. From these measurements, the statistical distributions of the layer thickness values were computed and the resulting descriptive statistics were outlined. This effort aimed at ensuring that particles which were exposed to burn-leach testing were of an acceptable integrity, possessing the layer thickness values that met the design specifications.

Figures 5.5-5.8 present the histograms for the layer thickness values for buffer, IPyC, SiC and OPyC for the particles used in this study. Tables 5.2-5.5 provide summaries of statistical data treatment computed using the equations in chapter 3.

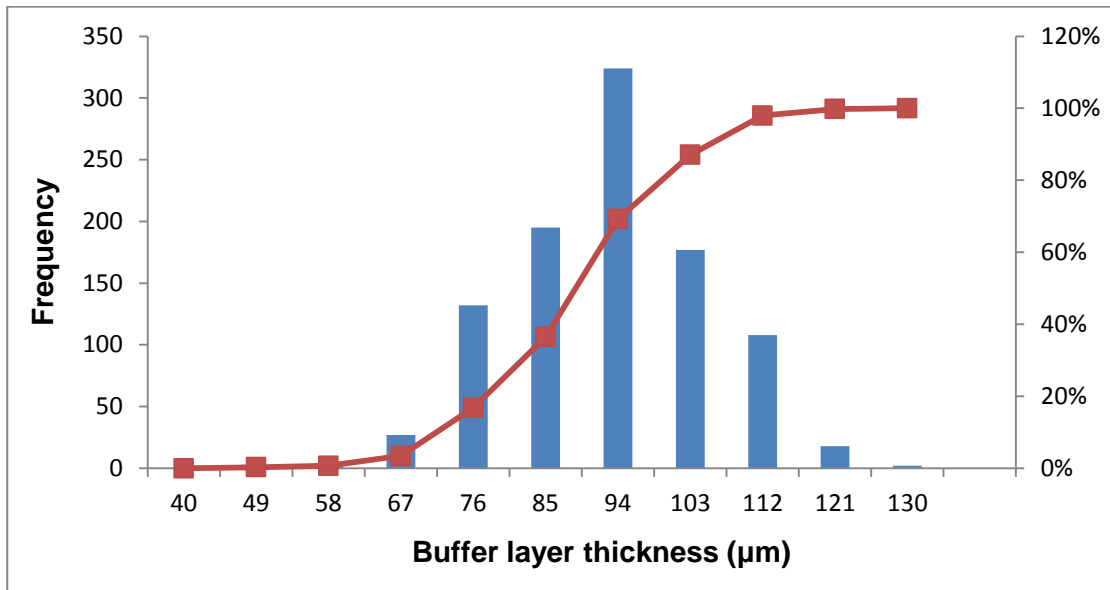


Figure 5.5: Statistical distribution of buffer layer thickness values of TRISO particles inspected in this dissertation for $n = 1\ 000$.

Table 5.2: Summary of statistical treatment of the buffer layer thickness values.

Attribute	B101 (µm)	B102 (µm)	B103 (µm)	B104 (µm)	B105 (µm)	B106 (µm)	B107 (µm)	B108 (µm)	B109 (µm)	B110 (µm)
Mean	87.0	86.1	93.1	91.0	89.3	87.5	85.4	91.1	88.0	84.7
StdDev	12.0	12.8	10.5	12.1	12.2	12.1	11.7	11.9	10.9	12.9
Skewness	-0.3	0.8	0.1	0.0	0.2	-0.4	0.2	-0.1	-0.2	-0.9
Minimum	54.2	64.1	69.0	64.0	57.5	60.8	57.5	62.4	62.5	42.7
Maximum	113.3	128.2	118.2	116.6	119.9	110.0	115.5	115.0	108.4	111.7
Count	100.0	100.0	100.0	100.0	100.0	100.0	100.0	100.0	100.0	100.0
C.L.(95%)	2.4	2.6	2.1	2.4	2.4	2.4	2.3	2.4	2.2	2.6

All the computed statistics indicated that the measure of centrality depicted by the mean layer thickness values lay within a 95% confidence interval of 2.4 µm for the buffer layer, 0.7 µm for the IPyC layer, 0.4 µm for the SiC layer and lastly 0.7 µm for the OPyC layer throughout the inspected populations. The skewness values were all found to be close to zero confirming a near normally distributed layers of the populations examined.

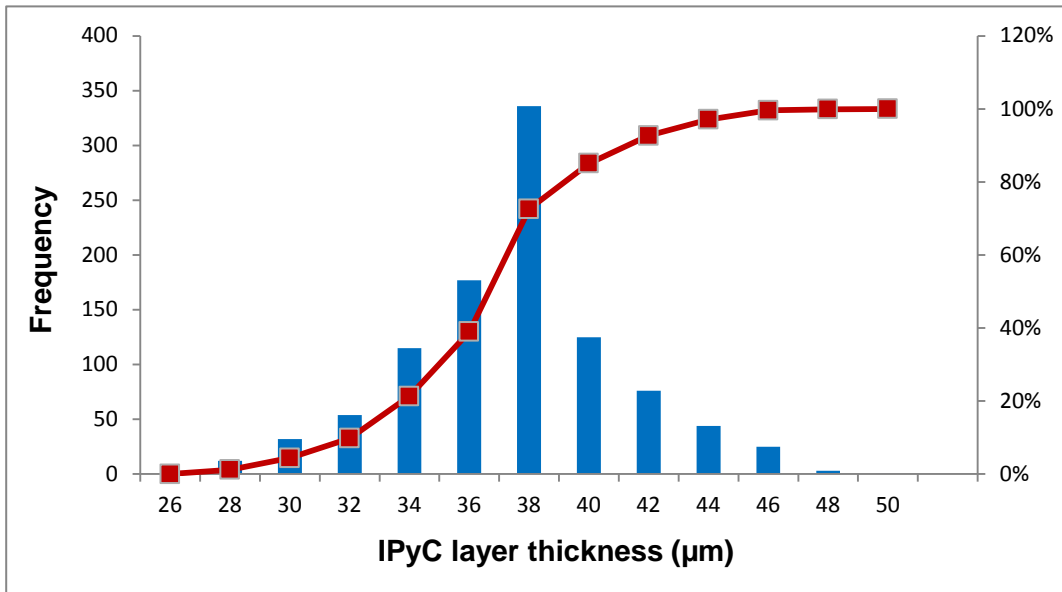


Figure 5.6: Statistical distribution of IPyC layer thickness values of TRISO particles used in this study for

$n = 1\ 000.$

Table 5.3: Summary of statistical treatment of the IPyC layer thickness values.

Attribute	B101 (µm)	B102 (µm)	B103 (µm)	B104 (µm)	B105 (µm)	B106 (µm)	B107 (µm)	B108 (µm)	B109 (µm)	B110 (µm)
Mean	37.8	36.8	36.4	36.5	37.8	35.5	35.0	37.1	35.8	35.9
StdDev	3.7	3.7	3.6	3.3	3.7	3.4	3.7	3.3	3.4	3.6
Skewness	0.4	0.0	0.1	-0.1	-0.3	0.7	-0.1	-0.1	0.2	0.4
Minimum	29.6	26.3	28.0	29.6	29.6	29.6	26.3	26.3	26.3	27.9
Maximum	46.0	46.0	44.4	44.4	46.0	49.4	44.4	44.5	42.7	47.6
Count	100.0	100.0	100.0	100.0	100.0	100.0	100.0	100.0	100.0	100.0
C.L.(95%)	0.7	0.7	0.7	0.6	0.7	0.7	0.7	0.7	0.7	0.7

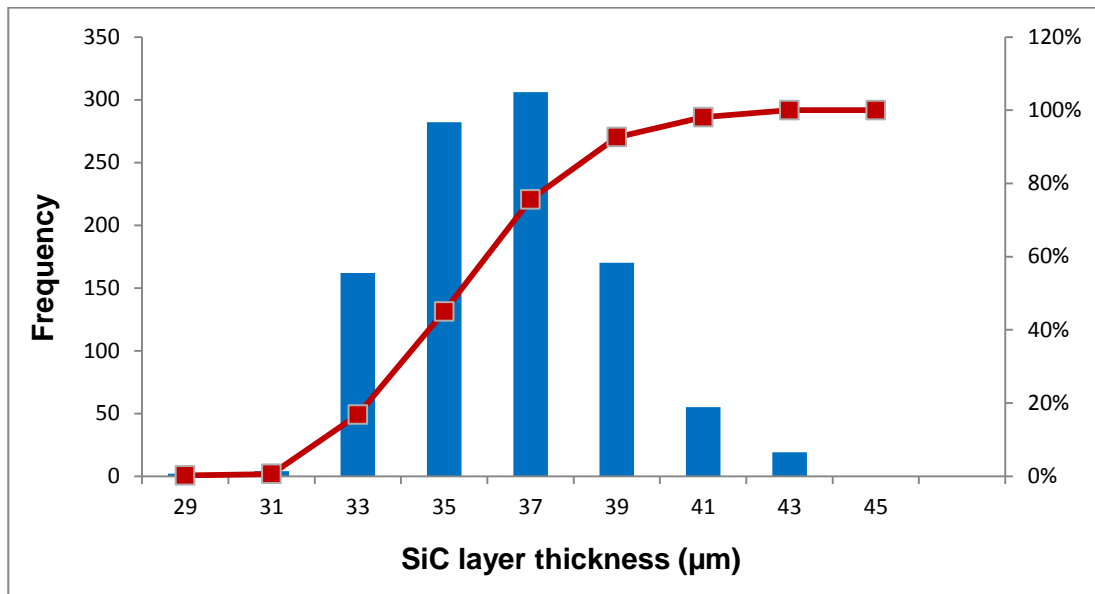


Figure 5.7: Statistical distribution of SiC layer thickness values of TRISO particles used in this study for

$n = 1\ 000.$

Table 5.4: Summary of statistical treatment of the SiC layer thickness values.

Attribute	B101 (µm)	B102 (µm)	B103 (µm)	B104 (µm)	B105 (µm)	B106 (µm)	B107 (µm)	B108 (µm)	B109 (µm)	B110 (µm)
Mean	35.2	35.1	35.8	35.8	36.8	35.4	35.3	35.4	35.9	35.1
StdDev	1.8	2.2	2.1	2.3	2.2	2.3	2.2	1.9	2.0	2.2
Skewness	-0.3	0.2	0.4	-0.1	0.0	-0.2	-0.2	-0.1	0.3	0.2
Minimum	31.2	27.9	31.2	29.6	31.2	29.6	29.6	31.2	31.2	27.9
Maximum	37.8	42.7	41.2	41.1	41.4	41.1	39.6	39.4	41.1	42.7
Count	100.0	100.0	100.0	100.0	100.0	100.0	100.0	100.0	100.0	100.0
C.L.(95%)	0.4	0.4	0.4	0.5	0.4	0.5	0.4	0.4	0.4	0.4

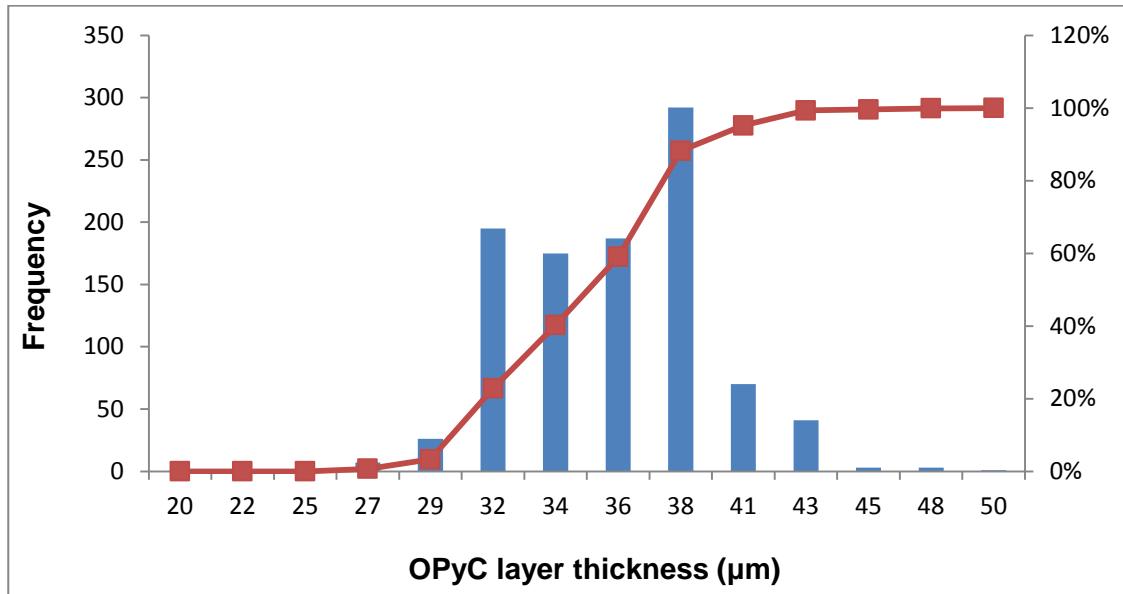


Figure 5.8: Statistical distribution of OPyC layer thickness values of TRISO particles used in this study for $n = 1\ 000$.

Table 5.5: Summary of statistical treatment of OPyC layer thickness values.

Attribute	B101 (µm)	B102 (µm)	B103 (µm)	B104 (µm)	B105 (µm)	B106 (µm)	B107 (µm)	B108 (µm)	B109 (µm)	B110 (µm)
Mean	35.0	34.8	35.2	35.0	35.2	33.7	35.3	34.6	34.1	33.3
StdDev	3.4	3.0	3.1	3.7	3.6	3.0	3.6	3.8	3.4	2.8
Skewness	0.1	-0.3	0.5	0.4	0.3	-0.2	-0.2	0.4	0.0	0.4
Minimum	27.9	27.9	29.6	27.9	27.9	24.6	26.5	26.3	26.3	27.9
Maximum	42.7	41.1	46.0	47.7	46.0	39.7	44.3	46.0	41.1	41.1
Count	100.0	100.0	100.0	100.0	100.0	100.0	100.0	100.0	100.0	100.0
C.L.(95%)	0.7	0.6	0.6	0.7	0.7	0.6	0.7	0.8	0.7	0.5

5.2.3 Analysis of Variance (Anova) of the SiC and IPyC layers

Variance in the SiC and IPyC carbon layers was computed. The reason for selecting only these two layers was because they were highly central to the failure or the structural integrity of the TRISO particle.

The null hypothesis is that the means of the layer thickness values of the SiC are equal at the 5% significance level:

- H_0 : Mean 1 = Mean 2 = Mean 3 = Mean 4 = ... = Mean 10

SiC

<i>Groups</i>	<i>Count</i>	<i>Sum</i>	<i>Average</i>	<i>Variance</i>
101	100	3520.35	35.2035	3.233009
102	100	3506.58	35.0658	4.915631
103	100	3576.46	35.7646	4.266651
104	100	3581.53	35.8153	5.116429
105	100	3681.08	36.8108	4.93627
106	100	3539.06	35.3906	5.456044
107	100	3529.47	35.2947	4.714532
108	100	3537.37	35.3737	3.564217
109	100	3591.87	35.9187	3.84488
110	100	3506.58	35.0658	4.915631

<i>Source of</i>	<i>SS</i>	<i>df</i>	<i>MS</i>	<i>F</i>	<i>P-value</i>	<i>F crit</i>
Between Groups	254.8482	9	28.3165	6.2977	1.06E-08	1.8892
Within Groups	4451.366	990	4.4963			
Total	4706.214	999				

The *P-value* of 1.06E-08 is less than the significance level (0.05), so we can reject the null hypothesis and safely assume that the mean layer thickness values of at least one or more runs of the SiC produced in the CVD coater are different.

F (6.2977) is greater than F_{crit} (1.8892), so again, we can reject the null hypothesis that the variances are all equal.

The null hypothesis is that the means of the layer thickness values of the inner pyrolytic carbon are equal at the 5% significance level:

- H_0 : Mean 1 = Mean 2 = Mean 3 = Mean 4 = ... = Mean 10

IPyC

Groups	Count	Sum	Average	Variance
101	100	3776.6	37.766	13.61733
102	100	3675.28	36.7528	13.77108
103	100	3643.39	36.4339	12.57163
104	100	3648.01	36.4801	10.55974
105	100	3780.04	37.8004	13.49036
106	100	3548.83	35.4883	11.63097
107	100	3503.4	35.034	13.57259
108	100	3710.23	37.1023	11.1439
109	100	3583.29	35.8329	11.4773
110	100	3591.04	35.9104	12.78245

Source of	SS	df	MS	F	P-value	F crit
Between Groups	767.4666	9	85.2740	6.8429	1.37E-09	1.8893
Within Groups	12337.12	990	12.4617			
Total	13104.59	999				

The *P*-value of 1.37E-09 is less than the significance level (0.05), so we can reject the null hypothesis and safely assume that the mean layer thickness values of at least one or more runs of the IPyC produced in the CVD coater are different.

F (6.8429) is greater than *F crit* (1.8893), so again, we can reject the null hypothesis that the variances are all equal.

5.3 Quantitative analysis of TRISO particles by BL method

5.3.1 Introduction

BL testing reagents and critical equipment were evaluated for their cleanliness before performing the experiments. The purpose of this was to validate that the water and the nitric acid solution was free of the residual uranium content that would contaminate the analyte solutions. Water samples were analysed directly by the ICP-Mass spectrometry technique. Nitric acid reagent (Merck AR grade) was prepared by diluting 5 mL of 6 M HNO₃ in 250 mL flask with ultra-pure water. In addition a 100 µg/L uranium standard

solution was prepared to validate the accuracy of the ICP-MS method. The results are shown in Table 5.6.

Table 5.6: ICP-MS results ($\mu\text{g/L}$) of water, reagents and reference samples

Sample	ICP- MS result in $\mu\text{g/L}$
Tap water	<2
Demineralised water	<2
Ultrapure water	<2
100 $\mu\text{g/L}$ standard	112

The measured uranium value of 112 $\mu\text{g/L}$ versus the known value of 100 $\mu\text{g/L}$ gave the author confidence in the accuracy of the ICP-MS technique. The calibration and the sensitivity of the method led to the conclusion that uranium is present in levels less than 2 parts per billion (the limit of detection of the ICP-MS method) in all the samples analysed. The ultra-pure water and the AR grade nitric acid was therefore of more than adequate purity to perform the burn-leach test for broken particles. All subsequent tests were performed using the ultrapure water and AR grade nitric acid.

To validate that properly cleaned equipment such as glassware, oven, and crucibles did not introduce uranium contamination, a BL test on uranium free dummy samples was performed with equipment that had previously been used. The equipment was first thoroughly cleaned and dried and then used to perform the BL tests on the dummy samples of pure ZrO_2 kernels and coated particles deposited on ZrO_2 kernels. The complete BL test was performed on each sample. For a 100% leaching of a single TRISO particle the expected ICP-MS result is 5mg/L. The final solutions were made up to 250 mL. The results of the ICP-MS analyses on the two samples are shown in Table 5.7.

Table 5.7: Results ($\mu\text{g/L}$) of uranium contamination studies on dummy samples.

Sample	Total mass (g)	ICP-MS result ($\mu\text{g/L}$ U)
ZRO-A	20.0085	6
CPT-B-A21-A	20.0012	2

The results showed that for purposes of identifying failed particles, the cleaning and the testing procedures practically introduced no contamination. Some contamination due to the equipment and the glassware was expected at these extremely low concentration levels.

5.3.2 Fresh TRISO particles

A total of 60 samples (20 g each) were subjected to burn-beach testing. Figure 5.9 illustrates the spread of the uncontained uranium plotted as the function of the total uranium content per 20 g sample. The results obtained were as follows:

- 73% of the 60 tested samples did not indicate the presence of a cracked or broken SiC layers in their TRISO particles;
- 20% of the 60 tested samples indicated the presence of at least a single TRISO particle with a cracked or broken SiC layer;
- 3% of the 60 tested samples indicated the presence of at least two TRISO particles with a cracked or broken SiC layer;
- 3% of the 60 tested samples indicated the presence of at least two TRISO particles that had partial or incomplete leaching of uranium.

An analysis to evaluate the presence or absence of a correlation between the mean layer thickness of the SiC and the IPyC layers was performed because these two layers are highly central to the failure or the structural integrity of the TRISO particle.

Figure 5.10 shows the relationship between the mean layer thickness of SiC for various batches and the cumulative amount of leached uranium. The results suggested that there was generally no correlation between the mean layer thickness values and the amount of the leached uranium. The batch that leached the least amount of 546 μg uranium had a mean layer thickness value of 35.07 μm , whereas the batch that leached more than 3 times this amount (1898 μg) had a mean layer thickness value of 35.92 μm . Figure 5.11 is a summary of the relationship between the amount of uranium leached and the mean layer thickness of the inner pyrolytic carbon layer. Here also, there was no evidence of a correlation between these. The batch that leached the least amount of uranium (546 μg) had a mean layer thickness value of the IPyC of 36.75 μm , whereas

the batch that leached the most uranium (1898 μm) had a mean layer thickness of 35.83 μm .

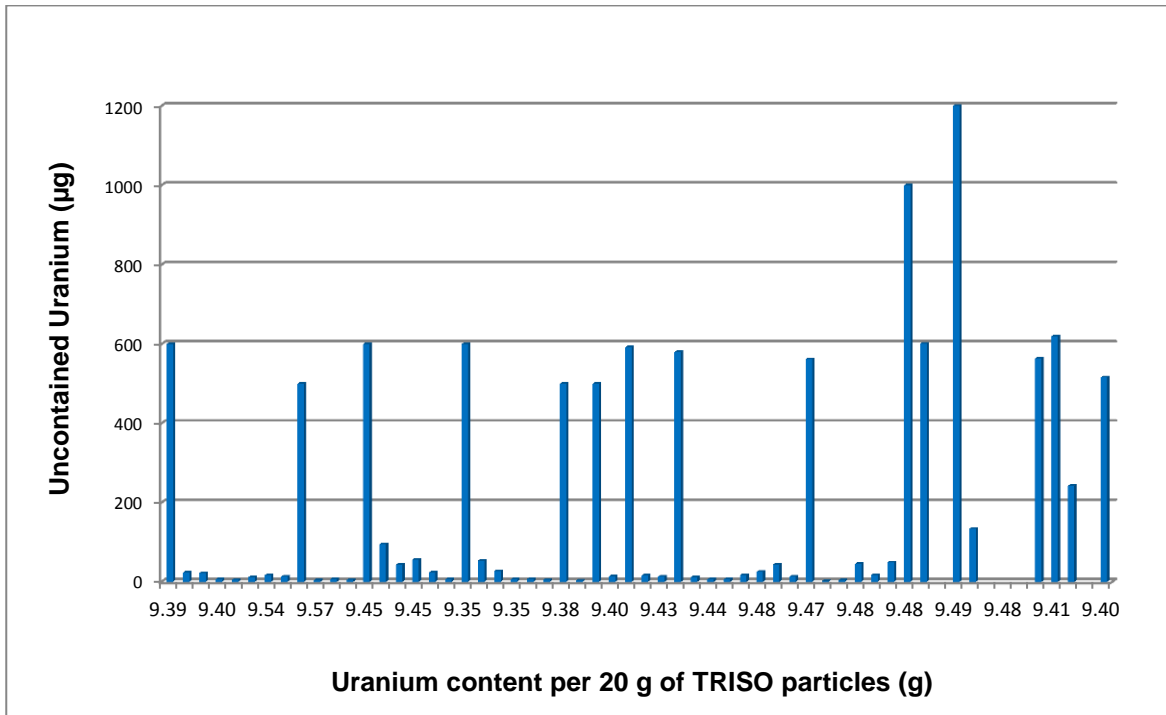


Figure 5.9: Amount of uncontained uranium for each of the 60 BL tested samples. 20 g of each sample were tested.

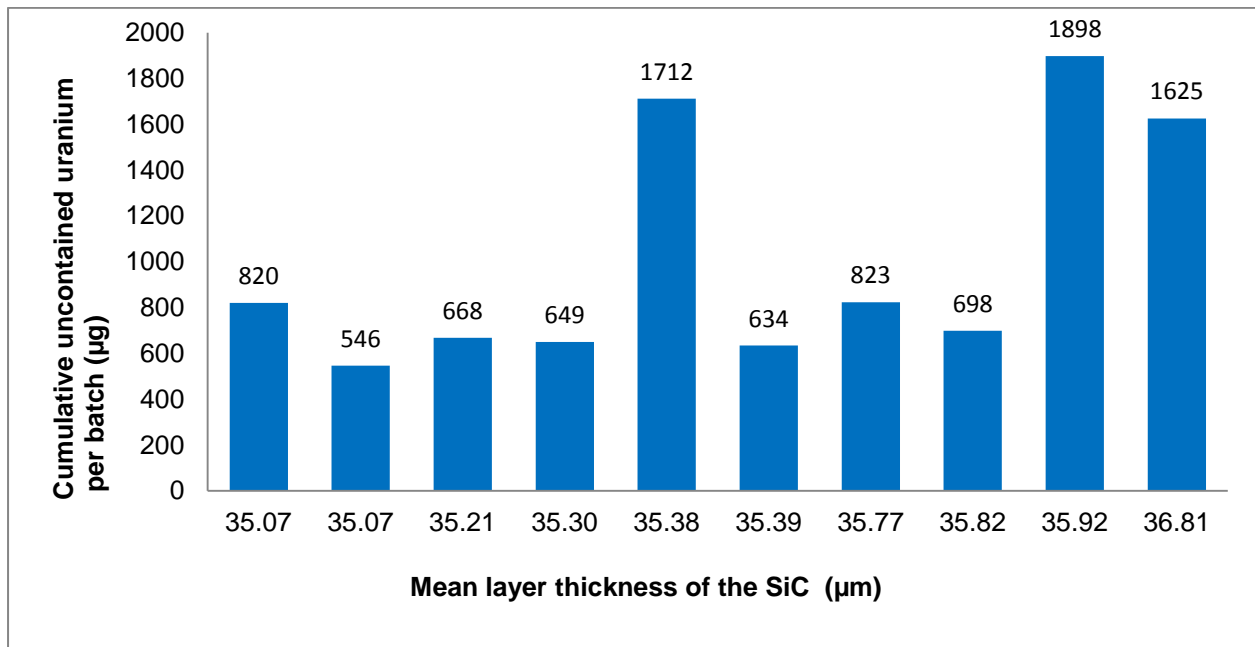


Figure 5.10: Total uncontained uranium as a function of the mean layer thickness of the silicon carbide layer for the batches SiC 101- SiC 110.

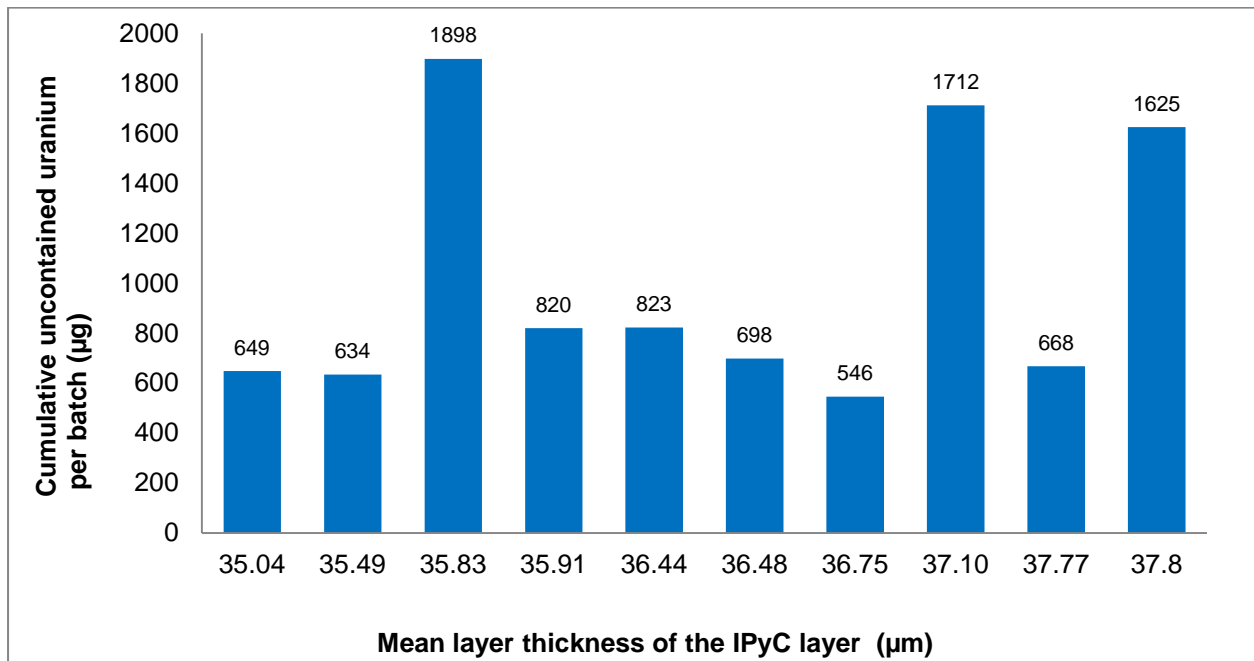


Figure 5.11: Total uncontained uranium as a function of the mean layer thickness of the inner pyrolytic carbon layer for the batches IPyC 101- IPyC 110.

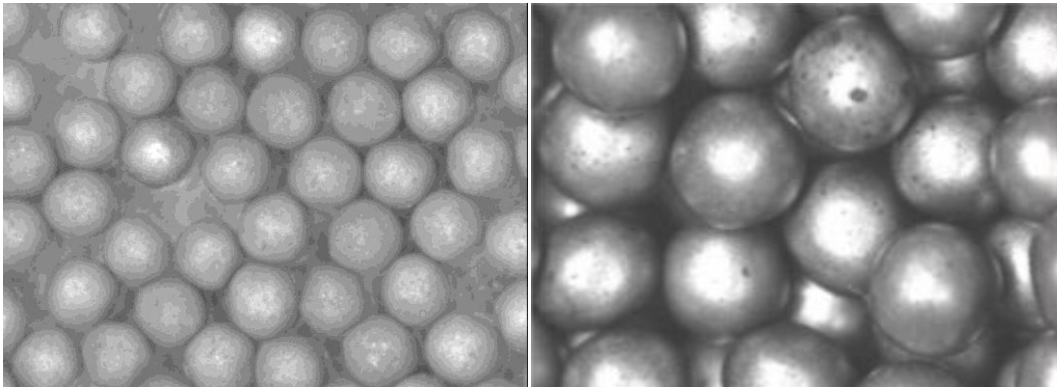
5.3.3 BL results by PBMR

LBL test is generally viewed as a better test than the direct BL test due to its ability to detect free uranium dioxide kernels before the burn step of BL test (Partain 1984, Weldon 1987).

Figures 5.12(a) and 5.12(b) show optical photomicrographs taken of the TRISO particles before and after leach-burn-leach (LBL) investigation performed in this study. A combination of HNO₃ and HF acids was used for the LBL study. Black spots on the TRISO particles in Figure 5.12(b) were observed, it was supposed that these resulted due to the use of hydrofluoric acid. Using just HNO₃ did not result in the formation of black spots. For all but one sample exposed to LBL analysis, there was no evidence of naked or exposed kernels after the first leach. Results obtained from LBL are summarised in Table 5.8. The amount of uranium leached was not artificially high compared to normal BL.

Of the 110 g (84 300 particles), only a single sample was found to have a failed TRISO particle. This result suggested that PBMR should consider performing the LBL to some extent until the coating conditions of the CVD were optimised, since it was evident that

the TRISO particles with exposed kernels were likely to be inherent in the manufacturing process.



a. 16X magnification

b. 64X magnification

Figure 5.12 (a) TRISO particles before LBL testing and (b) Particles after LBL testing.

Note: 5 mg/L is equivalent to 1 failed particle.

Table 5.8: Results (mg/L) of uranium leached during BL test of B₅ TRISO particles.

Sample number from batch	ICP-MS result	Equivalent particles
1	<2	0
2	6	1
3	<2	0
4	<2	0
5	<2	0

This LBL study could not distinguish if the exposed kernel was either due to the chemical manufacturing process or to the mechanical shock breakage when the particles were extracted from the coater after the CVD process.

One disadvantage of LBL testing was the length of time taken as there was an additional 16 hours of testing compared to the burn-leach (BL) test. The low proportion of the defective TRISO particles with exposed kernels found in this study of 1 in 84 300 particles could lead to a debate with regards to the benefits of performing the leach-burn-leach test as opposed to the burn-leach when costs considerations came to the fore.

5.3.4 LBL results by ORNL

As part of this study a 1 kg sample of the PBMR TRISO batch CPU-L-H101 with 9.6% LEU enrichment was sent to the Oak Ridge National Laboratory (ORNL). This population had been manufactured on the PBMR CVD reactor, using the same conditions used thus far. For the purpose of this study the focus would be on LBL results obtained for this population.

At the ORNL, TRISO particles were used to manufacture 203 compacts. The particles from this population were used for the fabrication of the cylindrical compacts with a nominal 12.3 mm diameter and 25.2 mm length. The compacting was performed by over-coating the particles with MGP and pressing them into the final fuel shape. A random selection of the compacts was taken and the selection is outlined in Table 5.9. The leach-burn-leach analysis was performed on sets of 20 compacts at a time, in four sample groups with five compacts in each sample. The uranium contamination fraction or effective number of the exposed kernels before the burn and the defective SiC layer fraction or number of exposed kernels after the burn were calculated from the combined results of all the relevant sample groups. Table 5.9 is a summary of the exposed kernels before and after burning. After the compacts were electrolytically deconsolidated and leached, the uranium was detected at a level equivalent to 5.3 kernels. According to the leaching procedure, the contribution from the uranium on the surface of TRISO particles coming from dust during the CVD process versus that from the defective particles was not distinguishable. For this procedure, the acceptance test value of the effective number of the exposed kernels was 5.3 out of 243 516 particles analysed.

Table 5.9: Summary of the SiC defect analysis for CPU-L- H101.

Compact ID	Number of	Effective number of exposed kernels	Number of kernels leached
181, 048, 202, 081, 096	5	0.0	0
007, 001, 174, 040, 194	5	0.0	0
099, 179, 070, 141, 151	5	0.0	0
197, 163, 166, 199, 157	5	0.0	0
068, 066, 036, 090, 025	5	0.0	0
109, 186, 055, 159, 041	5	0.0	0
059, 196, 069, 132, 110	5	0.0	0
032, 045, 079, 060, 147	5	0.0	1
028, 185, 100, 005, 112	5	0.9	1
097, 117, 203, 122, 086	5	2.0	0
158, 200, 029, 030, 113	5	0.0	0
124, 182, 116, 167, 089	5	0.0	0
049, 135, 018, 139, 119	5	0.0	0
114, 193, 065, 082, 017	5	0.0	0
009, 175, 064, 071, 169	5	0.0	0
165, 103, 095, 189, 073	5	0.0	0
035, 067, 125, 143, 033	5	0.6	Not Analysed
177, 012, 093, 027, 013	5	0.3	Not Analysed
085, 104, 149, 077, 118	5	0.0	Not Analysed
062, 004, 074, 140, 078	5	0.0	Not Analysed
178, 094, 042, 047, 002	5	0.0	Not Analysed
198, 171, 046, 056, 120	5	0.0	Not Analysed
061, 176, 003, 187, 039	5	0.5	Not Analysed
108, 121, 192, 026, 142	5	0.0	Not Analysed
084, 098, 101, 127, 076	5	0.0	Not Analysed
034, 190, 191, 148, 072	5	0.0	Not Analysed
011, 038, 080, 164, 024	5	0.0	Not Analysed
102, 087, 019, 092, 152	5	0.6	Not Analysed
014, 058, 154, 146, 050	5	0.0	Not Analysed
173, 183, 111, 150, 021	5	0.4	Not Analysed
022, 016, 123, 0754, 091	5	0.0	Not Analysed
083, 088, 153, 015, 128	5	0.0	Not Analysed
Total	160	5.3	2

However, 5 of the last 16 sample groups listed in Table 5.9 had uranium levels that ranged from 0.3 to 0.6 effective number of exposed kernels before burn. More than 90% of the average uranium content per kernel was detected when leaching uranium from a particle with a broken TRISO coating.

However, as observed at ORNL, this batch exhibited unusually slow or delayed leaching, which apparently resulted in only partial leaching of some kernels. For instance, the third from the last samples in Table 5.9 (compact numbers 173, 183, 111, 150, 021) indicated ~ 20 times more uranium in the second 24 hour leach than in the first, and additional leaching was expected to show more uranium release.

It is likely that all the leached uranium came from the defective particles in each of the samples that showed a fraction of the exposed kernel; therefore, the total number of the defective particles is probably at least 8. This would correspond to a uranium contamination defect fraction of $< 6.0E-5$ at a 95% confidence level. An unusual leaching mechanism was suspected. Two particles out of 121 758 analysed showed significant uranium leaching in the post-burn part of the LBL analysis, an indication of a defective SiC layer in particles with otherwise intact coated layers. However, five other samples which were not counted as having any defects showed traces of uranium release after burn, which may indicate additional particles with defective SiC layers. Typical uranium levels detected ranged from 0.10 μg to 0.30 μg for each 5 compact. However, the five abnormal compacts showed traces of uranium from 5.0 μg to 16 μg . These levels were less than one tenth of the uranium in a single kernel (average uranium per kernel was 649 μg), so they were not registered as defects using the LBL analysis. However they clearly showed uranium levels above the background level. In addition, for all five cases, the uranium released increased in the second 24 hours after burn-leach.

The CPU-L-H101 particles apparently possessed a failure mechanism that was not accounted for in the development of the BL test. The very slow leaching that was exhibited required longer leaching time, or the sensitivity level for the determination of a particle defect could be reduced.



Figure 5.13a: High resolution x-ray tomography of a SiC defect particle after the kernel was removed by acid leaching at ORNL. The white ring shows the SiC layer, the damaged porous layer below the white ring pointed by the arrow is the IPyC layer.

Even the two samples that were identified as containing SiC defects after the BL test exhibited unusually slow leaching. One sample released only 45% of the average uranium per kernel in the initial 24-hour leach, followed by 19% in the subsequent leach. However, two additional leaches did not release any additional uranium, even though the total had only reached 64%. After the fourth leach the defective particle was identified and analysed using X-ray imaging. A high resolution tomography of the particle is shown in Figure 5.13a. It was interesting to note that the IPyC layer was not removed during the burn step. This indicated that the SiC defect was not open at this stage, or it might have been blocked by the formation of the silicon dioxide. There appeared a partial IPyC layer in the upper hemisphere of the particle pointed by the arrow in Figure 5.13a. Figure

5.13b shows the same particle closer to the mid-plane. A crack in the SiC layer was evident, presumably showing the path through which leaching of the kernel occurred. The second sample that was identified to contain a particle with a SiC defect also exhibited unusually slow leaching of the uranium. Again, 24-hour leaches were performed after the burn and the fraction of an average kernel leached at each stage was 4%, 23%, 22% and 11%. After the fourth leach it was decided to stop and analyse again using X-ray tomography even though the particle did not appear to be completely leached.

The deviation from sphericity of the examined particles is noticeable in Figures 5.13 and 5.14. These observations are not new to the PBMR particles. Similar non-spherical particles were observed from the German reference fuel. This non-sphericity is not due to leaching. It was observed from particles that did not undergo BL test. Metallographic sections of those particles indicated non-sphericity.

The only explanation is that the observed deviations from sphericity are from flawed manufacturing procedures.



Figure 5.13b: The same particle as in Figure 5.13a showing a crack in the SiC layer (arrow).

Figure 5.14 shows that some of the kernel still remained in this particle. The buffer and IPyC layers were removed during the burn. A defect on the surface of the SiC layer could be seen as marked by the arrow. The uniformity of the SiC layer in the particle of Figure 5.14 was much greater than the previous particle. This suggested the need for further investigations on the kinetics of leaching.

It was also noted that the area closest to the defect did not leach as much as the backside. There was no clear explanation at the time for this observation. Several particles would have to be studied to establish whether this was a once off occurrence or it occurred more frequently.



Figure 5.14: High resolution tomography of a SiC defect after the kernel was partially removed by acid leaching.

The results above suggested that partial leaching of uranium was a phenomenon that existed for certain defective TRISO particles shown in Figures 5.13 and 5.14. Such an observation seemed to fully agree with other workers (Myers 1989, Adams 1983, Adams and Partain 1987). These results indicated that neither BL nor LBL analysis was sufficient to be used alone to characterise the number of particles with defective SiC layers in a given TRISO particle population. A technique such as high resolution X-ray tomography needed to be used on particles that indicated partially leached uranium fractions. Also, the current burn time and leach time needed to be extended substantially. In addition to large sample sizes that needed to be evaluated using the BL analysis, the above findings pointed out the weaknesses and the shortfalls of the BL analysis. The efficiency of the BL method was shown above to be questionable, in addition to that, the

unpredictability of partial leaching of uranium posed the biggest challenge due to the significant variation in uncontained uranium from one sample to the next.

For cases where the burn-leach test gave inconclusive results, it was advisable to count the number of shards to augment the analysis.

Results above suggest that there is at least circumstantial evidence that BL method combined with X-ray tomography provides information about the integrity of the SiC layer and why one particle leaches versus another.

An interesting spin-off discovery of the BL study within both the PBMR company and the ORNL company (see next section) was that a modified BL test could be designed to test for the layer integrity on a microscopic level as opposed to testing for the broken shells only as was done by the normal BL. Both the burn time and the leach time were not sufficient in their present form. Further studies in conjunction with a complementary technique such as high resolution tomography were recommended to fully understand the slow leach mechanism that was discovered for various defective TRISO particles. It is obvious that the defective TRISO particles could not be described by cracked or broken particles; a defective layer description should go beyond this. The BL method indicated consistency with regard to determining the particles with broken SiC layers in all samples of fresh TRISO particles which were tested in this section.

5.3.5 Fuel spheres by BL

Fuel spheres manufactured from depleted uranium were deconsolidated by means of isothermal oxidation at a temperature of 750 °C for 96 hours (second last row of Table 5.10). The total carbonaceous material (primarily the MGP) was removed by this process, revealing the SiC layer. The denuded particles were placed in 6 M HNO₃ and heated at a temperature of 95 °C for 16 hours to leach out the uranium from the defective SiC shells.

The failed fractions were determined by measuring the uncontained uranium using the ICP-MS technique. The visual counting of the SiC shards coming from the failed particles was performed in addition to the quantitative BL test. It was worth noting that with fuel spheres a new failure fraction of 3 broken SiC layer particles per single sphere was revealed by the BL test. This result could be ascribed to the breakages caused by

the mechanical pressing during the fuel sphere manufacturing process. Fresh TRISO particles did not reveal such a high failure rate as was indicated by the previous sections. As before, after the BL test, particles were mixed with methylene iodide. The particles that floated on the solvent were selected and are shown in Figure 5.15.

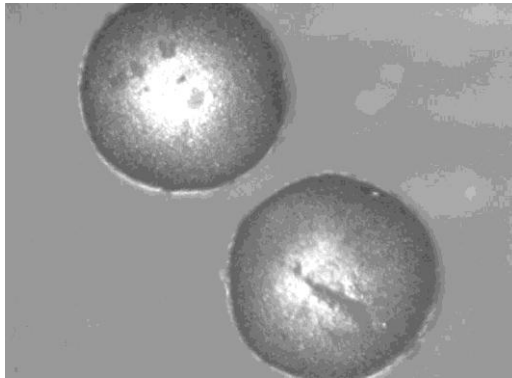


Figure 5.15: J10-FSA-G12, particles that floated in methylene iodide after BL test (48X magnification).

BL test was successfully applied in determining broken particles from fuel spheres. Figure 5.16 indicates strange-looking particles from a fuel sphere after BL test (32X and 48X magnification respectively). These particles were further imaged on the micro X-ray system to see if they still contained their uranium dioxide kernel. Figure 5.17 shows their X-ray images. It was noticed that their uranium dioxide kernel remained intact.

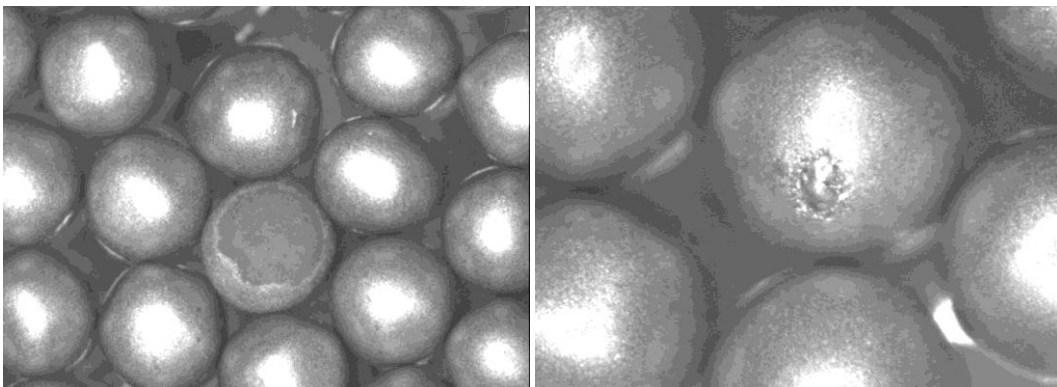


Figure 5.16: Photomicrographs showing strange-looking particles (from fuel sphere) after BL test. Magnification is 32X and 48X respectively.

The source of the damage to the SiC layer was not clear. It might have been due to any of the following: fuel sphere manufacturing; chemical attack from acid during BL test; and damage due to particle handling after the removal of methylene iodide.

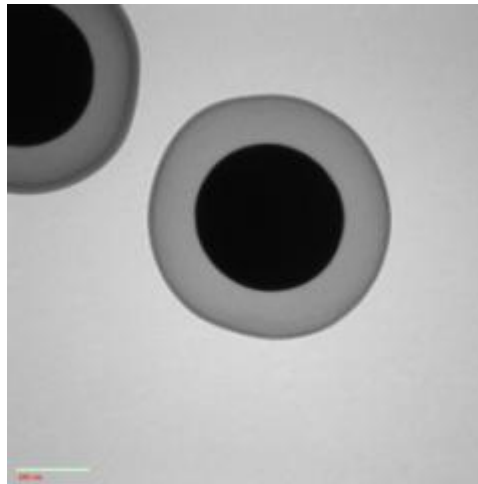


Figure 5.17: Micro X-rayed images of particles with a peculiar SiC layer.

5.3.6 Comparison of results with Nukem fuel testing

It was worthwhile to compare the integrity of the PBMR fuel spheres versus the integrity of the Nukem fuel spheres (the reference organization) using the BL method.

The release of the fission products in the PBMR core will depend largely on the quality of the fuel spheres in the core, and more specifically on the amount of free uranium within the fuel spheres. Two periods are distinguishable in the German fuel production, i.e., fuel produced before 1985 and the fuel produced after 1985. It was expected that the free uranium fraction values for the PBMR coater would be close to the German values obtained after 1985, since the fuel integrity had significantly improved after that period. Table 5.10 gives a summary of the German failure fractions and the PBMR actual values determined in this dissertation. Post 1985, the German fuel production consisted of 14 000 AVR 21-2 fuel spheres produced for bulk irradiation testing in the AVR and 200 fuel spheres produced for the HTR-Modul Proof Test in the High Flux Reactor (HFR) at Petten. The free uranium fractions were measured by means of the BL test for 40 of the AVR 21-2 fuel spheres and 10 Proof Test fuel spheres. It was obvious that either the fuel manufacturing processes at the PBMR company induced SiC breakages on the particles or the SiC layer from the PBMR CVD was not strong enough, since there was a significantly large number of defective PBMR particles (18) that were manufactured

using depleted uranium, 0.3% U-235, versus only (3 and 3) for the Nukem company in the data that were being compared.

Table 5.10: Comparison of the failure fractions between PBMR fuel versus Nukem fuel after 1985.

Production year	1985	1988	2009	2009
Designation	AVR 21-2	Proof test	PBMR	PBMR
Number of FSs produced	14 000	< 200	120	70
U-235 enrichment	16.7 %	10.6 %	0.3%	9.60 %
Number of particles per FS	9 560	14 600	15 250	14 000
Coating batch size (kg UO ₂)	3	5	5	5
Number of FSs burn-leach tested	40	10	30	5
Number of FSs with 0 particle defects	38	8	19	4
Number of FSs with 1 particle defect	1	1	5	1
Number of FSs with 2 particle defects	1	1	5	0
Number of FSs with 3 particle defects	0	0	1	0
Number of FSs with 4 particle defects	0	0	0	0
Number of FSs with 5 particle defects	0	0	0	0
Number of FSs with 6 particle defects	0	0	0	0
Number of FSs with 7 or more particle defects	0	0	0	0
Total number of defective particles observed	3	3	18	1
Total number of measured particles (thousands)	382.4	146	457.5	70
Proportion of defective particles ($\times 10^{-6}$)	7.8	20.5	39	14.3
Measured free uranium fraction ($\mu\text{g}\cdot\text{g}^{-1}$)	7.8	13.5	36	13.6

Following the above observations, some experiments were performed to investigate the steps involved in the manufacturing of the fuel spheres using BL test.

There were several stages involved during the production of fuel spheres. A fuel sphere contains around 15 000 TRISO-coated particles. It was of interest to investigate which of the stages were likely to break or weaken the SiC layers during fuel sphere manufacturing processes. An attempt was made in this dissertation to study these stages using BL method.

Twelve samples at each stage of the process were taken and half of these were subjected to BL analysis with the test extended to 96 hours at 750 °C. The reason to extend all the tests to 96 hours was to investigate the thermal strength of the SiC layer, as this was the temperature at which BL test of the fuel spheres was performed. Table 5.11 gives a summary of BL results obtained for each stage of the fuel sphere manufacturing process. The samples were approximately 20 g of TRISO-coated particles (9 g of U. Note that samples 5, 6 and 7 were received after burning off the OPyC layer. Sample 3 was washed free of the over-coating for this study.

It was interesting to note that there appeared to be a difference between the good fraction and the rejected fraction from the production sorting (Samples 1 and 2). Odd shaped particles have ‘some stressed layers’ since their sphericity is far from 1.0. As a result they are likely to fracture easily when exposed to pressure during the pressing step of fuel manufacturing. What was surprising was that the difference might be considered marginal. Perhaps not all the ‘stressed layers’ were immediately to be considered ‘breakable’ by the process of the test and an additional applied pressure was required to increase the probability of failure. Certainly, although there was an extra fraction of the rejected particles from the QC sorting table, over and above those removed by the production sorting table, these did not seem to indicate any increased probability of failure.

Table 5.11: BL test results (number of failed particle equivalents) in fuel sphere manufacturing.

Manufacturing step	Sample	#1	#2	#3	#4	#5	#6
1	Good fraction	0	1	1	0	0	0
2	Bad fraction	2	0	0	2	0	1
3	QC sort of (1) bad fraction	0	0	0	1	1	0
4	O/C and washed	0	1	1	2	1	1
5	Pre-mix	0	0	0	0	0	0
6	Core pressed	0	1	0	0	0	0
7	FS before Carbonising and annealing	1	0	2	3	27	0
8	Fuel sphere	0	0	2	2	1	0

A UO_2 kernel has a mass of 649 μg . Between the product at stage 1 of the process and stage 4 (the over-coating and washing steps) there appeared to be a significant change in the failure rate. Five of the six samples exhibited a damaged or broken particle within the coated particle fraction. However this must be compared in conjunction with particles recovered from steps 5 and 6, where there was no evidence of increased particle failure.

No evidence of increased failure was observed between steps 1 and 5 whereas there was obvious damage at step 4. This would tend to suggest that the washing of particles induced damage which resulted in the failure of an increased number of particles during the test as the coating process did not appear to have induced any discernable damage (see results from stages 5 and 6). The washing step was conducted purely for economical reasons to re-use uranium coming from scrapped over-coated particles. Whether this step would be implemented in the Pilot Fuel Production Plant (PFP) was not within the scope of this work. This study suggests that if this step was not carefully controlled, adequacy of fuel quality was likely to be compromised.

Proceeding to stage 7, there was an anomaly that resulted in a massive leaching of the uranium amounting to 27 failed particles (17 500 μg). This was an observation not confirmed by the deconsolidation of the spheres during stage 8. This would tend to suggest that the damage was incurred during the extraction of the sample for testing rather than during the manufacturing process itself. At the time of these experiments the coater engineers did admit that sometimes the extraction process was not well controlled and can result in massive breakages. For this reason, this sample was treated here as an outlier.

At stage 8 three of the six spheres tested contained more broken or damaged particles than the core pressed sample itself. There was therefore a suggestion that this stage might well induce further damage.

It was thus obvious that BL method could be used to interrogate the manufacturing processes for the production of fuel spheres. BL test was able to recommend an investigation into the washing of the over-coated particles. In the graphite laboratory, processes up to and including the core pressing appeared to be satisfactory. The reasons for the damage caused to the particles that were received before the carbonising and the annealing stages were another area where attention might need to

be focused. The process of the re-incorporation of the badly over-coated particles into the main stream of the production by washing and re-using should be carefully studied. The shell pressing step should be investigated. Such investigations were outside the scope of this dissertation. The study indicated that ‘handling’ of the production sub-stages could influence the final BL result and this was achieved using the decision-making process based on the BL test.

5.4. Variants of BL method

5.4.1 Effect of burn time on the amount of leached uranium

Results of extending the burn time from 16 hours to 90 hours are summarised in Table 5.12 and graphically shown in Figure 5.18.

Table 5.12: Summary of BL results of TRISO-coated particles burned for various times.

Sub-sample (20 g):	1A	2A	3A	4A	5A
Time in the furnace (hrs):	90.37	69.48	45.70	21.50	16.25
U (mg/L) ICP:	6.9	6.5	5.6	3.9	3.6

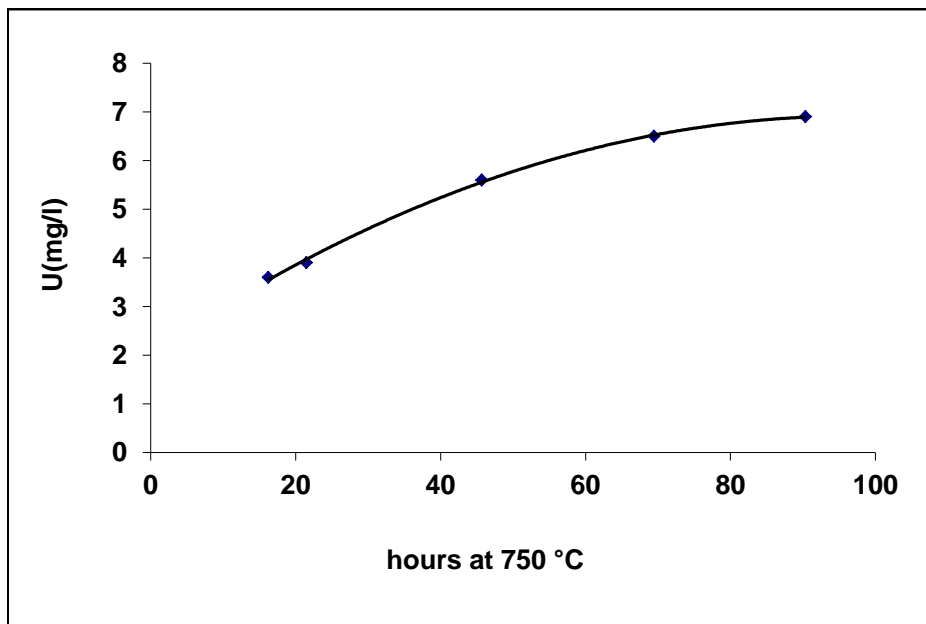


Figure 5.18: Uncontained uranium (mg/l) released as a function of the burn time (hours).

The amount of uncontained uranium leached was increasing as observed in Figure 5.18 with either two or three broken particles but clearly increasing monotonically between 16 and 46 hours. This could be observed by the smooth spacing of the concentration values, which did not reflect discrete particle breakage behaviour. It was observed that a gradual increase in the uranium concentration was smaller than one coated particle equivalent and it became even smaller as the curve levelled out.

These results were obtained for a fixed leach time of 16 hours whilst the burn time varied. Note that the results were obtained not from a single sample but from five randomly selected samples of ~ 15 000 coated particles each. If the results were due to random broken particles in the respective samples, without any effects due to varying burn times, it would be expected that the uranium content would vary statistically over the five samples. The smooth nature of the curve suggested that the samples released uranium due to a certain underlying mechanism, starting at the same baseline value for 16 hours burn time with increasing release as the burn time was increased.

The smooth increase and the small incremental uranium releases strongly argued against particle fracture as the function of time. Note also that the curve did not have a constant slope, which argued against failure mechanisms that predicted a fixed number of failures per unit time. An explanation that fitted the observations better was the following:

The apparent common baseline and smooth increase suggested that a fraction of the TRISO-coated particles, common to all the samples and large enough in number to smooth out statistical variations, was involved in the uranium release. This meant that BL results could be explained best by leaky particles. Figure 5.19 is a schematic representation of the proposed mechanism for the abnormal release of uranium from TRISO particles.

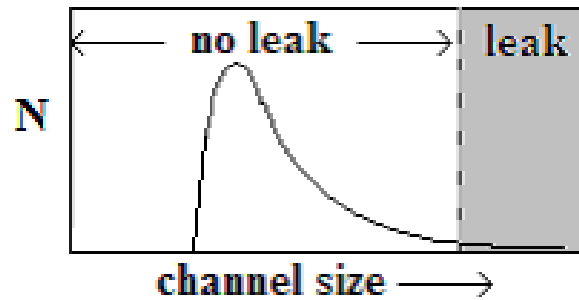


Figure 5.19: A schematic representation of a log normal leak channel size distribution.

Layers might have small meandering channels formed by linked porosity or some other defects such as carbon inclusions. The exact nature was not known and could not be derived from BL results alone. A fairly large and comparable number of particles in each sample might therefore leak at a rate much lower than broken or damaged particles. After 16 hours in the furnace a probably sufficient carbon was removed from these particles, causing a partial leaching of uranium. Because of the partial nature of the process, the 16 hours of leaching applicable to broken particles would now probably not be sufficient to remove all of the available uranium. Longer periods in the furnace might have opened up more channels, thus leading to an increase in uranium released. The gradual decrease in slope indicated saturation as fewer and fewer remaining channels became available with longer burning. The maximum uranium content was determined by the number of outliers at the tail end of the distribution which would have contained large enough channels to allow the leak mechanism to manifest. SiC layers which behaved in this way were not ideal for the fission product confinement. Fission gas, which was under high pressure inside the SiC layers in the reactor, would leak out at a steady rate into the coolant gas flow. A test with a fixed leach time and a variable burn time could be useful to test for the integrity of the SiC layers in this way as opposed to a normal BL test.

Another experiment was performed to validate that at least all the carbon outside the SiC layers of the coated particles was effectively removed after 16 hours of burning at 750°C in a muffle furnace. A known mass of coated particles from the batch CPT-T-D16 was placed in the furnace for 16 hours and accurately weighed after cooling. The same sample was placed in the furnace for a further 16 hours and the mass difference evaluated. The results are shown in Table 5.13.

Table 5.13: Mass difference for 16- and 32-hour burn times.

Sample	Burn time(h)	Mass in gram of crucible + sample
CPT-T-D16-A	16.87	71.5743
CPT-T-D16-B	32.43	71.5747

No significant difference in mass between 17 hours and 32 hours was observed, indicating completion of the burn process after 16 hours. This study also showed that there was no obvious corrosion of the SiC layer under these high temperature oxidising conditions. Vix-Guterl *et al.* 1993 found that the SiC-based fibers and SiC matrix are oxidised leading to the formation of silica layers at temperature ranges 900-1200 °C. It can be concluded that a temperature of 750 °C is low enough to prevent the corrosion of the SiC layer of TRISO particles as there was no observed changes in mass.

A 16-hour burn-off time was thus confirmed to be long enough to remove at least all the carbon outside the SiC layers. As it would be observed later, it was also long enough to remove all the inside carbon from broken or damaged particles. For all the experiments performed in this dissertation the burning/oxidation of TRISO particles was carried out under atmospheric pressure conditions and the diffusion of the oxygen was driven by the concentration gradient. There was no external pressurisation. The evidence obtained from the SiC shards after burning seemed to suggest that more often than not the cracked SiC shells broke into distinguishable shells during the burning step.

5.4.2 Effect of leaching time on the amount of uranium released

Multiple leaching results of samples 4A and 5A are summarised in Table 5.14. These samples were leached three more times than the usual, meaning that they were leached for three additional steps of 16 hours. Uranium leach solutions were analysed by the ICP-OES for the concentration values above 1 mg/L and with ICP-MS for the lower range. Sample 4A (21.5 h burn time) practically had all its uranium leached out after the first leach step whereas sample 5A (16.25 h burn time) had a further small release for the leach step two.

Table 5.14: Decrease in uranium concentration ($\mu\text{g/L}$) with successive leach steps.

Leach #	Uranium concentration in $\mu\text{g/L}$ for samples:	
	CPT-T-C7-4A (21.5 h burn)	CPT-T-C7-5A (16.25 h burn)
1	3900	3600
2	1	921
3	<1	27
4	27	33

Results of the leach experiments were in general agreement with the finding that batch CPT-T-C7 released uranium unlike the typical broken particles. Results seem to support the idea that 16 hours leach time was sufficient to leach uranium through the defects in SiC layers that were broken/cracked, and that other defects needed longer periods to be leached out completely.

5.4.3 Defective IPyC layer

IPyC layer forms the first defence in retaining the fission products within TRISO particles. The integrity of this layer was tested by sampling the particles from the PBMR's CVD reactor after only two layers, i.e the buffer and the IPyC, had been deposited by the CVD process. These particles were then exposed to a leaching acid by putting them in 6 M HNO_3 for 2 hours. The images obtained are shown in Figure 5.20. Such images were acquired after leaching IPyC layer in 6 M HNO_3 . IPyC leach experiment was carried out for 2 hours. In all the experiments, about 1% of particles (counted in every 5 g of particles) indicated defective IPyC layers. This amount was much higher than the failed fraction obtained for the defective SiC in fresh TRISO particles. Such results suggested that there was no direct correlation between the failed IPyC layers and the broken SiC layers.

These observations were also compared to open porosity results obtained at the Oak Ridge National Lab on the OPyC of the PBMR batch CPU-L-H101. The open porosity was determined to be 0.238 mL/m^2 using mercury porosimeter. In summary, the method followed was: the sample was first evacuated, then surrounded with mercury and, finally pressure was applied to force mercury into the void spaces whilst monitoring the amount

of mercury intruded. Data of intruded volume of mercury versus applied pressure were obtained and the pressures were converted to pore sizes.

It was not strange to assume that the IPyC layer would indicate open porosity characteristics shown by the experiments in this dissertation. Petti (1988) came to the conclusion that the reason why the German program produced a superior fuel to the American program could be largely attributed to the degree of the open porosity of the IPyC layer that the German coater facility produced. He reasoned that the bonding between the IPyC and the SiC layer was stronger in the German particles. On the other hand, the American IPyC layer lacked open porosity, and this led to a less physical bonding between the IPyC and the SiC layers on the layer boundaries. The debonding between these layers during the irradiation was a dominant factor that led to the high failure rate of the American fuel. The fact that the IPyC porosity appears to be varying during leaching then also suggests that the SiC/IPyC bonding would also vary. Further studies need to be carried out to investigate whether there is a relationship between this and the reactivity or behaviour observed during the BL method.

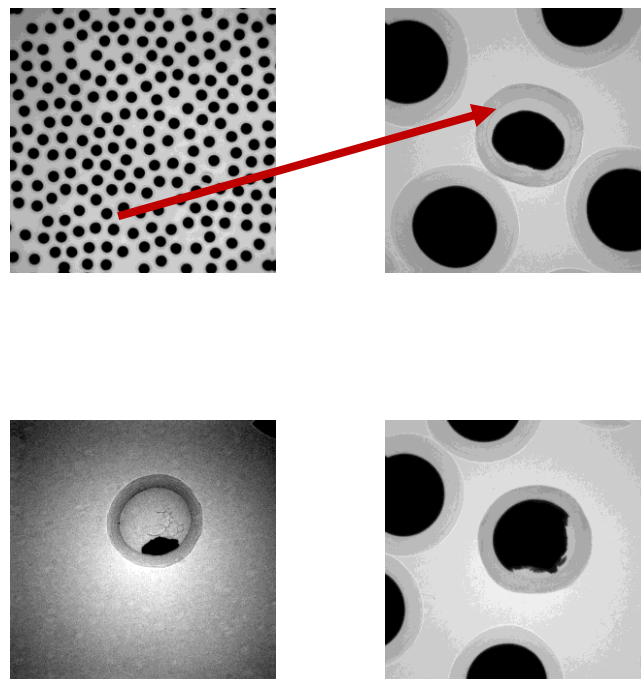


Figure 5.20: X-ray microradiographs of particles with two layers: buffer and IPyC. About 1 % of the population had defective IPyC layer that leached uranium within the first two hours in nitric acid.

It was no surprise that the PBMR ACF produced pyrolytic carbon layers with such a degree of open porosity, as the PBMR coater was manufactured according to the original AVR German coater specification.

ORNL performed characterisation of the PBMR CPU-L-H101 population as part of the collaboration in the AGR-2 fuel irradiation program. The focus here is on the findings of the characteristics of a defective IPyC layer using two different methods employed at PBMR and at ORNL. It was worth noting that at ORNL the uranium dispersion was used as an indicator of defective IPyC layers. ORNL performs this test by capturing an X-Ray image to specifically search for excessive uranium dispersion that may be caused by the high permeability in the defective IPyC layer. Particles from 40 compacts were analysed for uranium dispersion. Excessive permeability in the IPyC could result in chlorine intrusion during the deposition of the SiC, and subsequently uranium would diffuse out of the kernel into the buffer layer during heat treatment of the compact. Several anomalous particles were observed in the X-ray analysis of the CPU-L-H101 particles ($n = 60\ 879$) that were deconsolidated from 40 compacts. Three particles were identified as showing uranium dispersion that was evident of a defective IPyC layer. Figure 5.21 shows one of the defective IPyC particles. In this figure, the kernel appears as a bright circle in the centre, the dispersed uranium appears as the white arc beyond the kernel but before the SiC gray outer ring.

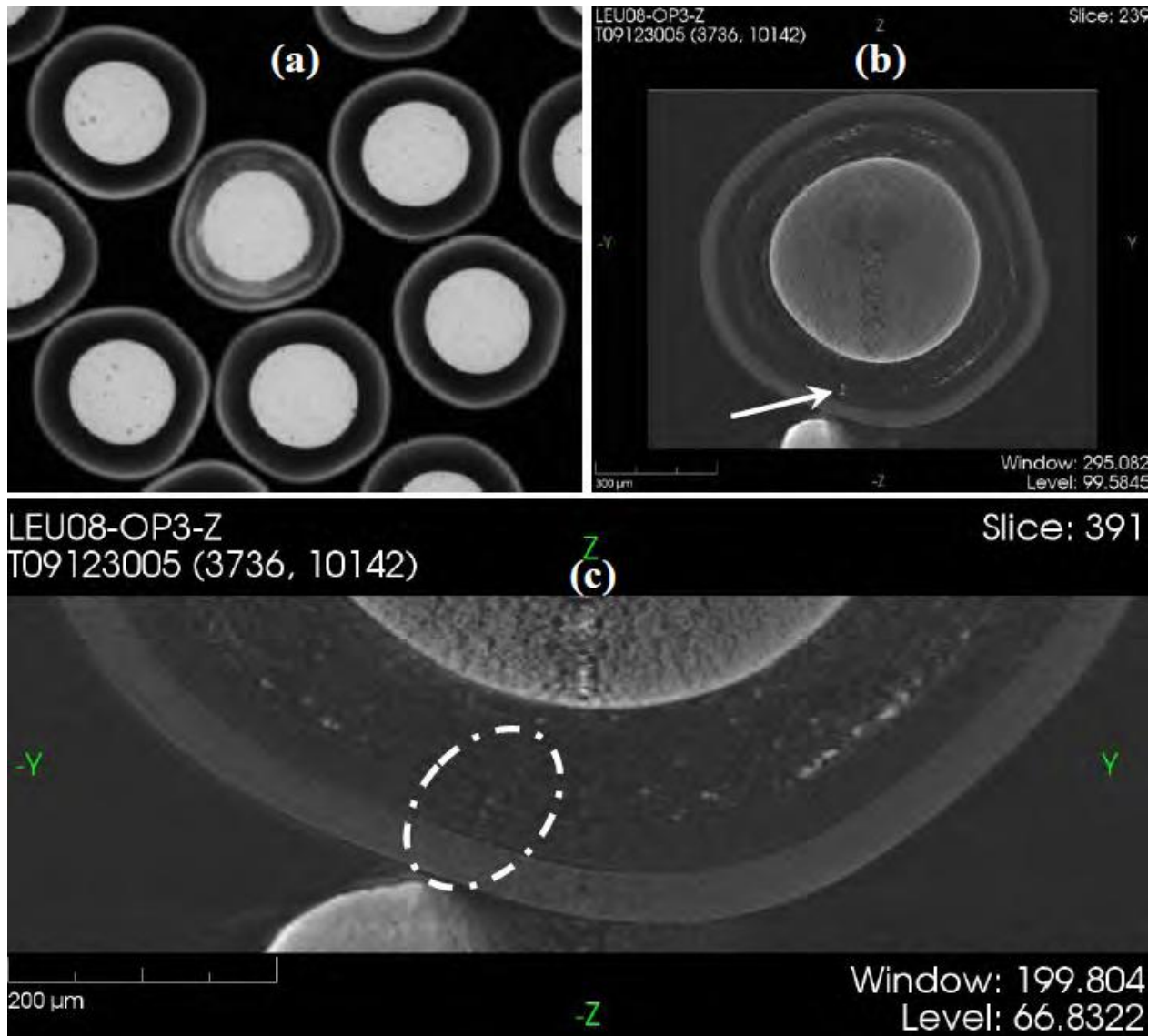


Figure 5.21: A particle with uranium dispersion caused by a crack in the IPyC layer. Low resolution X-ray image (a) and high resolution X-ray tomographs (b) and (c).

Buffer and IPyC regions should appear dark and that was not the case as shown by the arrow in Figure 5.21. However, in this particle, regions of higher density material (uranium) were dispersed throughout the buffer. Uranium tended to pile up at the buffer/IPyC interface where the outward diffusion was inhibited by the denser IPyC layer. Figure 5.22 shows another of the particles identified as having a defective IPyC layer.

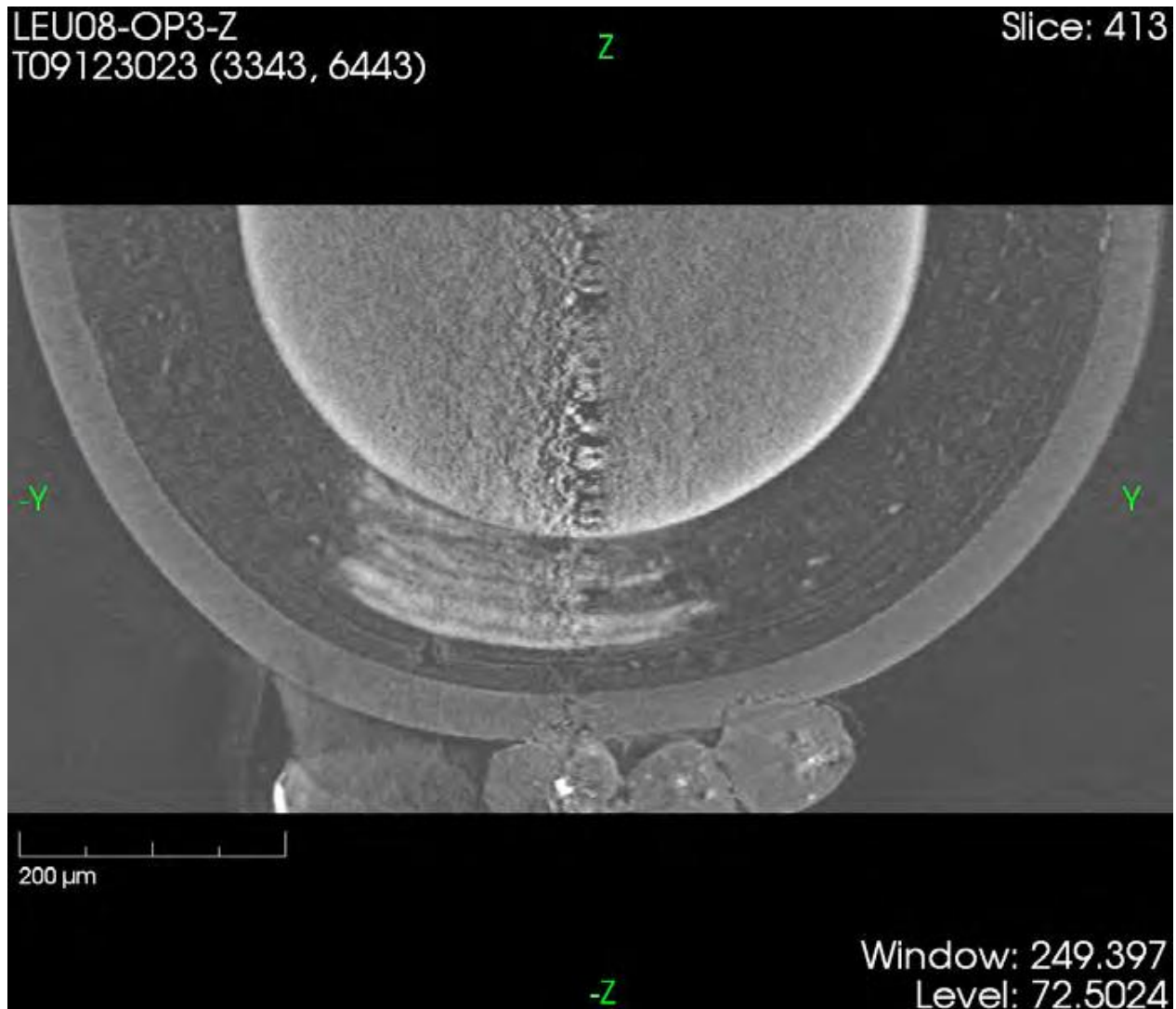


Figure 5.22: An image of a crack marked by a ring in the IPyC layer of a TRISO particle, showing uranium deposits through the crack, performed at ORNL.

This work showed that cracks on the IPyC can be successfully revealed by performing acid leach analysis of uranium in combination with X-ray imaging analysis of leached buffer + IPyC particles (as performed at PBMR) and uranium dispersion (as performed at ORNL). These works indicated that cracks do not automatically propagate from the IPyC through to the SiC and the OPyC. Some cracks will be singularly based on the IPyC alone and the uranium dispersion would cluster around that particular crack. There was no direct correlation between a defective IPyC layer and a defective SiC layer, in other words, cracks on IPyC did not propagate linearly into the SiC layer during the manufacture of TRISO particles. The fact that on average 1 in 100 particles indicated a defective IPyC and only 1 in 75 000 (see Advance fuel in Table 5.16) TRISO particles indicated a broken/cracked SiC layer, is in agreement with the above observations.

5.5 Statistical treatment of the BL results

5.5.1 Fresh fuel

In section 5.3.4, the results obtained from BL test of fresh fuel spheres were reported. In this section a statistical treatment of those results by the use of Poisson distribution was performed. Poisson distribution describes the statistical distribution of the number of failed coated particles per fuel sphere. BL test results of German Low Enriched Uranium (LEU) fuel spheres that were produced from 1985 to 1988 (AVR 21-2 and Proof Test batches) were compared to the advanced (LEU) fuel achieved so far at PBMR (Venter 2003). Table 5.15 summarises the results obtained by the two organisations. A total of 40 fuel spheres were tested for the AVR 21-2 program, a total of 10 fuel spheres for the Proof Test and a total of 5 fuel spheres for the PBMR's Advanced Fuel.

Table 5.15: A comparison of BL results of fuel spheres using Poisson distribution.

No of BL tests with	AVR 21-2	Proof test	Advance fuel
n = 0	38	8	4
n = 1	1	1	1
n = 2	1	1	0
n = 3	0	0	0
n = 4	0	0	0
n = 5	0	0	0
n = 6	0	0	0
n ≥ 7	0	0	0
Total	40	10	5
Failed coated particles	3	3	1
Total coated particles	382 400	146 000	75 000

Due to the average number of failed coated particles per fuel sphere being small and the lower limit close to zero, the one-sided upper confidence level was used for the statistical analysis of the Poisson distribution.

The observed average number of failed coated particles per fuel sphere was:

$$\lambda = \frac{3}{40} = 0.075 \text{ for the AVR 21-2 program;}$$

$$\lambda = \frac{3}{10} = 0.3 \text{ for the Proof test program;}$$

$$\lambda = \frac{1}{5} = 0.2 \text{ for the PBMR advance fuel program.}$$

The 95% upper limit confidence levels calculated using the modified Wald method (Clopper and Pearson 1934) for the campaigns were:

8.23 (for 382 400 particles), 6.08 (for 146 000 particles) and 3.20 (for 75 000 particles).

The PBMR seemed to have produced good fuel during the Advance Fuel production campaign conducted in 2008. There was a good agreement between the results of the German Proof test and the PBMR campaigns.

5.5.2 Sampling risks of the BL method

This section gives a summary of the calculations used to better understand the risks involved to appreciate the uncertainties during the process of sampling TRISO-coated particles.

The nominal mass of a single TRISO particle is ~ 1.3 mg, the mass of a single sample of TRISO particles taken in this study was 20 g. The total number of particles in 20 g is 15 385 discrete particles and 3 x 20 g corresponds to 46 154 particles, 6 x 20 g corresponds to 92 308 particles. A total population of 8kg TRISO particles is 400 x 20 g which corresponds to 6.2 million particles.

Risks associated with each sampling plan were computed and Table 5.16 and Figure 5.23 give summary of the findings of this study. Figure 5.23 was computed to demonstrate the relationship between the proportion of defectives and the probability of accepting a given sampling plan. It was worth noting that the consumer's risk, β (see chapter 3 for the definitions) was the highest, 92.5%, when only 15 385 TRISO particles were inspected by the burn-leach method. To reduce this risk to 5.6%, 10 x 20 g TRISO particles would have to be tested by the burn-leach method, and to reduce this risk to 0.1%, 20 x 20 g TRISO particles would have to be tested by the BL method. Of course, a zero risk occurred when 100% inspection of the TRISO particles was performed and that is economically meaningless as no fuel would be available to be loaded onto the nuclear

reactor if this was done. To reduce the risk of accepting a failed population of TRISO particles to 0.1% implied that a 99.9% confidence would be established on the integrity and quality of the TRISO particles that would be used to manufacture the fuel spheres. These computations demonstrated the evidence of the very high quality control costs inherent in the characterisation of TRISO fuel.

BL method is a destructive test, added to this, there were additional destructive tests that were performed during the characterisation of the TRISO particles such as the measurement of layer thicknesses, layer densities and the Bacon anisotropy factor to mention but a few. Also, after the manufacture of the fuel spheres, the burn-leach testing would be required for the quality assurance of the integrity of the fuel spheres. For quality control purposes, at least 20 fuel spheres would need to be tested. The ultimate consequence of these characterisation activities was that around 10% (800 g) of the original TRISO particle production would have been destroyed by the burn-leach test alone.

This study intended to determine the efficiency of BL test by examining at least ten different populations of TRISO particles which were manufactured under normal operating conditions known as Standard Quality. At such high sampling levels of 20 x 20 g TRISO particles, it would be impossible to perform all these tests for all the ten populations given the available resources. The investigator decided to settle for a sampling level of 6 x 20 g TRISO particles for the ten populations. Such a plan resulted in $\alpha = 23.7\%$ and $\beta = 23.1\%$ ($n = 92\ 308$). This meant that the risk of rejecting a good population of TRISO particles from the CVD coater based on the burn-leach results was 23.7%, whereas the risk of accepting a bad population of TRISO particles by the fuel sphere manufacture facility based on the burn-leach results was 23.1%. These values might look very high but for the purpose of completion and the establishment of trends in this study, these levels were deemed to be acceptable. The fuel that was used was depleted and was not going to be irradiated in a nuclear reactor.

Six samples of 20 g each were taken from each population of the ten populations used in this investigation. A total of 60 samples equivalent to 923 100 TRISO particles were inspected. Table 5.17 is summarised graphically in Figure 5.24 to show risks associated with each sampling plan.

Table 5.16: Design of acceptance sampling plans for BL test of particles.

Proportion defective	<i>Pa (Cumulative Poisson Probabilities) for values of n</i>							
<i>P</i>	46 154	76 923	92 308	123 077	153 846	230 769	307 692	769 231
0.000001	0.999	0.997	0.995	0.993	0.990	0.978	0.963	0.818
0.000002	0.995	0.990	0.986	0.974	0.963	0.925	0.870	0.542
0.000003	0.990	0.978	0.969	0.945	0.925	0.844	0.763	0.332
0.000004	0.982	0.963	0.945	0.910	0.870	0.763	0.663	0.188
0.000005	0.978	0.945	0.925	0.870	0.809	0.663	0.542	0.0995
0.000006	0.969	0.925	0.894	0.827	0.763	0.592	0.4485	0.056
0.000007	0.957	0.894	0.861	0.791	0.699	0.525	0.355	0.029
0.000008	0.945	0.870	0.827	0.736	0.663	0.4485	0.2875	0.015
0.000009	0.932	0.844	0.800	0.699	0.592	0.3805	0.231	0.008
0.00001 (AQL)	0.925	0.818	0.763	0.663	0.558	0.3315	0.185	0.004
0.000012	0.894	0.763	0.699	0.558	0.4485	0.231	0.1165	0.001
0.000014	0.861	0.718	0.627	0.493	0.355	0.171	0.085	0
0.000016	0.827	0.663	0.558	0.406	0.2875	0.1165	0.044	
0.000018	0.800	0.592	0.493	0.355	0.231	0.078	0.0265	
0.00002	0.763	0.542	0.4485	0.2875	0.185	0.056	0.015	
0.000022	0.736	0.493	0.406	0.249	0.147	0.037	0.009	
0.000024	0.699	0.449	0.355	0.199	0.1165	0.027	0.005	
0.000026	0.663	0.406	0.308	0.171	0.092	0.017	0.003	
0.000028	0.627	0.355	0.267	0.1365	0.072	0.011	0.002	
0.00003 (LTPD)	0.592	0.332	0.231	0.1165	0.056	0.008	0.001	
0.000032	0.558	0.288	0.199	0.0995	0.044	0.005	0.001	
0.000034	0.525	0.267	0.185	0.078	0.034	0.004	0	
0.000036	0.493	0.231	0.159	0.066	0.027	0.003		
0.000038	0.464	0.215	0.1365	0.052	0.019	0.001		
0.00004	0.449	0.185	0.1165	0.04	0.015	0.001		
0.000042	0.420	0.171	0.092	0.034	0.011	0.001		
0.000044	0.406	0.147	0.085	0.029	0.009	0		
0.000046	0.381	0.1365	0.072	0.024	0.007			
0.000048	0.355	0.1165	0.066	0.017	0.005			
0.00005	0.332	0.0995	0.056	0.015	0.004			
0.000052	0.308	0.092	0.048	0.012	0.003			
0.000054	0.288	0.078	0.04	0.01	0.003			
0.000056	0.267	0.072	0.034	0.009	0.002			
0.000058	0.249	0.061	0.029	0.007	0.001			
0.00006	0.231	0.056	0.0265	0.005	0.001			
0.000062	0.215	0.052	0.0225	0.004	0.001			
0.000064	0.199	0.044	0.019	0.003	0.001			
0.000066	0.185	0.037	0.016	0.003	0			
0.000068	0.180	0.034	0.0135	0.002				

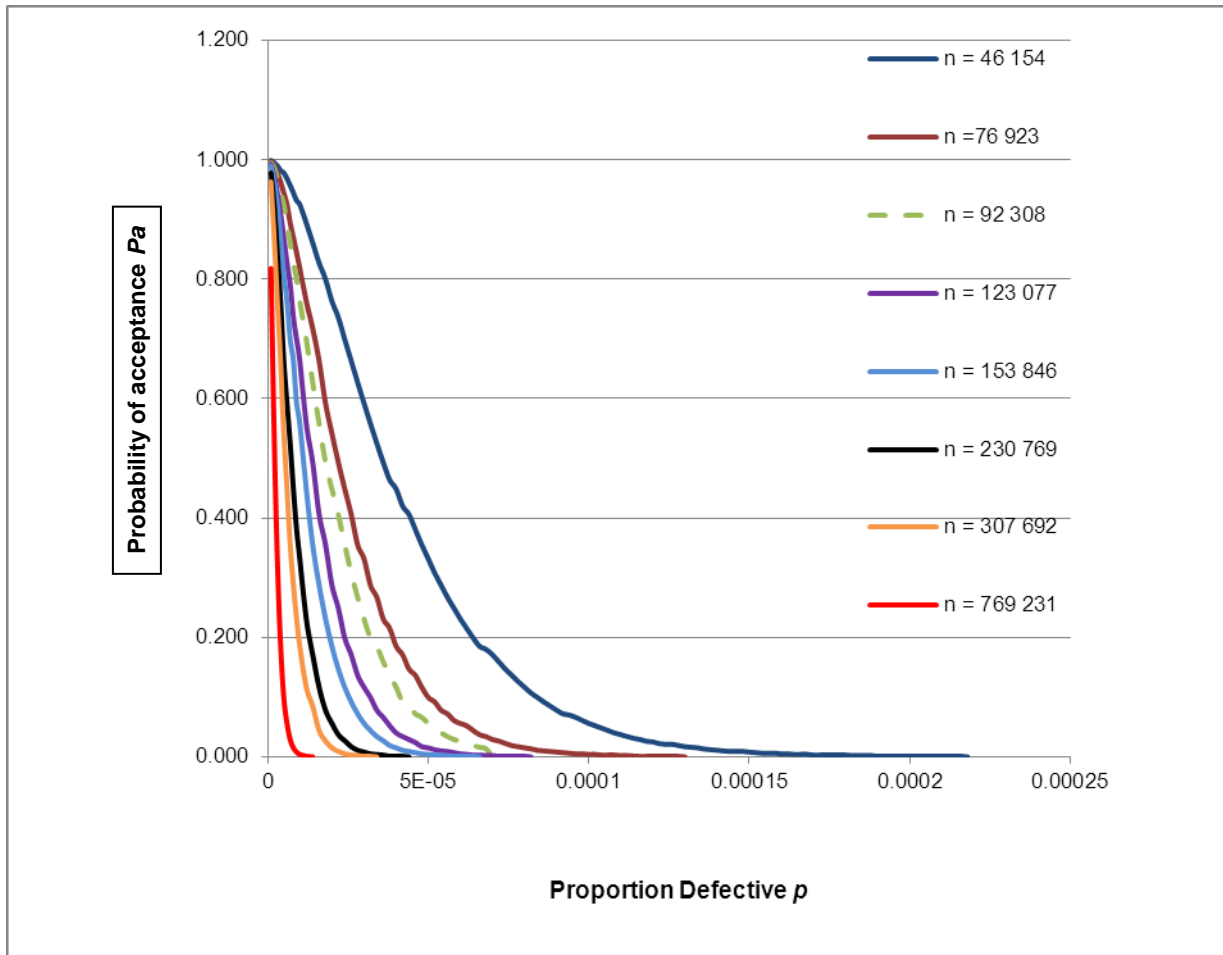


Figure 5.23: Design of acceptance sampling plans. Steep curves indicate high sampling rates or large sample sizes. Dashed line indicates the sampling rate employed in this study.

Table 5.17: Producer's risk (α) and consumer's risk (β) computed for each sampling plan.

Sample size n	Producer's risk (α)	Consumer's risk (β)
15 385	0.010	0.925
46 154	0.075	0.592
76 923	0.182	0.332
92 308	0.237	0.231
123 077	0.337	0.117
153 846	0.442	0.056
230 769	0.669	0.008
307 692	0.815	0.001
769 231	0.996	<0.001

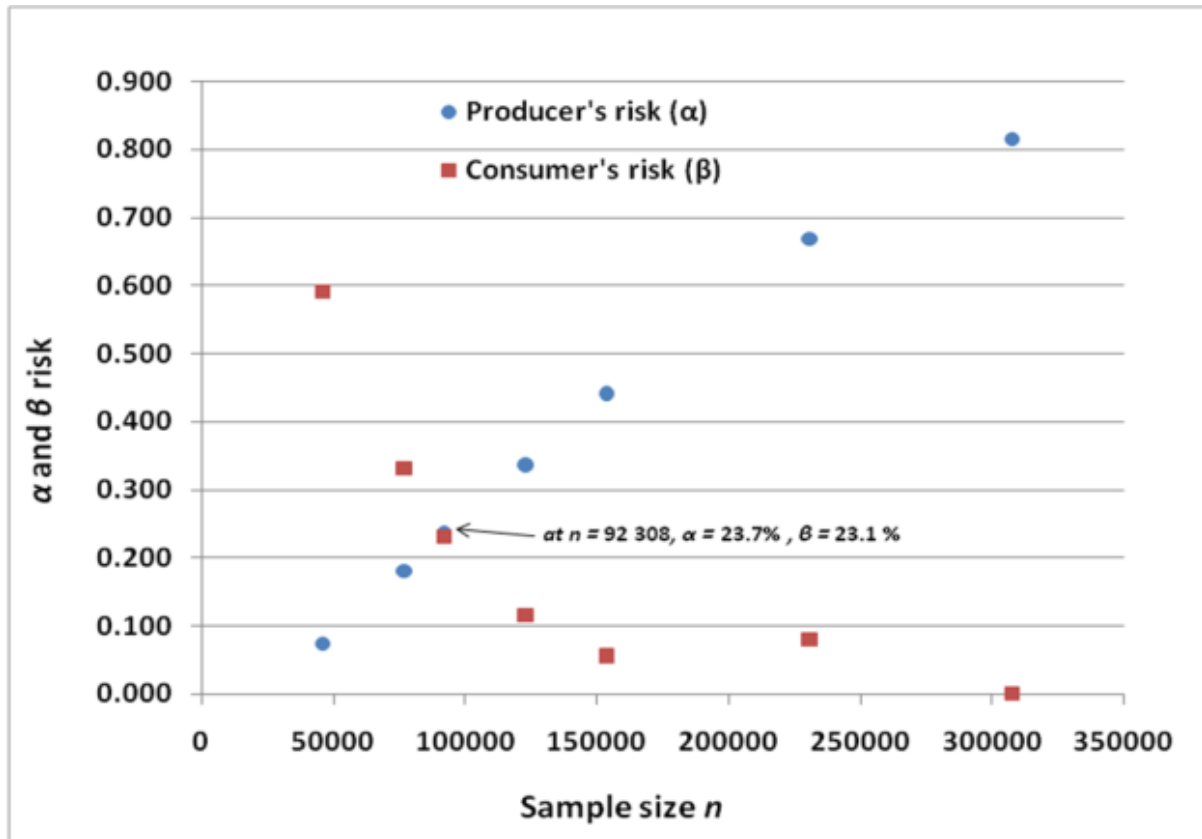


Figure 5.24: An outline of risks associated with each sampling plan.

CHAPTER 6

6. CONCLUSION AND RECOMMENDATIONS

6.1 Conclusion

Although particles with cracked or broken SiC layers were successfully determined by the BL method, few particles with a defective SiC layer indicated occurrences of 'slow leaching'. It is hereby concluded that 16 hours of leaching of TRISO particles in an acidic medium is not sufficient for defective particles that indicated the partial leach mechanism. Results from such particles were inconclusive. It became evident that defective TRISO particles could not only be described by cracked or broken particles. These findings seem to agree with other workers elsewhere (Myers 1989, Adams 1983, Adams and Partain 1987).

Some findings in this work are in slight conflict with the observations of the earlier researchers of TRISO particles. They documented that coated particles which partially leach uranium through the SiC layer did not exist.

It is hereby concluded that neither BL nor LBL is sufficient to be used alone to characterise the number of particles with defective SiC layers in a given TRISO particle population.

BL and LBL tests can only be used to indicate problems when uncontained uranium was above the background levels and those particular batches should be subjected to extended acid leach times, and the BL tests must be combined with complementary techniques that were employed in the study.

It is hereby concluded that oxidation times of 96 hours at 750 °C at standard pressure do not negatively affect the mechanical strength of the silicon carbide layer of fresh TRISO particles, as these did not indicate high failure fractions after BL test.

From the study of IPyC integrity it is hereby concluded that not all cracks on the IPyC layer propagate through to the SiC layer.

6.2 Recommendations

Further investigations, in conjunction with complementary techniques such as high resolution tomography and scanning electron microscopy, were recommended to fully understand the slow leach mechanism that was discovered in certain defective TRISO particles.

Thermogravimetric analysis (TGA/DTA or TGA/DSC) techniques should be explored in future to study the thermolysis of particles. Moreover, reactivity of the SiC layer with various reactive gases needs to be investigated.

Future studies should investigate the impact of the SiC/IPyC interface (bonding) on the reactivity or behaviour observed during the BL method as this area was not covered by this study. More work has to be performed to characterise the porosity of the IPyC layer as this is important in the better understanding of the failure mechanisms in IPyC layers.

More kinetic data has to be acquired from the extended leaching experiments. Such data should be fitted to either first, second or pseudo-order rate laws. Those efforts would help in determining whether the most likely leaching mechanism was diffusion limited or concentration limited.

BIBLIOGRAPHY

Adams, C.C. and Partain, K.E., Heavy Metal Removal QC Method Selection. GA Internal Memorandum, GA Technologies Inc., San Diego, 1987.

Adams, C.C., US/FRG TRISO Coated ThO₂ Particle Studies. GA Technologies Inc., 906932/1, San Diego, 1983.

Agresti, A. and Coull, B.A., Approximate is better than "Exact" for interval estimation of binomial proportions. *The American Statistician*, 52 (1998) 119-126.

Association of German Engineers (VDI), the Society for Energy Technologies. AVR-Experimental High Temperature Reactor, 21 Years of Successful Operation for a Future Energy Technology. Germany, ISBN-3-18-401015-5, (1990) 9-23.

Bassak, U., High Temperature Gas Cooled Reactor Fuels and Materials. Viena: IAEA, IAEA-TECDOC-CD-1645, ISBN:978-92-0-153110-0, 2010.

Clopper, C.J. and Pearson, E.S., The use of confidence or fiducial limits illustrated in the case of the binomial. *Biometrika*, 26 (1934) 404-413.

Cohen, M.E. and Whiting, C.D., Method of identifying Defective Particle Coatings. Patent, USA 4591478, Filed 26 August 1983.

Cohen, M.E., Preliminary Test Techniques for Defective Particle Detection. GA Technologies Inc., 906513/1, San Diego, 1982.

DelCul, G.D., Spencer, B.B., Mattus, H., Collins, E.D., TRISO Coated Fuel Processing to support High-Temperature Gas-Cooled Reactors. Oak Ridge National Laboratory, Tennessee, 2005.

Ehrburger, H. and Vix-Guterl, C., Effect of thermal treatment on the reactivity of SiC-based fibres. *J. Mat. Sci.*, 31 (1996) 5363-5371.

Fukasawa, T. and Ozawa, Y., Relationship between dissolution rate of uranium dioxide pellets in nitric acid solutions and their porosity. *Radioanalytical and Nuclear Chemistry*, 106 (1986) 345-356.

Goodin, D.T. and Nabelek, H., US/FRG Accident Condition Fuel Performance Model. GA Technologies Inc., DOE Report HTGR-85-107, GA Document 908293/N/C, San Diego, 1985.

Goodin, D.T., Final Report on FY-85 SiC Defect Detection. GA Technologies Inc., 907870/N/C, San Diego, 1985.

Guillermier, P. and Phelip, M., Areva and Cea Fuel Development and Qualification program of HTR Fuel, Proceedings of the HTR 2006 meetings, 3rd International Topical Meeting on High Temperature Reactor Technology, Johannesburg, South Africa, October 1-4, 2006.

Hasegawa, A., Kohyama, A., Jones, R.H., Snead, L.L. and Riccardi, B., Critical issues and current status of SiC/SiC composites for fusion. *J. Nucl. Mater.*, 283 (2000) 128-137.

Heit, W., Huschka, H. and Rind, W., Status of Qualification of High-Temperature Reactor Fuel Element Spheres. *Nucl. Technol.* 69 (1985) 44-54.

Helary, D., Dugne, O., Bourrat, X., Jouneau, P.H. and Cellier, F., EBSD investigation of SiC for HTR particles. *J. of Nucl. Mater.*, 350 (2006) 332-335.

Hirai, T. and Sasaki, M., Silicon Carbide Prepared by Chemical Vapor Deposition. *Silicon carbide ceramics*, 1 (1991) 77-98.

Huhn, J.D., Results from ORNL Characterisation of German Reference Fuel From EUO 2358-2365 Composite. Oak Ridge National Laboratory, Tennessee, 2002.

Ikawa, K., Kobayashi, F. and Iwamoto, K., Failure of Coated Fuel Particles during Thermal Excursion above 2000°C. *J. Nucl. Sci. Techno.*, 15 (1978) 774-779.

Inomata, Y., Crystal Chemistry of Silicon Carbide. *Silicon carbide ceramics*, 1 (1991) 1-11.

Kadak, A.C., A Future for Nuclear Energy: Pebble Bed Reactors. *International J. Critical Infrastructures*, 1(2005) 330-345.

Katoh, Y., Snead L.L. and Henagar, C., Current status and critical issues for development of SiC composites for fusion applications. *J. Nucl. Mater.*, 367 (2007) 659-671.

Katz, J.J. and Seaborg, G.T., *The Chemistry of the Actinide Elements*. London. John Wiley & Sons Inc., New York, 1957.

Kim, K.S., You, G.S., Min, D.K., Ro, S.G. and Kim, E.K. Oxidation Behaviour of Unirradiated and Irradiated UO₂ in Air at 150-375°C. *Korean Nuclear Society*, 29 (1997) 93-98.

Kim, W.K., Lee, Y.W., and Park, J.Y., Nondestructive Measurement of the Coating Thickness in the Simulated Triso-Coated Fuel Particle for the HTR. Proceedings of the HTR 2006 meetings, 3rd International Topical Meeting on High Temperature Reactor Technology, 2006.

Kim, Y.S., A thermodynamic Evaluation of the U-O system from UO₂ to U₃O₈. *J. Nucl. Mater.*, 279 (2000) 173-180.

Kleykamp, H., Schauer, V., and Skokan, A., Oxidation behaviour of SiC fibre reinforced SiC. *J. Nucl. Mater.*, 227 (1995) 130-137.

Kovacs, W.J., Characterisation of Defective SiC Coatings in TRISO HTGR Fuel Particles. General Atomics Company, DOE Report GA-A16215, San Diego, 1981.

Krajewski, L.J. and Ritzman, L.P., Operations Management, Processes and Value Chains, 7th Ed., Supplement i, pages I1-I15.

Krockel, H., Merz, M. and van der Biest, O., Ceramics in advanced energy technologies. Proceedings of the European Colloquium held at the Joint Research Centre, The Netherlands, Petten, 20-22 September 1982.

Kurishita, H., Yoshinaga, H., and Ikuhara, Y., Grain Boundary and High-Temperature Strength in SiC. *Silicon carbide ceramics*, 1 (1991) 185-211.

Layton, F.L., Evaluation of Techniques for Detecting Defective Silicon Carbide Coatings. Oak Ridge National Laboratory, ORNL/NFW-78/5, Tennessee, 1978.

McEachern R.J., A review of kinetic data on the rate of U_3O_7 formation on UO_2 . *J. Nucl.Mater.*, 245 (1997) 238-247.

Minato, K., Fukuda, K. and Ikawa, K., Strength of Silicon-Carbide Coating Layers of Fuel particles for High Temperature Gas-Cooled Reactors. *J. Nucl.Sci.Techno.* 19 (1982) 69-77.

Myers, B.F., An Assessment of the methods for determining defect or failure fractions in HTGR coated particle fuels and their relationship to particle microstructure: Oak Ridge National Laboratories, ORNL/TM-10805, Tennessee, 1989.

Nozawa, T., Hinoki, T., Hasegawa, A., Kohyama, A., Katoh, Y., Snead, L.L. and Henager, C.H., Recent advances and issues in development of silicon carbide composites for fusion applications. *J. Nucl. Mater.*, 386 (2009) 622-627.

Otsuka, A., Matsumura, Y., and Hosono, K., Long term oxidation of a SiC fibre-bonded composite in air at 1 500 °C. *J. Eur. Ceramic Society*, 23 (2003) 3125-3134.

Partain, K.E., Status Report-SiC Defect Detection. GA Technologies Inc., San Diego, 1984.

Petti, D.A., Maki, J.T., Buongiorno, J., Hobbins, R.R. and Miller, G.K., Key differences in the fabrication of US and German TRISO-coated particle fuel, and their implications on fuel performance. Oak Ridge National Laboratory, Tennessee, 1985.

Rogers, T., Vapour deposited silicon carbide. Extremely Hard Materials for Micromechanics (Digest No: 1997/059), Date 24 April 1997.

Ross, S.M., Probability Models, seventh ed., Orlando, Florida, Academic Press, (2000) 141-160.

Rousseau, G., Desgranges, L., Charlot, F., Millot, N., Niepce, J.C., Pijolat, M., Valdivieso, F., Baldinozzi, G. and Berar, F., A detailed study of UO_2 to U_3O_8 oxidation phases and the associated rate-limiting steps. *J. Nucl.Mater.*, 355 (2006) 10-20.

Safi, S. and Kazezamdeh, A., MCMB-SiC composites; new class high temperature structural materials for aerospace applications. *Ceramics International*, 39 (2013) 81-86.

Safi, S. and Rad, R.Y., In situ synthesis of nano size silicon carbide and fabrication of C SiC composites during the siliconization process of mesocarbon microbeads preforms. *Ceramics International*, 38 (2012) 5081-5087.

Sha, J.J., Hinoki, T., and Kohyama, A., Microstructural characterization and fracture properties of SiC-based fibers annealed at elevated temperatures. *J. Mat. Sci.*, 42 (2007) 5046-5056.

Snead, L.L, Nozawa, T., Katoh, Y., Byun, T.S., Kondo, S. and Petti, D.A., Handbook of SiC properties for fuel performance modelling. *J. Nucl.Mater.*, 371 (2007) 329-377.

Spencer, B.B., Del Cul, G.D. and Collins, E.D., Processing of spent TRISO-coated Gen IV Reactor fuels. Oak Ridge National Laboratory, 37831, Tennessee.

Terry, W.K., Ougouag, A.M., Kloosterman, J.L., van Rooijen, W.F.G. and Gougar, H.G. Investigation of Bounds on Particle packing in Pebble-Bed High Temperature Reactors. *Nucl. Eng. And Design* 236 (2006) 669-676.

Tremaine, P.R., Chen, J.D., Wallace, G.J. and Boivin, W.A., Solubility of uranium (IV) Oxide in alkaline aqueous solutions to 300°C. *J. Solution Chemistry*, 10 (2004) 221-230.

Venter, J.H., Free Uranium in Fresh Fuel, PBMR Document 025549, Pretoria, 2004.

Venter, J.H., Fuel design bases report revision 2. PBMR 025140, Pretoria, 2006.

Venter, J.H., Statistical base for irradiation test design and interpretation of results. Pretoria, PBMR Document 015089, 2003.

Wawner Jr., F.E., Boron and SiC Fibers. *Comprehensive Composite Maerials*, 1 (2000) 85-105.

Weber, G.W., Beatty, R.L., Tennery, V.J. and Lackey Jr., W.J. The Effect of Pyrocarbon Coating Permeability on Uranium Redistribution in High Temperature Gas-Cooled Reactor Fuels. International Conference on Metallurgical Coatings, San Francisco, USA, April 5-8, 1976.

Weldon, E.D., QC Laboratory. GA Technologies Inc., San Diego, 1987.

Wikipedia, The Free Encyclopedia, 2013, accessed 1 May 2013,
<http://en.wikipedia.org/wiki/Pebble_bed_reactor>.

Wruss, W., Kubel, F. and Wilhelm, M., XRD investigation of Si–SiC composites with fine SiC microstructure. *Powder Diff.*, 16 (2001) 42-45.

Zazula, J.M., Project Note On Graphite Transformations at High Temperature and Pressure Induced by Absorption of the LHC Beam. CERN-SL, 1997.

Zinkle, S.J., Ice, G.E., Miller, M.K., Pennycook, S.J. and Wang, X.L., Advances in microstructural characterisation. *J. Nucl. Mater.*, 386 (2009) 8-14.

APPENDICES

APPENDIX A: EQUIPMENT AND REAGENTS

1. Sample Preparation (metallographic cross sections)

- a. PR-10 Mounting Press (Leco)
- b. Tetrapol-2 (Struers)
- c. SiC used 1 200 μ m piano

2. OIAS System

- a. Olympus Microscope system
- b. Vanox-T, Olympus SZX9

3. RIFFLING

- a. Rotary Sample Divider (Fritsch)
- b. Vibratory Feeder system

4. SORTING

- a. Rwe Nukem GmbH
- b. Aviteq controllers, Vibtronic SFA

5. FURNACES

- a. UltraFurn, SA (Pty) Ltd

6. REFLUX SYSTEM

- a. P Selecta (Heating mantles)
- b. Julaba water-cooling system

7. ROTAVAP

- a. Laborota-4000

8. REAGENTS

- a. 65% HNO₃, Merck

Average volume of a TRISO particle = 0.00037 cm³. Average mass of a TRISO particle = 0.0013 g, so average density of a TRISO particle = 3.5 g/cc.

APPENDIX C: The uranium content in the TRISO coated particles

The uranium content, sometimes referred to as the uranium loading is defined in this study as the total grams of uranium in a 20 g sample of TRISO particles. The nominal uranium content was 9 g in a 20 g TRISO particle sample evaluated in this study. This determination was important for the quantification of the failed fractions of the SiC layers in a population.

Figure A1 gives a summary of the total uranium content in the TRISO coated particles for the samples that were investigated in this dissertation. The uranium content was determined by the gravimetric method described in chapter 4.2.3.

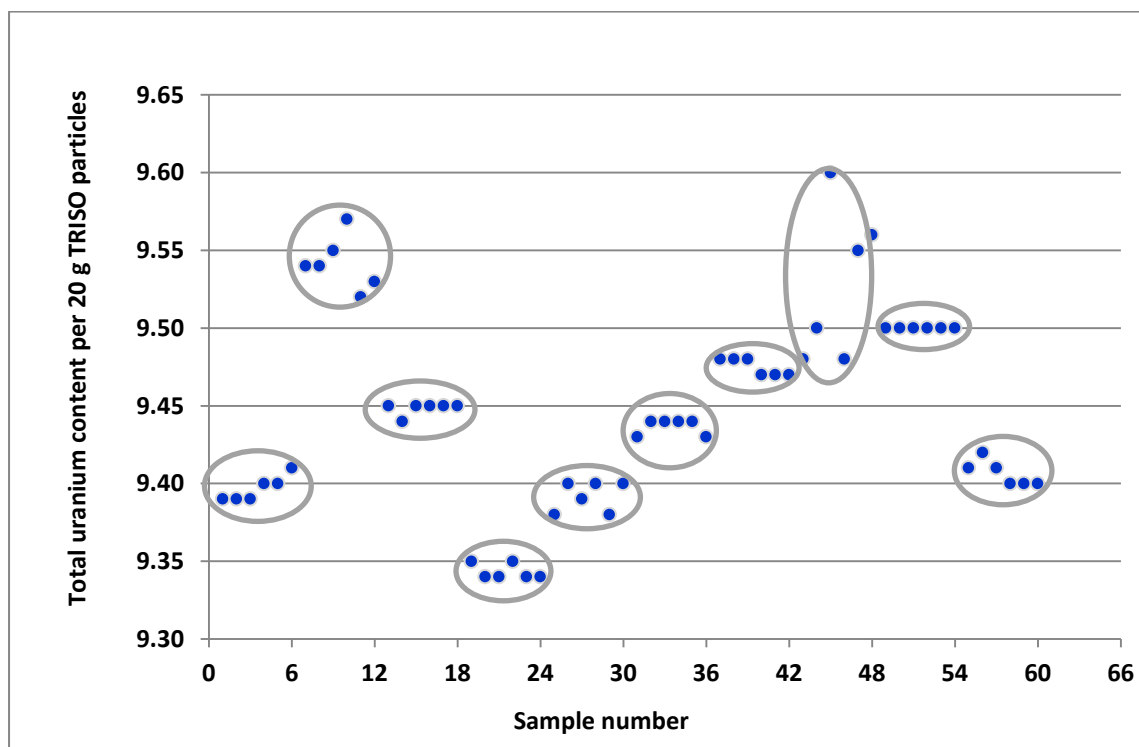


Figure A1: Total uranium content as determined for each 20 g TRISO particle sample. Sixty samples in total were analysed. The cluster analysis for each population is shown by each circle representing populations 1 through 10, produced from the PBMR ACF.

The targeted amount of the uranium content per 20 g of TRISO particles or per single fuel sphere was 9.0 g. The results obtained for the uranium content of each TRISO

particle population indicated that the conditions of the spouted bed of the furnace during the coating chemical reaction were reasonably consistent for each of the coating runs, this was seen by the clustering together of the uranium content values in Figure A1 except for the coating run number 8.

This study also noted that while the uranium content of the TRISO particles was similar within a single ACF run, the uranium content varied significantly from one coating run to the next. The reasons for this inconsistency were beyond the scope of this dissertation, and could be investigated better by the ACF scientists and engineers.

The mean total uranium present in each batch was determined as follows:

$$Total\ U = U_T = Mass\ of\ sample\ (g) \times gram\ uranium\ per\ gram\ TRISO\ coated\ particles$$

The uncontained uranium from the failed particles was determined as follows:

$$U_{uncontained}\ (\mu g) = (ICP-MS)\ result\ (mg/L) \times Volume\ (0.1L) \times (1000\ \mu g/1mg)$$

The failure fraction (ratio of uncontained uranium to total uranium present in mg/kg) was:

$$U_{uncontained}\ (mg / kg) = \frac{(ICP - MS) \times Volume}{U_T}$$

For the fuel spheres the theoretical value of 9.0 g was used for U_T .



APPENDIX D: BL results from 60 samples of TRISO coated particles

ACF population	Average uranium (g) content per batch	Uranium leached (µg) per 20 g sample
CPU-B-H101 47.0 %U/Triso particle	9.39	600
	9.39	23
	9.39	22
	9.40	6
	9.40	5
	9.41	12
CPU-B-H102 47.6 %U/Triso particle	9.54	17
	9.54	13
	9.55	500
	9.57	4
	9.52	7
	9.53	5
CPU-B-H103 47.2 %U/Triso particle	9.45	600
	9.44	95
	9.45	43
	9.45	56
	9.45	23
	9.45	6
CPU-B-H104 46.7 %U/Triso particle	9.35	600
	9.34	53
	9.34	27
	9.35	6
	9.34	7
	9.34	5
CPU-B-H105 46.9 %U/Triso particle	9.38	500
	9.40	3
	9.39	500
	9.40	14
	9.38	592
	9.40	16
CPU-B-H106 47.4 %U/Triso particle	9.43	13
	9.44	580
	9.44	12
	9.44	6
	9.44	6
	9.43	17
CPU-B-H107	9.48	25
47.3 %U/Triso particle	9.48	43
	9.48	13
	9.47	562
	9.47	2
	9.47	4
CPU-B-H108 47.4 %U/Triso particle	9.48	45
	9.50	17
	9.60	49
CPU-B-H108 47.4 %U/Triso particle	9.48	1000
	9.55	601
	9.56	*
CPU-B-H109 47.4 %U/Triso particle	9.50	1200
	9.50	134
	9.50	*
	9.50	*
	9.50	*
	9.50	564
CPU-B-H110 47.0 %U/Triso particle	9.41	62
	9.42	242
	9.41	*
	9.40	516
	9.40	*
	9.40	*

APPENDIX E: Cumulative Poisson Probabilities for Acceptance Sampling

c														
np	0	1	2	3	4	5	6	7	8	9	10	11	12	13
.05	.999	1.000												
.10	.905	.995	1.000											
.15	.861	.990	.999	1.000										
.20	.819	.982	.999	1.000										
.25	.779	.974	.998	1.000										
.30	.741	.963	.996	1.000										
.35	.705	.954	.994	1.000										
.40	.670	.938	.992	.999	1.000									
.45	.638	.925	.989	.999	1.000									
.50	.607	.910	.986	.998	1.000									
.55	.577	.894	.982	.998	1.000									
.60	.549	.878	.977	.997	1.000									
.65	.522	.861	.972	.996	.999	1.000								
.70	.497	.844	.966	.994	.999	1.000								
.75	.472	.827	.959	.993	.999	1.000								
.80	.449	.809	.951	.991	.999	1.000								
.85	.427	.791	.945	.989	.998	1.000								
.90	.407	.772	.937	.987	.998	1.000								
.95	.387	.754	.929	.984	.997	1.000								
1.0	.368	.736	.920	.981	.996	.999	1.000							
1.1	.333	.699	.900	.974	.995	.999	1.000							
1.2	.301	.663	.879	.966	.992	.998	1.000							
1.3	.273	.627	.857	.989	.998	1.000								
1.4	.247	.592	.833	.946	.986	.997	.999	1.000						
1.5	.223	.558	.809	.934	.981	.996	.999	1.000						
1.6	.202	.525	.783	.921	.976	.994	.999	1.000						
1.7	.183	.493	.757	.907	.970	.992	.998	1.000						
1.8	.165	.463	.731	.891	.964	.990	.997	.999	1.000					
1.9	.150	.434	.704	.875	.987	.997	.999	1.000						
2.0	.135	.406	.677	.857	.947	.983	.995	.999	1.000					
2.2	.111	.355	.623	.819	.928	.975	.993	.998	1.000					
2.4	.308	.570	.779	.904	.964	.988	.997	.999	1.000					
2.6	.074	.267	.518	.736	.877	.983	.995	.999	1.000					
2.8	.061	.231	.469	.692	.848	.935	.976	.992	.998	.999	1.000			
3.0	.050	.199	.423	.647	.815	.916	.966	.988	.996	.999	1.000			
3.2	.041	.171	.380	.603	.781	.895	.983	.994	.998	1.000				
3.4	.033	.147	.340	.558	.744	.871	.942	.977	.992	.997	.999	1.000		
3.6	.027	.126	.303	.515	.706	.844	.927	.969	.988	.996	.999	1.000		
3.8	.022	.107	.269	.473	.668	.816	.909	.984	.994	.998	.999	1.000		
4.0	.018	.238	.433	.629	.785	.889	.949	.979	.992	.997	.999	1.000		
4.2	.015	.078	.210	.395	.590	.753	.867	.936	.972	.989	.996	.999	1.000	
4.4	.012	.066	.185	.359	.551	.720	.844	.921	.964	.985	.994	.998	.999	1.000
4.6	.010	.056	.163	.326	.513	.686	.818	.905	.980	.992	.997	.999	1.000	
4.8	.008	.048	.143	.294	.476	.651	.791	.887	.944	.975	.990	.996	.999	1.000
5.0	.007	.040	.125	.265	.440	.616	.762	.867	.932	.968	.986	.995	.998	.999
5.2	.006	.034	.109	.238	.406	.581	.732	.845	.918	.960	.982	.993	.997	.999
5.4	.005	.029	.113	.237	.406	.572	.722	.835	.908	.950	.972	.983	.997	.999
5.6	.004	.024	.082	.191	.342	.512	.670	.797	.886	.941	.972	.988	.995	.998
5.8	.003	.021	.072	.170	.313	.478	.638	.771	.867	.929	.965	.984	.993	.997
6.0	.002	.017	.062	.151	.285	.446	.606	.744	.847	.916	.980	.991	.996	
6.2	.002	.015	.054	.134	.259	.414	.574	.716	.826	.902	.949	.975	.989	.995
6.4	.002	.012	.046	.119	.235	.384	.542	.687	.803	.886	.939	.969	.986	.994

APPENDIX F: Design of the acceptance sampling for the BL test

Proportion Defectives	# Particles		Probability of c=1 or less defects	Producer's risk	Consumer's risk
p	$n (3 \times 20g)$	np	P_a (Cumulative Poisson Probabilities)	α	β
0.000001	46154	0.05	0.999		
0.000002	46154	0.09	0.995		
0.000003	46154	0.14	0.990		
0.000004	46154	0.18	0.982		
0.000005	46154	0.23	0.978		
0.000006	46154	0.28	0.969		
0.000007	46154	0.32	0.957		
0.000008	46154	0.37	0.945		
0.000009	46154	0.42	0.932		
0.00001	46154	0.46	0.925	0.075	
0.000012	46154	0.55	0.894		
0.000014	46154	0.65	0.861		
0.000016	46154	0.74	0.827		
0.000018	46154	0.83	0.800		
0.00002	46154	0.92	0.763		
0.000022	46154	1.02	0.736		
0.000024	46154	1.11	0.699		
0.000026	46154	1.20	0.663		
0.000028	46154	1.29	0.627		
0.00003	46154	1.38	0.592		0.592
0.000032	46154	1.48	0.558		
0.000034	46154	1.57	0.525		
0.000036	46154	1.66	0.493		
0.000038	46154	1.75	0.464		
0.00004	46154	1.85	0.449		
0.000042	46154	1.94	0.420		
0.000044	46154	2.03	0.406		
0.000046	46154	2.12	0.381		
0.000048	46154	2.22	0.355		
0.00005	46154	2.31	0.332		
0.000052	46154	2.40	0.308		
0.000054	46154	2.49	0.288		
0.000056	46154	2.58	0.267		
0.000058	46154	2.68	0.249		
0.00006	46154	2.77	0.231		
0.000062	46154	2.86	0.215		
0.000064	46154	2.95	0.199		
0.000066	46154	3.05	0.185		

Proportion Defectives	# Particles		Probability of c=1 or less defects	Producer's risk	Consumer's risk
p	$n (6 \times 20g)$	np	P_a (Cumulative Poisson Probabilities)	α	β
0.000001	92308	0.09	0.995		
0.000002	92308	0.18	0.986		
0.000003	92308	0.28	0.969		
0.000004	92308	0.37	0.945		
0.000005	92308	0.46	0.925		
0.000006	92308	0.55	0.894		
0.000007	92308	0.65	0.861		
0.000008	92308	0.74	0.827		
0.000009	92308	0.83	0.800		
0.00001	92308	0.92	0.763	0.237	
0.000012	92308	1.11	0.699		
0.000014	92308	1.29	0.627		
0.000016	92308	1.48	0.558		
0.000018	92308	1.66	0.493		
0.00002	92308	1.85	0.449		
0.000022	92308	2.03	0.406		
0.000024	92308	2.22	0.355		
0.000026	92308	2.40	0.308		
0.000028	92308	2.58	0.267		
0.00003	92308	2.77	0.231		0.231
0.000032	92308	2.95	0.199		
0.000034	92308	3.14	0.185		
0.000036	92308	3.32	0.159		
0.000038	92308	3.51	0.137		
0.00004	92308	3.69	0.117		
0.000042	92308	3.88	0.092		
0.000044	92308	4.06	0.085		
0.000046	92308	4.25	0.072		
0.000048	92308	4.43	0.066		
0.00005	92308	4.62	0.056		
0.000052	92308	4.80	0.048		
0.000054	92308	4.98	0.040		
0.000056	92308	5.17	0.034		
0.000058	92308	5.35	0.029		



Proportion Defectives	# Particles		Probability of c=1 or less defects	Producer's risk	Consumer's risk
p	$n (15 \times 20g)$	np	P_a (Cumulative Poisson Probabilities)	α	β
0.000001	230769	0.23	0.978		
0.000002	230769	0.46	0.925		
0.000003	230769	0.69	0.844		
0.000004	230769	0.92	0.763		
0.000005	230769	1.15	0.663		
0.000006	230769	1.38	0.592		
0.000007	230769	1.62	0.525		
0.000008	230769	1.85	0.449		
0.000009	230769	2.08	0.381		
0.00001	230769	2.31	0.332	0.669	
0.000012	230769	2.77	0.231		
0.000014	230769	3.23	0.171		
0.000016	230769	3.69	0.117		
0.000018	230769	4.15	0.078		
0.00002	230769	4.62	0.056		
0.000022	230769	5.08	0.037		
0.000024	230769	5.54	0.027		
0.000026	230769	6.00	0.017		
0.000028	230769	6.46	0.011		
0.00003	230769	6.92	0.008		0.008
0.000032	230769	7.38	0.005		
0.000034	230769	7.85	0.004		
0.000036	230769	8.31	0.003		
0.000038	230769	8.77	0.001		
0.00004	230769	9.23	0.001		
0.000042	230769	9.69	0.001		
0.000044	230769	10.15	0.000		